

# **MULTILAYER IMPEDANCE PUMP:**

## **A Bio-inspired Valveless Pump**

### **with Medical Applications**

A thesis by

Laurence Loumes

In Partial Fulfillment of the Requirements

for the Degree of

Doctor of Philosophy



California Institute of Technology

Pasadena, California

2007

(Defended December 8, 2006)

© 2007

Laurence Loumes

All Rights Reserved

*I dedicate this thesis to my parents who  
always valued education and taught me hard work,  
perseverance, humility, honesty and integrity.*

## Acknowledgements

I am very thankful to my advisor Prof. Mory Gharib for his insights and support throughout my PhD. At his contact, I learned how to think outside the box and not to be afraid of taking risks.

I would like to thank John and Idit for their mentoring throughout my PhD. Dr. Idit Avrahami who was a post-doctoral scholar in the Gharib group, was constantly by my side to guide me through all the different steps a PhD student encounters and provided me with an exceptional mentoring. She became a great friend. I learned a lot from her, scientifically and emotionally. Dr. John Dabiri, now professor at Caltech, has been a constant support and guidance, always available and keeping track with my progress. I got to know John since the start of my PhD when, at the time we were both enrolled in the aero program. At a time I was not sure I wanted to go for a PhD, John told me about that research group on campus that uses fluid mechanics in biological context...

Finally, I would like to acknowledge my family and friends who kept me sane and bared my crazy moments.

## Abstract

This thesis introduces the concept of multilayer impedance pump, a novel pumping mechanism inspired from the embryonic heart structure.

The multilayer impedance pump is a composite two-layer fluid-filled elastic tube featuring a thick, gelatin-like internal layer similar in nature to the embryonic cardiac jelly, and that is used to amplify longitudinal elastic waves. Pumping is based on the impedance pumping mechanism. Elastic waves are generated upon small external periodic compressions of the elastic tube. They propagate along the tube's walls, reflect at the tube's extremities and drive the flow in a preferential direction. This fully coupled fluid-structure interaction problem is solved for the flow and the structure using the finite element method over a relevant range of frequencies of excitation. Results show that the two-layer configuration can be an efficient wave propagation combination, and that it allows the pump to produce significant flow for small excitations. The multilayer impedance pump is a complex system in which flow and structure exhibit a resonant behavior. At resonance, a constructive elastic wave interaction coupled with a most efficient energy transmission between the elastic walls and the fluid is responsible for the maximum exit flow. The pump efficiency reaches its highest at resonance, highlighting furthermore the concept of resonance pumping.

Using the proposed multilayer impedance pump model, we are able to bring an additional proof on the impedance nature of the embryonic heart by comparing a

peristaltic and an impedance multilayer pump both excited in similar fashion to the one observed in the embryonic heart.

The gelatin layer that models the embryonic cardiac jelly occupies most of the tube walls and is essential to the propagation of elastic waves. A comparison between the exact same impedance pump with and without the additional gelatin layer sheds light on the dynamic role of the cardiac jelly in the embryonic heart and on nature's optimized design.

Finally, several biomedical applications of multilayer impedance pumping are presented. A physiologically correct model of aorta is proposed to test the pump as an implantable cardiovascular assist device.

## Table of Contents

<b>Chapter 1 Introduction and Background</b> .....	<b>1</b>
1.1 The embryonic heart.....	2
1.1.1 Formation and structure.....	2
1.1.2 The embryonic beating heart as a pump.....	3
1.2 Properties of an impedance pump.....	6
1.2.1 The concept of impedance.....	6
1.2.2 The impedance pump function.....	6
1.3 Concept of multilayer impedance pump.....	8
1.4 Overview.....	10
<b>Chapter 2 The Multilayer Impedance Pump Model</b> .....	<b>12</b>
2.1 Physical model.....	12
2.2 Mathematical model.....	15
2.3 Numerical model.....	17
<b>Chapter 3 MIP Flow and Structure Behavior</b> .....	<b>18</b>
3.1 Model Verification.....	18
3.2 Model Validation.....	18
3.3 Identification of the natural frequencies of the system.....	19
3.4 Pulse velocity.....	21
3.5 Flow rate variation in time.....	22
3.6 Mean exit flow rate and frequency.....	22

3.7	Reynolds number and Womersley number.....	24
3.8	Wall motion .....	25
3.9	Wave interaction in a multilayer impedance pump .....	26
3.10	Velocity profiles .....	31
3.11	Wall position, axial velocity and axial pressure longitudinal distribution .....	34
3.12	Mechanical work done by the elastic tube.....	38
3.13	Pumping efficiency.....	43
<b>Chapter 4 Discussion .....</b>		<b>46</b>
<b>Chapter 5 Impedance Pumping in the Embryonic Heart .....</b>		<b>51</b>
5.1	The different embryonic heart pumping models.....	52
5.1.1	The peristaltic excitation.....	53
5.1.2	The impedance excitation .....	55
5.2	Flow, pressure, and energy expenditure in the two models of embryonic heart pumping .....	55
5.2.1	Flow and pressure in the peristaltic pump model .....	55
5.2.2	Flow and pressure in the impedance pump model.....	56
5.2.3	Energy expenditure .....	56
5.3	Discussion.....	58
<b>Chapter 6 Dynamic Role of the Cardiac Jelly .....</b>		<b>61</b>
6.1	Properties of the cardiac jelly .....	62
6.2	Numerical simulations .....	64
6.2.1	Models.....	64
6.2.2	Exit flow rate variation in time .....	64

6.2.3	Compared performances .....	65
6.2.4	Validation with a second MIP model.....	67
6.3	Nature's design: Importance of the cardiac jelly .....	68
<b>Chapter 7 Potential Cardiovascular Applications .....</b>		<b>70</b>
7.1	Medical applications of the MIP.....	70
7.1.1	Intra-aortic pump .....	71
7.1.2	Gelatin-coated graft .....	72
7.2	Physiologically correct model of an aorta .....	75
7.2.1	Nature of the flow in the descending aorta.....	75
7.2.2	Aorta model with pulsatile boundary conditions .....	77
7.2.3	Results.....	79
7.2.4	Summary.....	81
<b>Chapter 8 Conclusion .....</b>		<b>82</b>
<b>Appendix 1 Model Validation.....</b>		<b>84</b>
<b>Appendix 2 Wave dynamics.....</b>		<b>93</b>
<b>Appendix 3 MIP with a viscoelastic material.....</b>		<b>93</b>
<b>Appendix 4 Error in linearization.....</b>		<b>101</b>
<b>Appendix 5 High frequency results.....</b>		<b>102</b>
<b>Appendix 6 Viscous diffusion time.....</b>		<b>108</b>
<b>References .....</b>		<b>111</b>

## List of Figures

<b>Figure 1.</b> (Left) Schematic of a peristaltic pump. (Right) Schematic of an impedance pump. ....	2
<b>Figure 2.</b> Ventral views of the embryonic heart tube formation in the chick. ....	4
<b>Figure 3.</b> Cross section of the embryonic heart tube in the chick. ....	4
<b>Figure 4.</b> Illustration of the function of the Multilayer Impedance Pump (MIP) .....	10
<b>Figure 5.</b> (Top) 3D view and (Bottom) 2D view in longitudinal cross section of the physical model of the MIP. ....	13
<b>Figure 6.</b> 2D axisymmetric longitudinal outline of the MIP model with excitation and boundary conditions .....	16
<b>Figure 7.</b> 2D axisymmetric longitudinal view of the mesh. ....	17
<b>Figure 8.</b> (Top) Impulse response: exit flow rate variation in time under triangular impulse excitation. (Bottom) The associated Power Spectrum Density (PSD). ....	20
<b>Figure 9.</b> Typical exit flow rate history plot. ....	23
<b>Figure 10.</b> Mean exit flow rate ( $\bar{Q}$ ) as a function of the excitation frequency ( $f$ ). ....	24
<b>Figure 11.</b> Gelatin maximum positive radial strain in time and space as a function of the frequency of excitation ( $f$ ). ....	26
<b>Figure 12.</b> Illustration of the propagating waves in the multilayer impedance pump. (Top) Outline of the model. Walls position against longitudinal axis. (Middle) Corresponding snapshots of the axial velocity fluid field. (Bottom) Axial pressure longitudinal distribution. ....	31

<b>Figure 13.</b> Velocity profiles. (a) Instantaneous axial velocity field and velocity profiles at 11 cross sections along the tube. (b) Enlarged view of the different velocity profiles. (c) Velocity profile at the exit of the pump (#11) for selected times over a period of time...	34
<b>Figure 14.</b> Wall displacement, axial pressure longitudinal distribution and axial velocity longitudinal distribution over a period of time once periodicity in the flow is achieved.	38
<b>Figure 15.</b> (Top) Input and Output cross sections. (Bottom) Control volume and fluid energy balance. ....	39
<b>Figure 16.</b> Pumping work of the elastic tube ( $W_{pump}$ ) as a function of frequency of excitation ( $f$ ). ....	42
<b>Figure 17.</b> Equivalent model: Poiseuille flow driven by a pressure gradient. ....	44
<b>Figure 18.</b> Efficiency ( $\varepsilon$ ) of the MIP as a function of the frequency of excitation ( $f$ )....	45
<b>Figure 19.</b> Model peristaltic embryonic heart pump. 2D longitudinal cross-sectional view of the multilayered tube with an imposed peristaltic displacement wave. ....	54
<b>Figure 20.</b> Schematic and conventions of the imposed peristaltic wave motion. $c$ is the wave velocity. ....	54
<b>Figure 21.</b> Flow and pressure in the PerisEHM. (Left) Exit flow rate and time. (Right) Axial pressure longitudinal distribution over 1 period. ....	57
<b>Figure 22.</b> Flow and pressure in the ImpEHM. (Left) Exit flow rate and time. (Right) Axial pressure longitudinal distribution over 1 period. ....	57
<b>Figure 23.</b> Simplified model of embryonic heart tube. Cross sections in relaxed and contracted states. ....	63
<b>Figure 24.</b> Comparative 2D axisymmetric longitudinal views. (Top) Single layer IP. (Bottom) Gelatin-coated multilayer IP. ....	65

<b>Figure 25.</b> (Top) Exit flow rate history plot for the SLIP. (Bottom) Exit flow rate history plot for the gelatin-coated MIP.....	66
<b>Figure 26.</b> Exit flow rate history plot for the second test case of MIP with a modified gelatin layer.....	68
<b>Figure 27.</b> Illustration of the MIP fitting the inside of the aorta.....	73
<b>Figure 28.</b> A schematic illustration of blood flow in the TCPC Fontan circulation. ....	75
<b>Figure 29.</b> Schematic of the aorta model and the boundary conditions.....	77
<b>Figure 30.</b> Imposed inlet velocity waveform. Plot of the axial velocity $v_z$ is normalized by its peak value $v_z^{\max}$ over one period ( $f=1\text{Hz}$ ). ....	78
<b>Figure 31.</b> Physiologically correct model of aorta. 2D cross sectional view. Geometry and boundary conditions. ....	79
<b>Figure 32.</b> Resulting inlet axial pressure from the inlet imposed velocity profile.....	80
<b>Figure 33.</b> (Right) Axial velocity variation in time.(Left)axial pressure variation in time . Plots are for the node located at mid length of the test domain on the axis of symmetry. 81	

## List of Tables

<b>Table 1.</b> Physical parameters of the MIP.....	14
<b>Table 2.</b> The different test cases (mesh and time steps refinements) and the associated error with respect to the finest mesh.....	19
<b>Table 3.</b> Comparison of the flow, typical pressure inside the pump, pumping work, actuation work, and efficiency between the PerisEHM and the ImpEHM .....	58
<b>Table 4.</b> Comparison of the flow, typical pressure inside the pump, pumping work, actuation work, and efficiency between the SLIP and MIP for the same excitation conditions.....	67

# Chapter 1

## Introduction and Background

The heart is a robust pump capable of beating rhythmically for over 2 ½ billion times in a lifetime. At very early stages of development, the embryonic heart is basically a thick-walled tube. It is during later stages that it will take its four chambers shape. The tubular heart is a remarkable pump that achieves unidirectional pumping even before valve formation.<sup>25</sup> A periodic contractile wave down the embryonic heart flexible walls drive the red blood cells through it.

There are two ways to achieve pumping in valveless elastic tubes: by peristalsis or by the use of impedance mismatch (figure 1). In a peristaltic pump successive sections of the elastic tube are compressed pushing fluid from one end of the tube to the other by positive displacement. In an impedance pump (IP) however, a single actuation location is sufficient to produce a net unidirectional flow. The driving mechanism is the result of the interaction of elastic waves created by local periodic excitations of the tube at an off-center longitudinal position, and their reflection at the tube's extremities where a mismatch of impedance is present.<sup>5</sup>

Recent experimental investigations have revealed that the embryonic heart was an impedance and not a peristaltic pump as commonly thought.<sup>25</sup> The embryonic heart possesses an interesting multilayered wall structure. We use it as an inspiration point for the design of an innovative valveless impedance pump: the multilayer impedance pump.

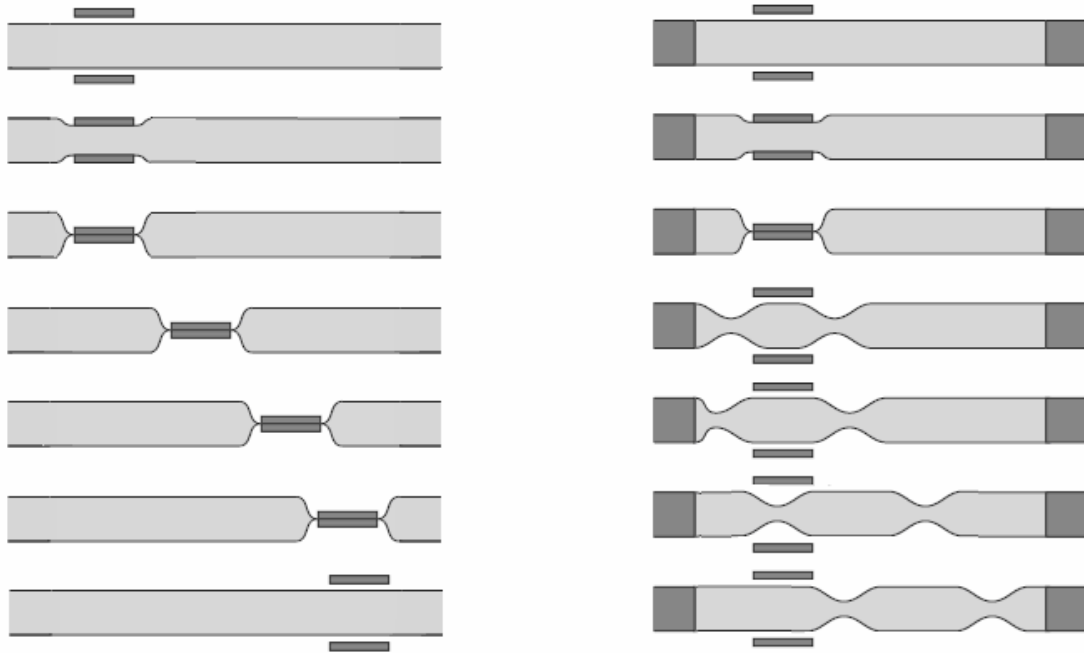


**Figure 1.** (Left) Schematic of a peristaltic pump. The pump functions by positive displacement, a propagating compression zone pushes the fluid along the tube. (Right) Schematic of an impedance pump. The pump functions by elastic wave propagation and reflection. The dark colored edges of the pump represent a mismatch of impedance.

(adapted from Hickerson<sup>27</sup>)

## 1.1 The embryonic heart

### 1.1.1 Formation and structure

An adult vertebrate heart is formed out of four chambers, but at early stages the primitive heart is a simple tube. The heart morphogenesis is done by first the looping of the primitive heart tube on itself. Later, cell differentiation ensures the shaping of the ventricles.<sup>41</sup>

More specifically, the very first stages of the heart development begin with a pair of epithelial tubes formed on opposite sides of the embryo (figure 2.A). Fusions of those tubes along the ventral midline lead to the formation of the cardiac tube (figure 2.B). In the chick, contractions begin soon after the tube forms (Hamburger and Hamilton<sup>26</sup> stage 9 (HH-9)), but before effective blood flow occurs (HH-12, figure 2.D). Flow is driven by a wave propagating along the length of the tube, and becomes pulsatile at HH-stage 17.<sup>23</sup>

The heart tube is composed of three layers: myocardium, cardiac jelly and endocardium (figure 3)<sup>56</sup>. The myocardium is a highly organized tissue composed of smooth muscle cells, fibroblasts and cardiac myocytes. This two- to three-cell-thick layer is the only layer of the tube containing contractile elements, the myofibrils, which slide toward each other upon contraction. The second layer is the cardiac jelly, accounting for the bulk of the tube walls. It is a gelatinous acellular connective tissue matrix playing a central role in septation of the heart and formation of the atrioventricular canals. As the heart differentiates, the cardiac jelly disappears to the profit of the myocardium. Finally, the endocardium is a single layer of cells lining the wall of the heart and is directly in contact with the blood.

### ***1.1.2 The embryonic beating heart as a pump***

Of particular interest is the heart tube before valve formation (HH-9 &10). It is mainly straight tube composed of three layers –endocardium, cardiac jelly and myocardium-. This primitive pump produces a net unidirectional flow. A wave propagates along the tube driving flow through it. Long thought to be a peristaltic wave<sup>21, 52</sup>, Forouhar et al.<sup>25</sup> were able to contradict this hypothesis and proposed instead that the embryonic heart functions as an impedance pump.

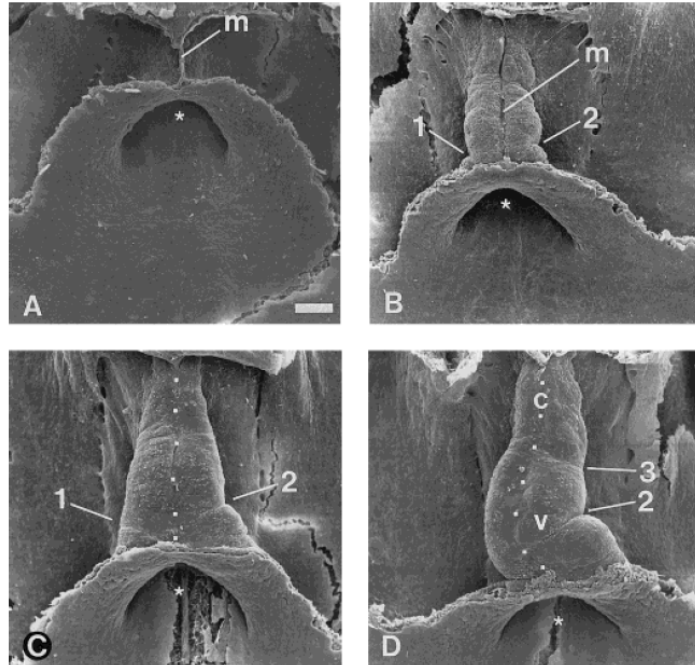


**Figure 2.** Ventral views of the embryonic heart tube formation in the chick (reproduction of Manner<sup>41</sup>). HH-9 &10. Scale bar = 100  $\mu$ m.

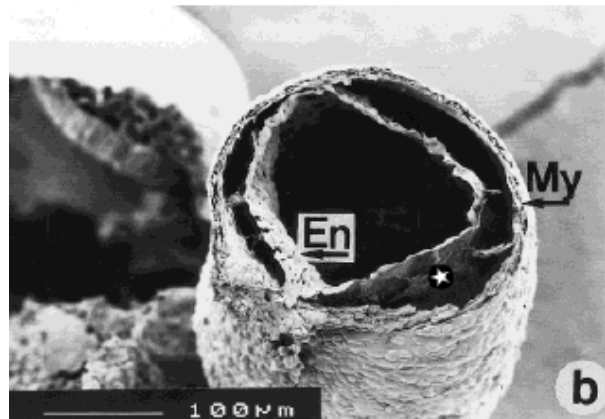


**Figure 3.** Cross section of the embryonic heart tube in the chick (reproduction of Sedmera<sup>56</sup>). My=myocardial mantle, \*=cardiac jelly, En= endocardium. Scale

bar = 100  $\mu$ m

To understand the pumping mechanism they used confocal microscopy and 4D reconstruction protocols on zebrafish, a canonical model for vertebrate development.<sup>22</sup>

Forouhar et al. identified three mechanical properties of embryonic heart tube contractions that contradict the peristaltic hypothesis:

- (i) a bidirectional, as opposed to unidirectional, wave traversing the endocardial layer
- (ii) blood cell trajectories that do not follow local endocardial wave trajectories and that exhibit velocities greater than those of the traveling wave
- (iii) a nonlinear frequency-flow relationship that exceeds the maximum flow rate a peristaltic pump would produce.<sup>a</sup>

In addition to having contradicted the peristaltic hypothesis, they found several elements suggest that the embryonic heart may function as a hydroelastic impedance pump instead:

- (i) resonance peaks in the frequency-flow relationship;
- (ii) mismatched impedance at inflow and outflow tracts and visible wave reflections at the heart tube boundaries
- (iii) a pressure-flow relationship that exhibits a phase difference between the maximum acceleration of blood and the maximum local pressure gradient.

In conclusion, the embryonic heart can be seen as a valveless impedance pump that uses elastic wave propagation and reflection to drive the flow unidirectionally.

---

<sup>a</sup> In a peristaltic pump the flow rate is linearly dependant with the frequency of excitation.

## 1.2 Properties of an impedance pump

### 1.2.1 *The concept of impedance*

Impedance represents the measure of opposition to flow presented by a system. Conventionally impedance is resistance in the case of oscillatory systems. The term impedance is used in the electric current theory (electrical impedance), vibrating solid systems (mechanical impedance) or gas-filled systems (acoustic impedance). We are here referring impedance as the hindrance to flow, which is expressed as the ratio of the instantaneous pressure over the instantaneous flow rate at the section considered (input impedance).<sup>47,50</sup> In the case of a fluid-filled elastic tube IP, mismatch of impedance can be practically achieved by connecting the system to tubes of different stiffnesses or different radii. The mismatch of impedance creates a wave reflection site, a necessary condition to achieve pumping.

### 1.2.2 *The impedance pump function*

The first demonstration of valveless pumping, known as Liebau effect, has been done by Gerhart Liebau in 1954.<sup>37</sup> Using an elastic tube connected to reservoirs at different heights, he was able to pump against the pressure head by periodically compressing the elastic tube at a unique location. He suggested that elasticity, viscosity, and inertia affected the performance of the device, but he was not able to explain how these parameters contributed to the pumping.

Since these first observations, mathematical<sup>4,34,51,59</sup>, experimental<sup>13,28,29,51,53</sup> and lately numerical<sup>5,12,32,42</sup> models have been proposed. These models consist of fluid-filled elastic tubes in open and closed loops excited by a periodic total or partial compression of the

tube. Their limited assumptions (1D, inviscid, linear) and the lack of description of the physics of fluids failed to completely explain this fascinating phenomenon. Although flow dependence on excitation frequency has been observed since Bredow's experiment<sup>13</sup> in 1968, it is only recently that the resonant behavior of the system had been characterized.<sup>5,29,42</sup> Hickerson's experiment<sup>27</sup> was a fluid-filled elastic tube in a closed loop that was connected to reservoirs at the extremities of the tube. These reservoirs were filled with water and allowed to adjust the pressure head. By varying the parameters defining the pump, she was able to show some interesting features of the impedance pump:

(i) Exit flow rate (flow rate at the distant extremity to pinching) is pulsatile

(ii) Mean exit flow is:

- non linear with respect to the frequency of excitation;
- maximum when the pump is excited at resonant frequency or at harmonics of the resonant frequency;
- linearly dependant to the amplitude of pinching (up to 90% radial compression);
- increased with the asymmetry in pincher location;
- linearly increasing with the shortening of the duty cycle;
- linearly decreasing with resistance (increase of pressure head).

The latest numerical work done by Avrahami and Gharib<sup>5</sup> based on the experiment of Hickerson<sup>27</sup>, allowed to understand for the first time the interplay of pressure flow and elasticity in an impedance pump. Pumping is the result of a constructive wave interaction located at the extremity of the elastic tube distant to the pincher, the *pumping region*.

This interaction location is very sensitive to the timing, and therefore to the frequency of excitation. The wave interaction mechanism can be decomposed in three fundamental factors that participate in driving the flow: volume suction, pressure gradient and inertia. In addition, a velocity node is present toward the extremity of the tube. The energy used to compress the tube is transmitted as elastic energy to deform the tube and kinetic energy to push the fluid. Considering the energy exchanged in the system *pump*, they concluded that the velocity node was the point where the elastic energy of the tube starts to be converted into kinetic energy in the fluid. Only at resonance is that energy exchange the most efficient. Their open-looped fluid-filled elastic tube model demonstrated that pumping is not driven by inertia<sup>59</sup> or asymmetry in losses<sup>42</sup> as proposed in closed loop systems, but rather by a resonant wave interaction.

### **1.3 Concept of multilayer impedance pump**

This work proposes a new kind of IP that features a multilayered wall similar to the geometry of the embryonic heart. The main advantage of a multilayer pump over a single-layer impedance pump is that it requires only small excitations to produce significant flow.

The Multilayer Impedance Pump (MIP) is modeled as a valveless composite fluid-filled elastic tube of circular cross section that is periodically excited at a unique location following the impedance pumping mechanism. The tube walls are made of a thick gelatin-like layer modeling the cardiac jelly, and a thin stiffer external layer modeling the myocardium layer. They form together an efficient wave propagation system (figure 4). Elastic waves are generated by periodic compressions of the elastic tube at a single off-

centered location on the external surface of the tube. The elastic waves emitted by the excitation location reach maximum amplitude at the fluid-gelatin interface. They are propagated along the length of the pump and are reflected at the two reflection sites. Because the flexible stiffer layer is compressible but not distensible, all large wave motion is confined inside the pump. The tube's extremities are fixed, creating an impedance mismatch, to allow full reflection of the traveling longitudinal elastic waves. Their interaction results in the driving of the net flow in a preferential direction. Numerical and experimental studies on SLIP<sup>5,27,42</sup> have shown that, in order to achieve significant flow, an IP must typically be compressed at relatively high amplitudes (about 70% of the tube's external radius). This strong compression can strain the tube walls, create large outward radial motion of the tube that would make the pump not compatible with confined environments, or also occlude the flow that would make the device not suitable to many biomedical applications. The proposed MIP addresses these difficulties with the combined use of gelatin and the stiffer layer. The presence of the stiffer layer forbids large radial outward motion, while the softness and thickness of the gelatin are used to amplify and efficiently propagate elastic waves.

Therefore, in a MIP only small excitations are needed to generate elastic waves that last longer and are of greater amplitude than the ones in a SLIP. In addition to its special design, the pumping is based on resonance, meaning that the pump performance is frequency dependant and maximizes at resonance. One of the features of resonant pumping is that the pump requires minimal input energy to operate when excited at resonance.<sup>5</sup>

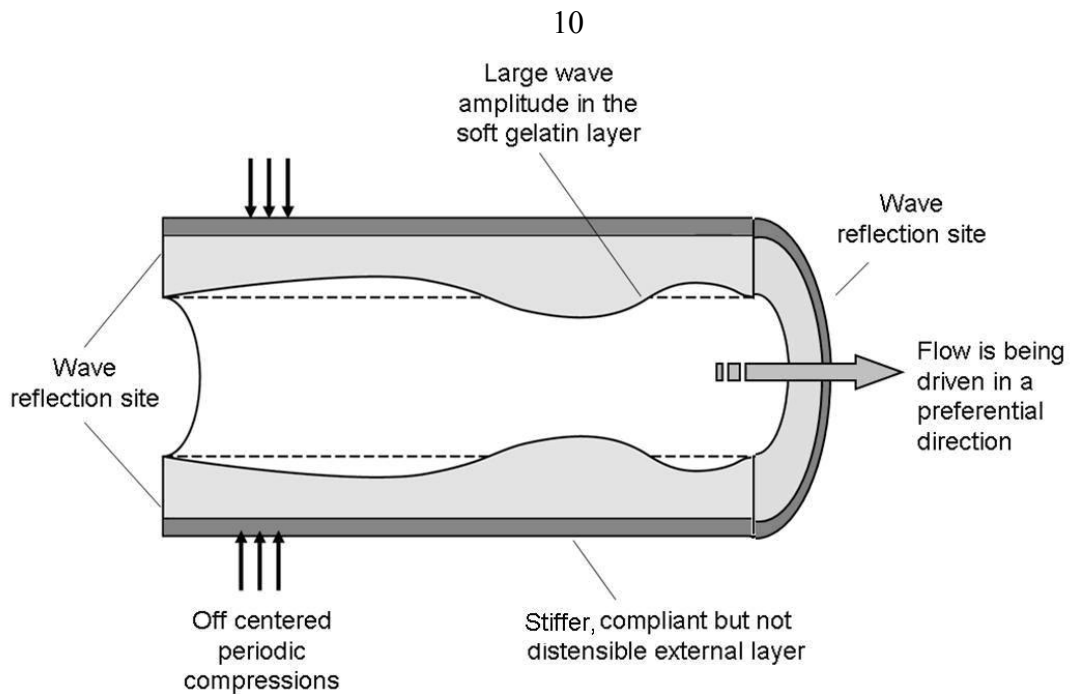


**Figure 4.** Illustration of the function of the Multilayer Impedance Pump (MIP).

## 1.4 Overview

We propose to investigate the potential of a Multilayer IP using numerical simulations. The novelty of the design requires a large design optimization as well as characterization of the pump under dynamical conditions. The choice of numerical simulations is motivated by the possibility of extensive use in design optimization and by the fact that one can isolate factors which in many cases cannot be separated experimentally. In addition, they provide detailed description of the unsteady flow field and the solving of structural behavior at any point in the elastic tube.

This thesis presents the innovative MIP design in Chapter 2. In Chapter 3 flow and structure response to periodic excitation is explored, with an emphasis on the system's behavior at resonance conditions. The energy exchange between the elastic tube and the

fluid that leads to resonance pumping is especially investigated. Chapter 4 is a discussion on the MIP model, its strength and its limitations. In Chapter 5, using an impedance and a peristaltic multilayer pump model, we bring an additional proof that the embryonic heart is a multilayer impedance pump. The role of the gelatin layer in pumping is assessed through the comparison the multilayer pump performances with the exact same pump without gelatin in Chapter 6. Several biomedical applications of the MIP are given in Chapter 7. A physiologically correct model of an adult descending aorta is used to test the pump as a fully implantable intra-aortic pump. Chapter 8 contains concluding remarks over the previous chapters.

## Chapter 2

# The Multilayer Impedance Pump Model

### 2.1 Physical model

The MIP was a fluid-filled elastic tube with an excitation zone located asymmetrically with respect to the length of the pump. The pump had an aspect and a layered wall structure similar to the embryonic heart. The fluid domain accounts for only 35% of the total volume occupied by the pump. The layered walls of the elastic tube were made of a thick gelatin layer for about 80% of the elastic tube volume, and a thin stiffer layer for the remaining 20%, following the heart tube geometry (figure 5). Each layer constituting the tube walls was made of an isotropic linear elastic material. The material properties of each layer have been chosen so that a large enough stiffness ratio between the elastic layers enables the combined effect of wave amplification through the gelatin and the prevention of outward motion at the external layer. In addition, following the embryonic heart structure, the gelatin-like layer has been given some compressibility ( $\nu_{gel}=0.3$ ), while the stiffer layer was relatively incompressible ( $\nu_{st}=0.49$ ) (table 1).

The periodic excitation consisted of imposed radial displacements  $y(t, z)$  on a section of the outer surface of the tube (1). The pump was actuated for 20% of the period time  $T$ . The tube's external radius was maintained to original position during the remaining 80% of the period time. During actuation, the elastic tube was compressed following a

sinusoidal time function  $g(t)$  that depended on the frequency of excitation  $f$  (2). The amplitude  $A$  of the compression was set to 10% of the pump external radius, so that to model the displacement resulting from the myocytes' contractions. The spatial repartition of the compression zone followed a quadratic spatial function  $s(z)$  to simulate a physical pincher (3):

$$y(t, z) = g(t) * s(z), \quad (t, z) \in [0, T] * [a_l, a_l + a_w], \quad (1)$$

$$g(t) = A * \sin(5\pi f t) * \text{Heaviside}\left(\frac{T}{5} - t\right), \quad (t) \in [0, T], \quad (2)$$

$$s(z) = 1 - \left(\frac{1}{13}z - \frac{14}{13}\right)^4, \quad (z) \in [a_l, a_l + a_w]. \quad (3)$$

The impedance mismatch was achieved by fixing the tube's extremities, ensuring total reflection of the elastic waves. The fluid filling the tube was water.

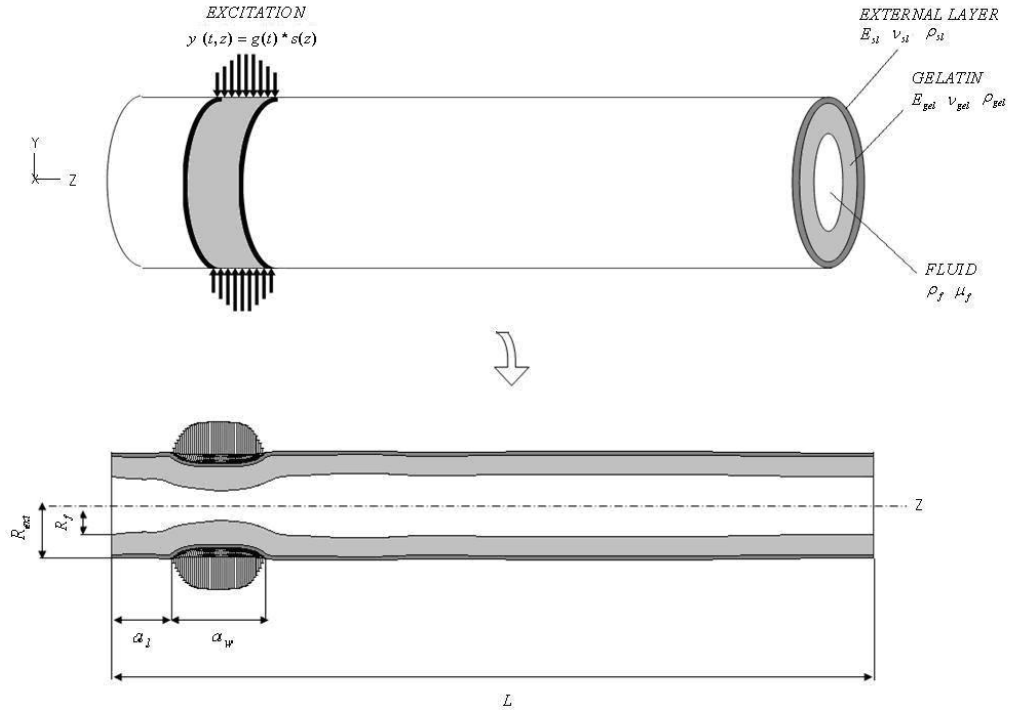


**Figure 5.** (Top) 3D view and (Bottom) 2D view in longitudinal cross section of the physical model of the MIP.

**Table 1.** Physical parameters of the MIP.

Physical parameter	Symbol	Value
Length of the pump	$L$	15.2 cm
External radius of the pump	$R_{ext}$	1.03 cm
Fluid domain radius	$R_f$	0.55 cm
Gelatin thickness	$h_{gel}$	0.405cm
Stiffer layer thickness	$h_{sl}$	0.075 cm
Actuator location with respect to the tube's nearest extremity	$a_l$	1.2 cm
Actuator width	$a_w$	1.8 cm
Gelatin stiffness	$E_{gel}$	5 e+ 4 dyn/cm <sup>2</sup>
Stiffer layer stiffness	$E_{sl}$	1 e+ 7 dyn/cm <sup>2</sup>
Gelatin Poisson's ratio	$\nu_{gel}$	0.3
Stiffer layer Poisson's ratio	$\nu_{sl}$	0.49
Gelatin density	$\rho_{gel}$	1 g/cm <sup>3</sup>
Stiffer layer density	$\rho_{sl}$	1 g/cm <sup>3</sup>
Fluid viscosity	$\mu_f$	0.01 g/cm s
Fluid density	$\rho_f$	1 g/cm <sup>3</sup>
Excitation amplitude	$A$	0.1 cm
Frequency	$f$	7 Hz to 12.2 Hz

## 2.2 Mathematical model

The fluid motion was derived by the conservative Navier-Stokes equations using the Arbitrary Lagrange Eulerian formulation:

$$\nabla \cdot \mathbf{v} = 0, \quad (4)$$

$$\rho_f \left( \frac{\partial \mathbf{v}}{\partial t} + (\mathbf{v} - \mathbf{v}_g) \cdot \nabla \mathbf{v} \right) + \nabla \cdot \boldsymbol{\tau}_f = 0, \quad (5)$$

where  $\boldsymbol{\tau}_f$  is the stress tensor,  $\mathbf{v}$  is the flow velocity vector and  $\mathbf{v}_g$  is the local coordinate velocity vector,  $\rho_f$  is the density of the fluid and  $t$  is the time.

The fluid is Newtonian, incompressible and viscous, and its state of stress  $\boldsymbol{\tau}_f$  follows:

$$\boldsymbol{\tau}_f = -P\mathbf{I} + \mu_f(\nabla \mathbf{v} + \nabla \mathbf{v}^T), \quad (6)$$

where  $P$  is the static pressure and  $\mu_f$  is the dynamic viscosity.

The dynamics of each layer of the flexible wall were calculated using the balance of momentum equation in Lagrangian form (7) and the constitutive relation for a linear isotropic elastic material (8):

$$\nabla \boldsymbol{\tau}_s + \mathbf{b}^f = \rho \ddot{\mathbf{u}}, \quad (7)$$

$$\boldsymbol{\tau}_s = \lambda \text{Tr}(\boldsymbol{\varepsilon}_s)\mathbf{I} + 2\mu \boldsymbol{\varepsilon}_s, \quad (8)$$

where  $\boldsymbol{\tau}_s$  is the Cauchy stress tensor,  $\boldsymbol{\varepsilon}_s$  the strain tensor,  $\mathbf{b}^f$  the body forces vector per unit volume,  $\ddot{\mathbf{u}}$  the acceleration vector  $\rho$  the density, and  $\lambda$  and  $\mu$  the Lamé constants of the considered structural domain.

At the fluid-structure interface the fluid is fully coupled to the gelatin. The fundamental conditions applied to the fluid-structure interface are displacement compatibility and traction equilibrium between the two surfaces:

$$\mathbf{d} = \mathbf{u}, \quad (9)$$

$$\mathbf{n} \cdot \boldsymbol{\tau}_f = \mathbf{n} \cdot \boldsymbol{\tau}_s, \quad (10)$$

where  $\mathbf{d}$  and  $\mathbf{u}$  are the fluid and solid displacement vectors respectively, and  $\mathbf{n}$  is the unit normal.

To ensure total wave reflection, fixed ends in both layers are modeled by imposing zero displacements in all directions and at all time at the two tube extremities:

$$\mathbf{u} = \mathbf{0} \quad \text{at } z=0 \text{ and } z=L. \quad (11)$$

The no-slip condition ( $\mathbf{n} \times \dot{\mathbf{u}} = \mathbf{n} \times \mathbf{v}$ ) is applied at the fluid-structure interface, and the tube lies in a stress-free and pressure-free environment (figure 3):

$$\mathbf{n} \cdot \boldsymbol{\tau}_s = 0 \quad \text{on the lateral surface of the tube}, \quad (12)$$

$$P = 0 \quad \text{at } z = 0 \text{ and } z = L. \quad (13)$$

Initial conditions are resting state: zero pressure and zero velocity in the fluid, no stress or strain in the structure.

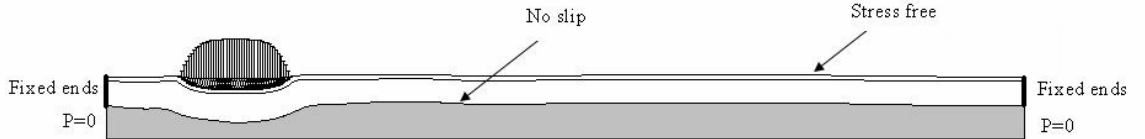


**Figure 6.** 2D axisymmetric longitudinal outline of the MIP model with excitation and boundary conditions (the shaded region represents the fluid domain).

## 2.3 Numerical model

The finite elements method was used to discretize both the fluid and structure domains, and the fully coupled problem was solved using the commercial package ADINA (ADINA R&D, MA).

The fluid and the solid domain were meshed using 4-noded axisymmetric elements. The solid mesh was refined at the pinching zone. A total of 10,500 elements were used, 6,000 for the fluid and 4,500 for the solid (figure 7). An embedded actuation pincher was modeled by imposing radial displacements on a series of nodes corresponding to the pincher location, at the outer surface of the tube. The solid part is solved using the small strain, small deformation hypothesis, and the flow is assumed to be laminar. A constant number of 1,000 time steps per pinching cycle are used to march throughout the transient simulations.

The time integration scheme is implicit Euler backward ( $\alpha=1$ ), which is first-order accurate in time. The equations of motion are integrated by using the implicit damped Newmark scheme ( $\delta=0.5$ ,  $\alpha =0.25$ ), and the full Newton Method was used for the non linear equations. The fluid and solid are 2-ways direct fully coupled, and the fluid mesh is updated at each time step using Arbitrary Lagrange Eulerian formulation. All computations are starting from resting state and are carried on until periodicity in the fluid motion is achieved (mean exit flow is constant within 1% for at least 5 periods).

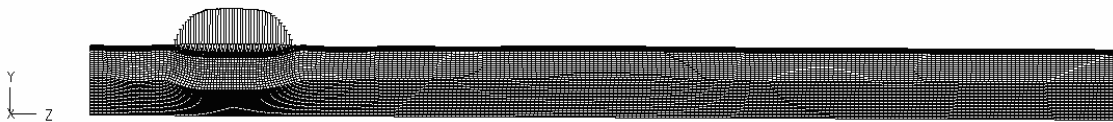


**Figure 7.** 2D axisymmetric longitudinal view of the mesh.

## Chapter 3

# MIP Flow and Structure Behavior

### 3.1 Model Verification

Please see appendix 1.

### 3.2 Model Validation

We perform the same computation for different mesh and time step refinements keeping constant the product  $C = t_s * N$  where  $t_s$  is the time step and  $N$  the total number of elements. We perform the mesh and time step independence tests for the model excited at one of the highest excitation frequency ( $f=11$  Hz) so that the accuracy of the simulation for lower frequencies will be ensured. Our model has a total of 10,500 elements (6,000 fluid elements and 4,500 solid elements) and we use 1,000 time step per each excitation period ( $C=0.9545$ ). We compare our model to 4 other cases (see table 2), and each computation runs until periodicity in the flow is achieved.

We define the instantaneous error in mesh refinement to be the mean error in axial velocity relative to the finest mesh at a specific point  $(y_o, z_o)$  (14).

$$Error_{(y_o, z_o)} = \mathit{mean}_{t \in [t_o, t_o + T]} \left| \frac{v_z^{test}(t, y_o, z_o) - v_z^{finest}(t, y_o, z_o)}{v_z^{finest}(t, y_o, z_o)} \right| \quad (14)$$

The time average of the error calculated for the point belonging to the axis of symmetry at the exit of the pump decreases with mesh refinement and our model has an average relative difference with the finest mesh possible  $Error_{(0,L)}$  of about 3%.

**Table 2.** Mesh and time steps refinements test cases and associated error with respect to the finest mesh.

Case #	Number of elements	Time steps per period	Mean Error
1	13,650	1,300	0
2	12,600	1,200	0.0069
3	10,500	1,000	0.0315
4	8,400	800	0.0565
5	5,200	500	0.0583

### 3.3 Identification of the natural frequencies of the system

A free vibration test is performed. The model is impulsively actuated and the pincher is held to resting position until every motion in the fluid and solid domains disappears. The triangular impulse duration is  $1.66 \text{ e-}2 \text{ s}$ , corresponding to 200 time steps of  $8.3 \text{ e-}5 \text{ s}$  each. The time step length  $t_s = 8.3 \text{ e-}5 \text{ s}$  corresponds to the smallest time step duration used throughout the computations ( $f=12 \text{ Hz}$ ).

Because the model is fairly complex, the spectral analysis of the impulse response is carried on for different parameters extracted from the flow (pressure, axial velocity) and

the structure (radial displacement), and at different points throughout the model. Each of these observables {point, parameter} has an associated Power Spectrum Density (PSD) that exhibits several frequencies.

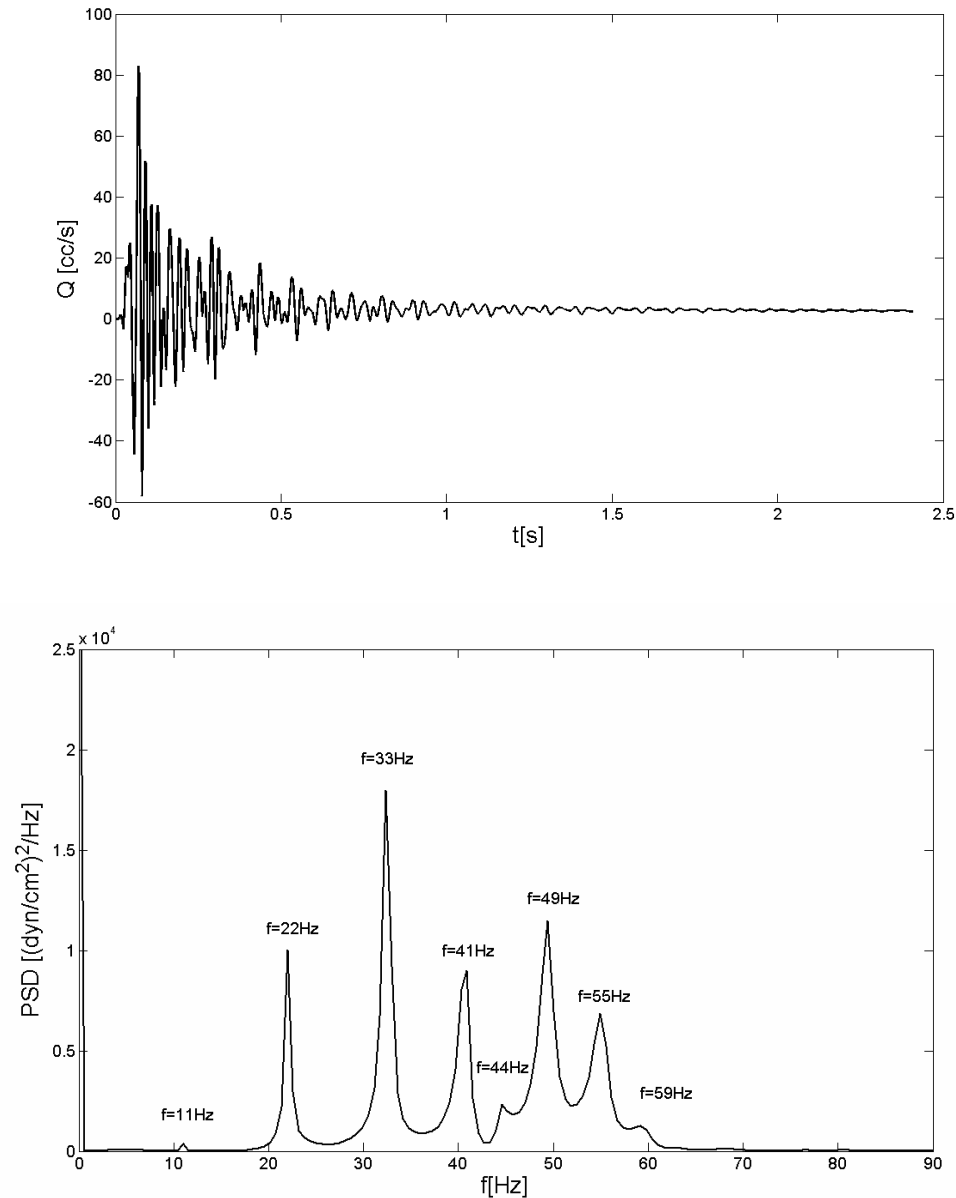


**Figure 8.** (Top) Impulse response: exit flow rate variation in time under triangular impulse excitation. (Bottom) The associated Power Spectrum Density (PSD). The Fourier transform was calculated using 4,096 points, and a time resolution of  $4 \times 10^{-4}$  s.

However, throughout the model the different observables' PSD contains the same frequencies, but expressed at different strengths (amplitude of the PSD). We chose to present the exit flow rate variation in time and its associated PSD (figure 8) because in addition to exhibiting all the natural frequencies present in the system, it is a relevant observable for the system *pump*. We identify  $f_n=11$  Hz as a natural frequency and  $f=22$  Hz,  $f=33$  Hz,  $f=44$  Hz,  $f=55$  Hz as harmonics. Additional natural frequencies are  $f=41$  Hz,  $f=49$  Hz and  $f=59$  Hz.  $f_d=33$  Hz is the dominant frequency of the spectrum. We choose to study the system around the natural frequency  $f_n=11$  Hz because the dominant frequency is its harmonic.

### 3.4 Pulse velocity

The pressure wave speed was calculated using a single pressure step at one extremity of the tube of magnitude. The pressure is modeled as a normal traction force of magnitude  $1e+4$  dyn/cm<sup>2</sup>. The time step resolution for the computation is  $t_s=9.0909$  e-5 s. The pressure wave speed is estimated to  $172.7$  cm.s<sup>-1</sup>, based on the time needed for the pressure step to propagate along the model ( $L=15.2$  cm) at rest. This velocity is closed to the value  $c_0 = 155.6$  cm.s<sup>-1</sup> found using the Moens-Korteweg formula<sup>49</sup> (15) (derived for inviscid flow in a thin walled elastic tube that possesses some material compressibility):

$$c_0 = \sqrt{\frac{Eh}{2\rho a(1-\nu^2)}}, \quad (15)$$

where  $E$  is the stiffness of the gelatin layer ( $E_{gel}=5e+4$  dyn/cm<sup>2</sup>),  $h$  the thickness of the gelatin layer ( $h_{gel}=0.405$  cm),  $\rho$  the density of the gelatin layer ( $\rho_f=1$  g/cm<sup>3</sup>) and  $a$  the fluid domain radius ( $R_f=0.55$  cm) and  $\nu$  the Poisson's ratio of the gelatin ( $\nu_{gel}=0.3$ ).

### 3.5 Flow rate variation in time

Instantaneous flow rate  $Q(t, z_o)$  at a cross section located at  $z = z_o$  of the tube is, by convention, positive when flow is exiting the pump (flow in  $Z$  direction), and is expressed as:

$$Q(t, z_o) = 2\pi \int_0^{R_f(t)} v_z(y(t, z_o), z_o) y(t, z_o) dy(t, z_o), \quad (16)$$

where  $v_z$  is the axial velocity,  $y$  is the radial position,  $R_f$  is the fluid domain radius and  $z_o$  the longitudinal position of the considered cross-section and  $t$  the time. For each excitation frequency, we compute the cross sectional flow at the pump extremity distant to the actuator  $Q(t, L)$ . Exit flow history plots show a transient phase where the flow is building up before reaching a steady state of periodic oscillations and constant mean value (figure 9).

### 3.6 Mean exit flow rate and frequency

For the various frequencies of excitation, the mean exit flow rate ( $\bar{Q}$ ) is calculated by averaging at steady state conditions, the instantaneous exit flow rate  $Q(t, L)$  over one excitation period.

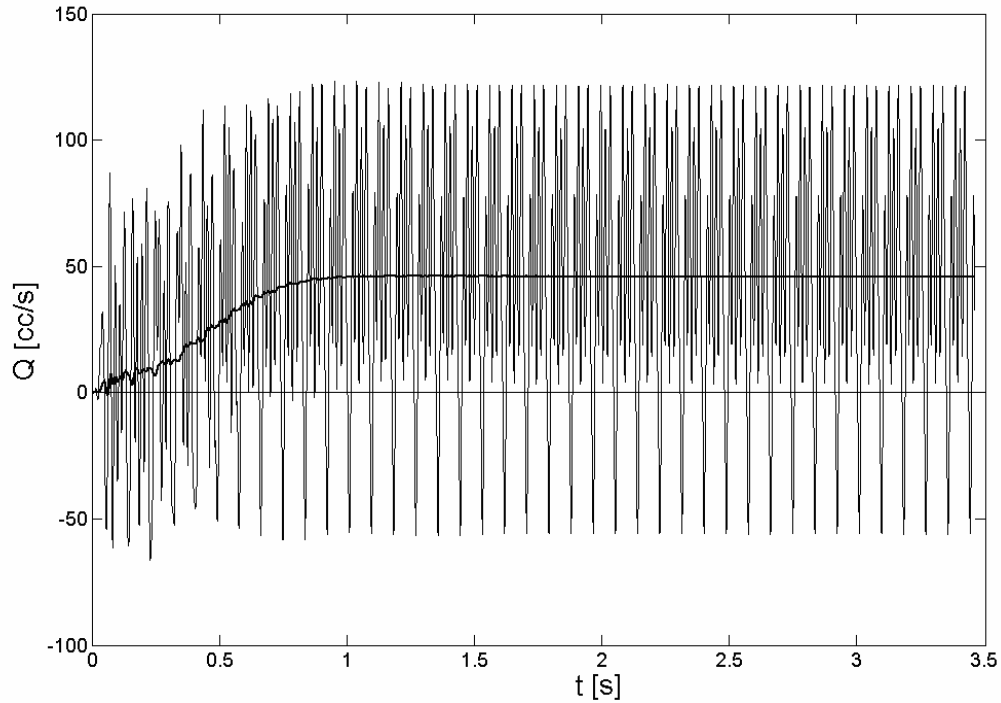


**Figure 9.** Typical exit flow rate history plot. Excitation frequency is  $f=11.5$  Hz.

Periodicity is achieved after 15 pinching cycles and mean flow at steady state is 45.7 cc/s.

The solid line is a filtered curve of the flow rate using a moving average window of one cycle.

The mean exit flow rate is nonlinearly dependent on frequency as expected for an IP. In addition, it exhibits a zone of negative flow for frequencies below 9 Hz (figure 10). Maximum positive flow reaches 86.87 cc/s when the pump is excited at 10.1 Hz. Therefore, for the system *pump*  $f_{res}=10.1$  Hz will be referred it as the resonant frequency of the system. Flow resonance has been also observed in single layer impedance pumps.<sup>5,29,42</sup>

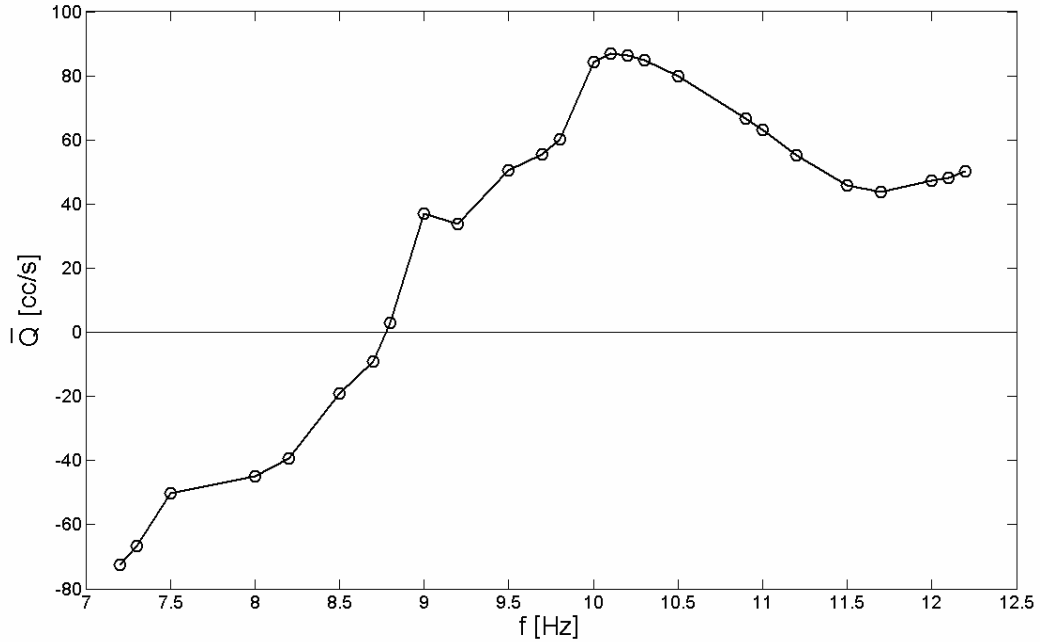


**Figure 10.** Mean exit flow rate ( $\bar{Q}$ ) as a function of the excitation frequency ( $f$ ).

### 3.7 Reynolds number and Womersley number

The Reynolds number in a steady flow is defined as the

$$R_e = \frac{\bar{u} d}{\nu}, \quad (17)$$

where  $\bar{u}$  is a characteristic velocity,  $d$  is a characteristic length, and  $\nu$  the kinematic viscosity of the fluid. For the fluid-filled elastic tube problem  $\bar{u}$  is defined as the mean axial velocity  $\bar{v}_z$ ,  $d$  as the fluid domain radius  $R_f$ , and  $\nu$  as the ratio of the dynamic

viscosity of water over the density of water  $\frac{\mu_f}{\rho_f}$ . The Reynolds number can be expressed

as a function of the mean exit flow:

$$R_e = \frac{25}{\pi d \nu} \frac{4\bar{Q}}{\pi d \nu}. \quad (18)$$

For the different frequencies of excitation, the mean exit flow ranges from -78cc/s to +86cc/s leading to mean Reynolds number up to  $R_e^{mean} = 9,959$ . The instantaneous Reynolds number based on the maximum axial velocity for each frequencies of excitation ranges between 2,000 and 20,000.

The Womersley number ( $\alpha$ ) is defined as the ratio of the inertial forces to the viscous forces for pulsatile flows and can be seen as the equivalent of the Reynolds number but for pulsatile flow. It is expressed as:<sup>50</sup>

$$\alpha = R_f \sqrt{\frac{\omega}{\nu}}, \quad \omega = 2\pi f, \quad (19)$$

where  $R_f$  is the fluid domain radius,  $\omega$  is a characteristic frequency in radians per second of the oscillatory motion, and  $\nu$  the kinematic viscosity of the fluid. For the fluid-filled elastic tube problem  $\omega$  is expressed in terms of the frequency of excitation of the system  $f$ , and  $\nu$  is the ratio of the dynamic viscosity of water over the density of water  $\frac{\mu_f}{\rho_f}$ . For

the frequency range 7.2Hz to 12.2Hz studied, the Womersley number spans 36.9 to 48.1.

### 3.8 Wall motion

Each layer of the tube has a distinct thickness and distinct material properties which influences the speed, damping and amplitude of the traveling elastic waves. The thickness and softness of the gelatin layer are used to amplify wave motion, while the stiffness of

the external layer is used to limit outward radial motion. The concept of multilayer pumping relies on large amplitude wave motion at the fluid-gelatin interface combined with a very limited motion of the external surface of the pump. The maximum wall deflection in the stiffer layer outer surface is found to range from 0.37% to 6.10% from resting position, while the gelatin inner surface deflects from 24% to 32% from resting position, depending on the frequency of excitation. At resonance  $f_{res} = 10.1$  Hz, gelatin stretch is particularly important (figure 11) and plays a role in the pumping performance.

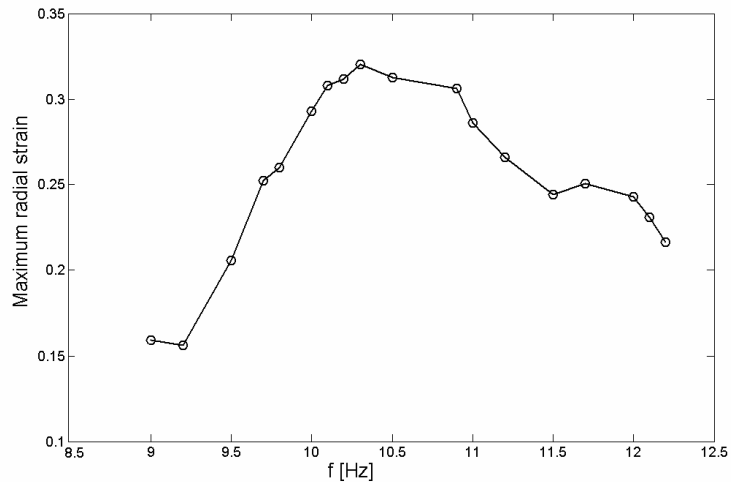


**Figure 11.** Gelatin maximum positive radial strain in time and space as a function of the frequency of excitation ( $f$ ).

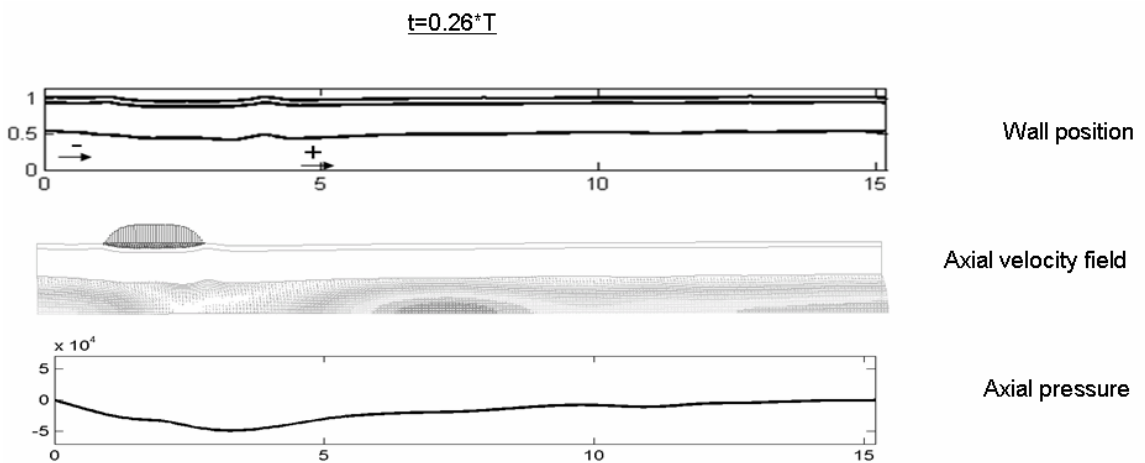
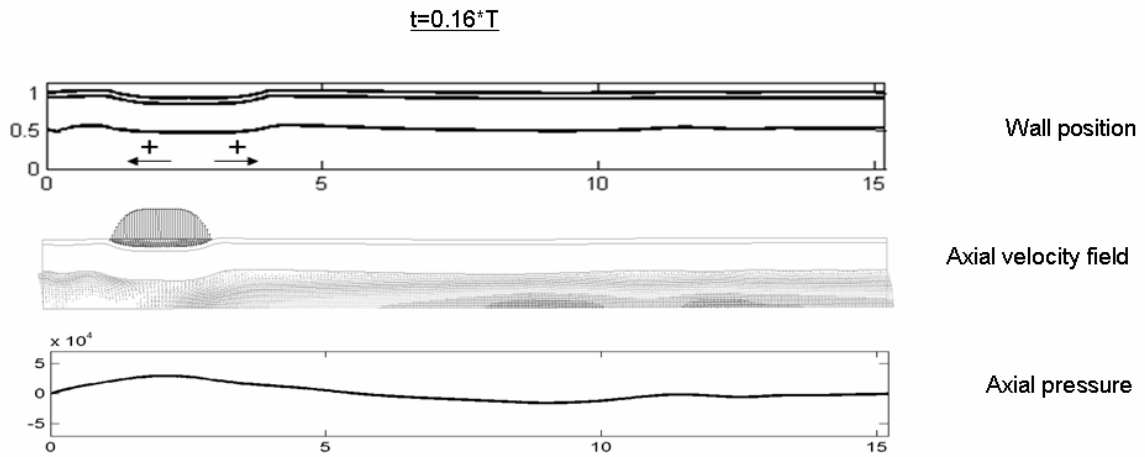
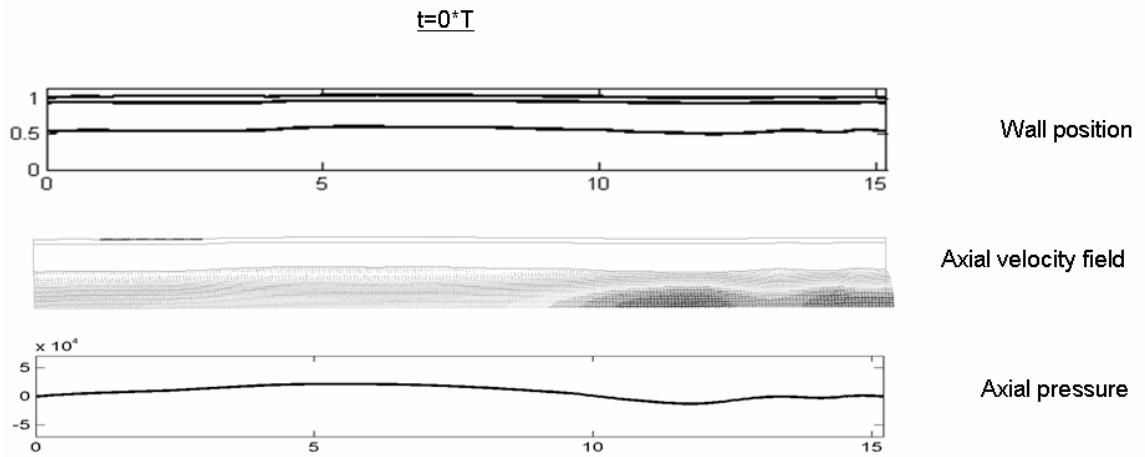
### 3.9 Wave interaction in a multilayer impedance pump

Upon compression elastic waves are created in both layers of the tube. They travel along the length of the tube and reflect at the tube extremities. The constructive wave mechanism occurring in the tube's walls of a MIP (mainly in the gelatin layer) is similar to the one described by Avrahami and Gharib<sup>5</sup> for a SLIP. When the pump is excited at resonance a strong wave interaction occurs toward the pump extremity distant from the

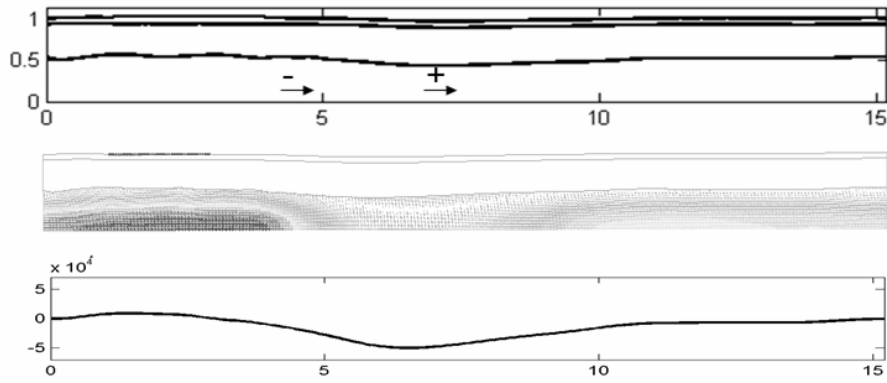
pincher. This interaction creates a suction zone where fluid fills quickly the newly created cavity. As this cavity travel downstream toward the tube's extremity a strong pressure gradient is created between the cavity and the extremity of the tube. A net exiting flow is created by inertia. More specifically, the wave mechanism over a period of time  $T$  is as follows (figure 12 and appendix 2).

The cycle begins with the elastic tube at resting state ( $t=0*T$ ). Upon compression ( $t=0.16*T$ ), two primary positive elastic waves are created on each side of the pincher. The positive elastic wave close to the short side of the tube reflects into a negative wave ( $t=0.26*T$ ). At  $t=0.36*T$  the pinching action is over and the result is the creation of a pressure gradient associated with a reflected negative elastic wave ( $z=4.8$  cm) and a primary positive elastic wave ( $z=7$  cm) traveling toward the exit of the tube. While traveling, the positive wave ( $t=0.45*T$ ,  $z=10$  cm) steepens due to the influence of the nearby forward negative wave ( $t=0.45*T$ ,  $z=7$  cm). Small amplitude secondary waves ( $t=0.45*T$ ,  $z=[0,3]$  cm) that have being created from the release action of the pincher and have reflected on the short side of the pincher, are now traveling toward the exit of the tube. The forward positive wave reaches the tube's extremity ( $t=0.57*T$ ), and reflects in a negative wave traveling now toward the pincher ( $t=0.67*T$ ). At that instant, a strong wave interaction occurs between this reflected wave and the still-forward-traveling negative wave creating a large suction zone ( $t=0.67*T$ ). Fluid fills quickly the newly created opening, and a strong pressure gradient is present between the cavity and the extremity of the tube as the cavity travels further downstream. Fluid is washed out by inertia and exits the pump ( $t=0.74*T$ ). The suction zone reflects at the tube extremity

( $t=0.8T$ ), squeezing the fluid out of the pump ( $t=0.9T$ ). Motion in the tube damps and a new cycle is about to begin ( $t=1T$ ).



$t=0.36 \cdot T$

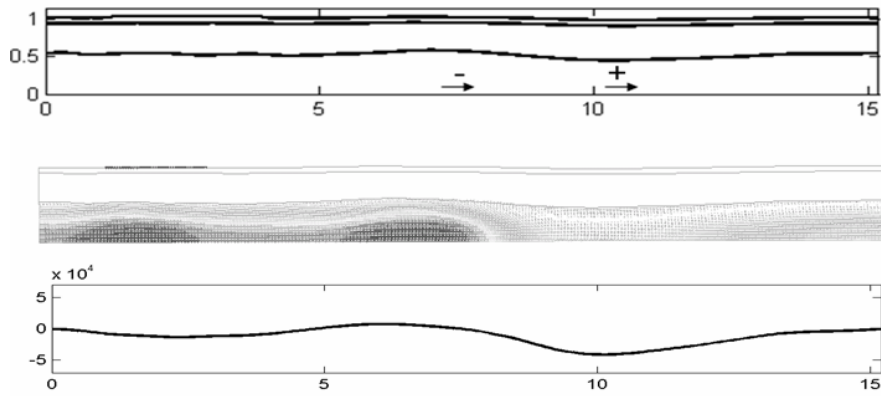


Wall position

Axial velocity field

Axial pressure

$t=0.45 \cdot T$

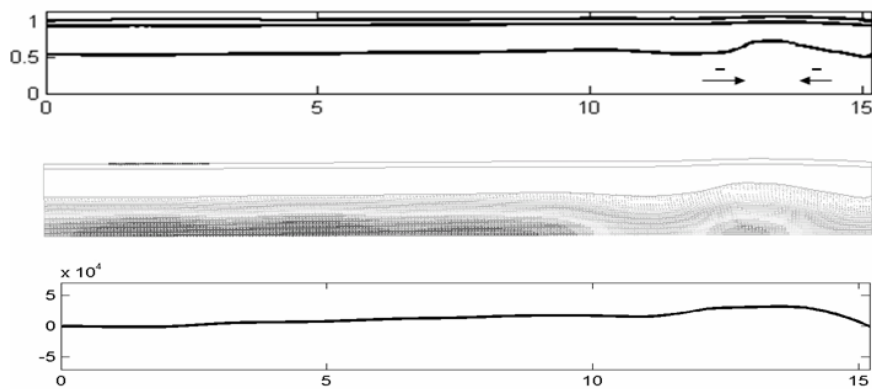


Wall position

Axial velocity field

Axial pressure

$t=0.67 \cdot T$



Wall position

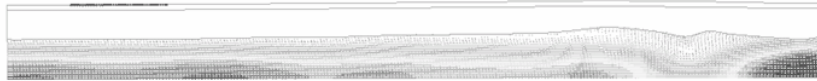
Axial velocity field

Axial pressure

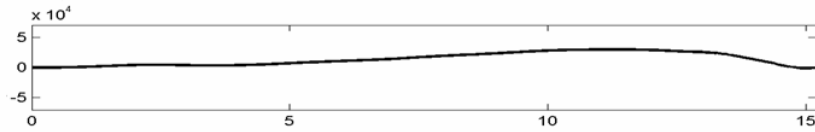
$t=0.74^*T$



Wall position



Axial velocity field



Axial pressure

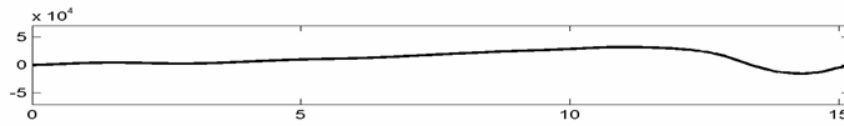
$t=0.8^*T$



Wall position



Axial velocity field



Axial pressure

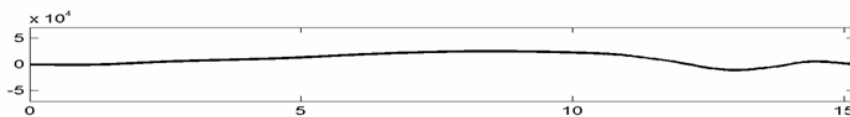
$t=0.9^*T$



Wall position



Axial velocity field



Axial pressure

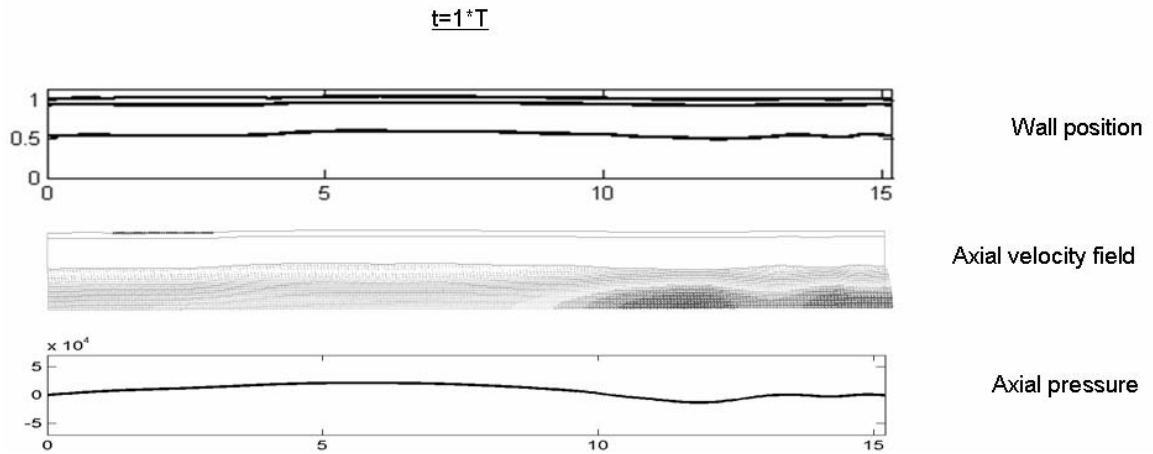


**Figure 12.** Illustration of the propagating waves in the multilayer impedance pump. Example for  $f=10.1$  Hz. Selected frames at time  $t$  as a fraction of the period time  $T$ . (Top) Outline of the model. Walls position against longitudinal axis. (Middle) Corresponding snapshots of the axial velocity fluid field. (Bottom) Axial pressure longitudinal distribution.

### 3.10 Velocity profiles

For the MIP excited at 10.1Hz, we select a specific time ( $t=8.77129$  s) and plot the velocity profiles for discrete cross sections along the tube.

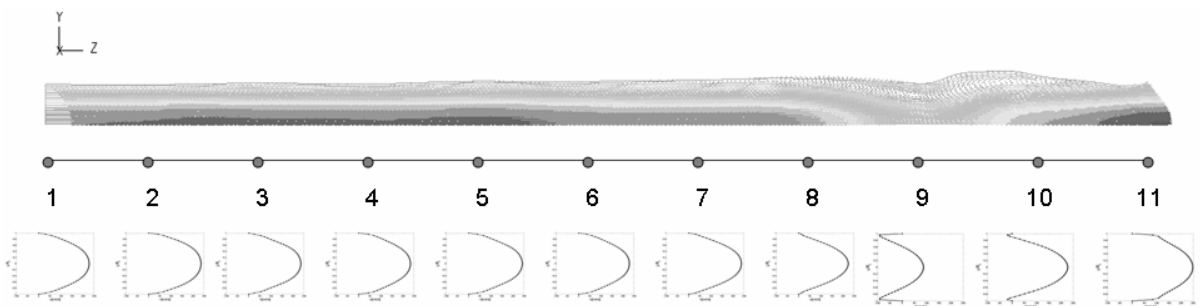
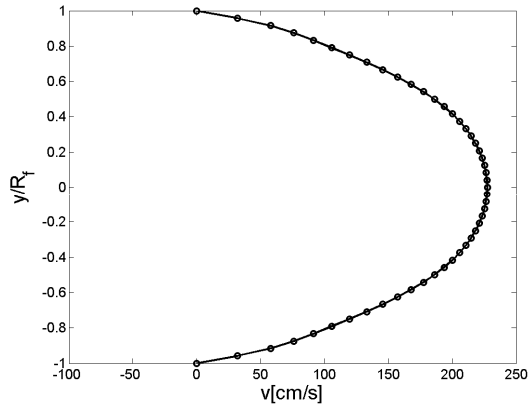
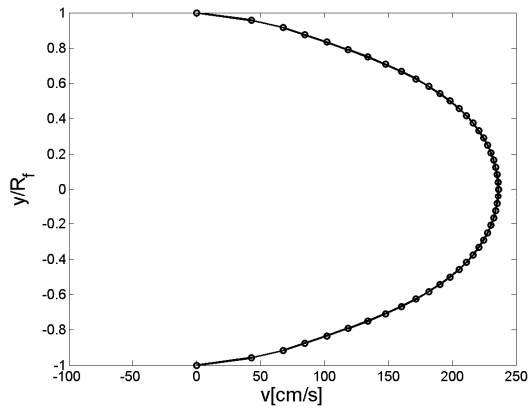


**Figure 13 (a)**

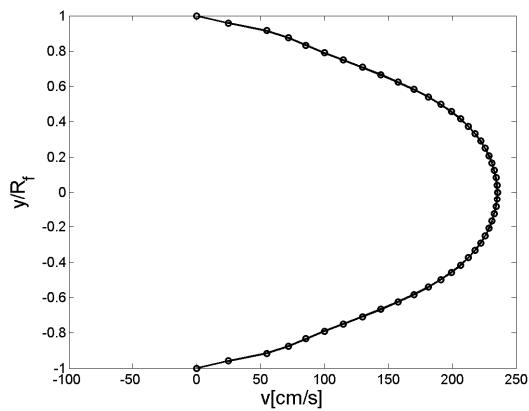
1



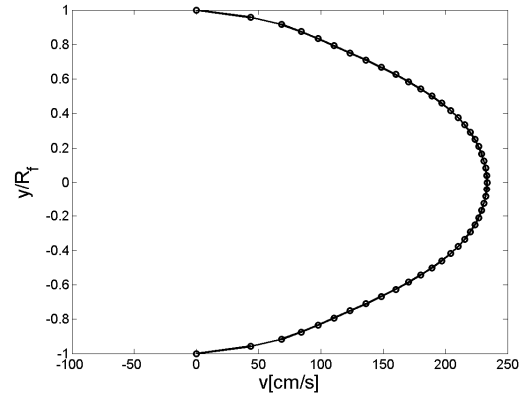
2



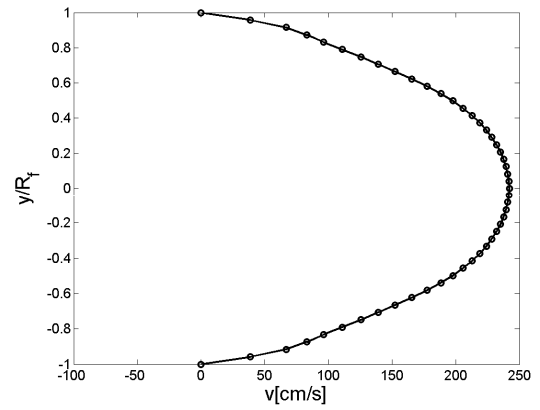
3



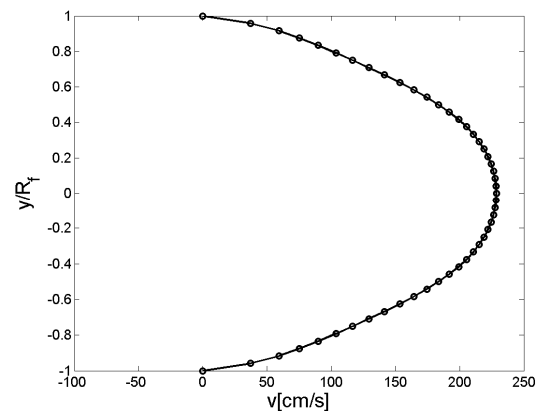
4



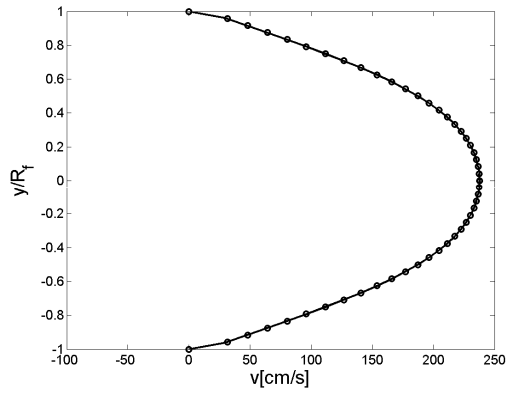
5



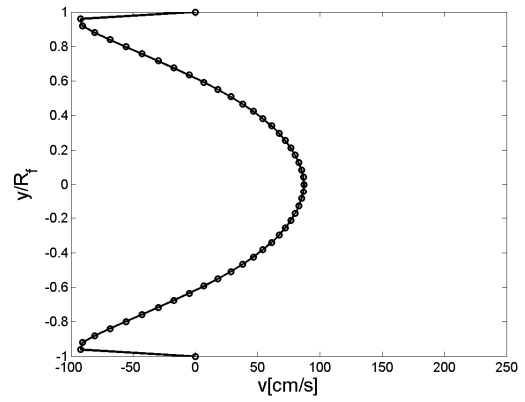
6



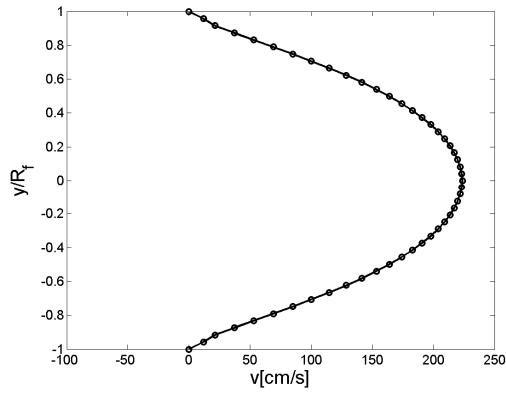
7



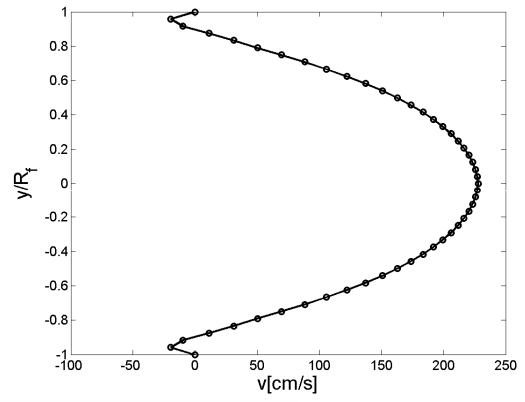
9



8



10



11

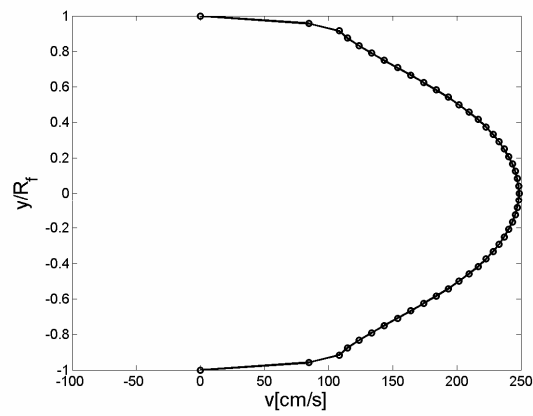
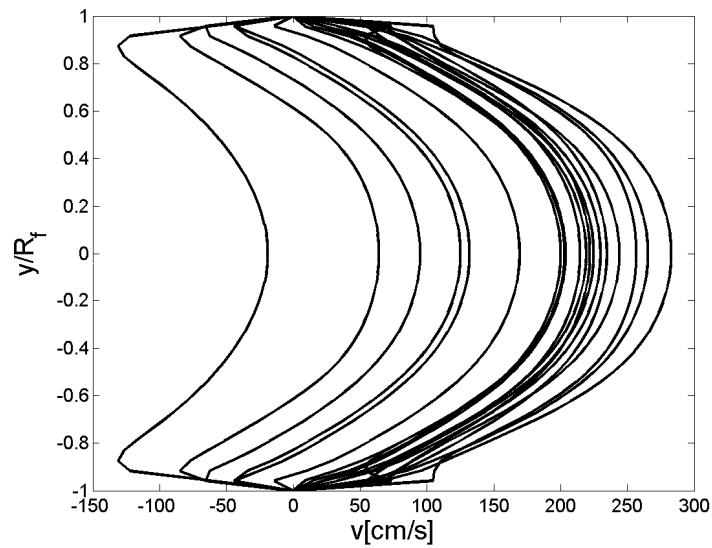


Figure 13 (b)

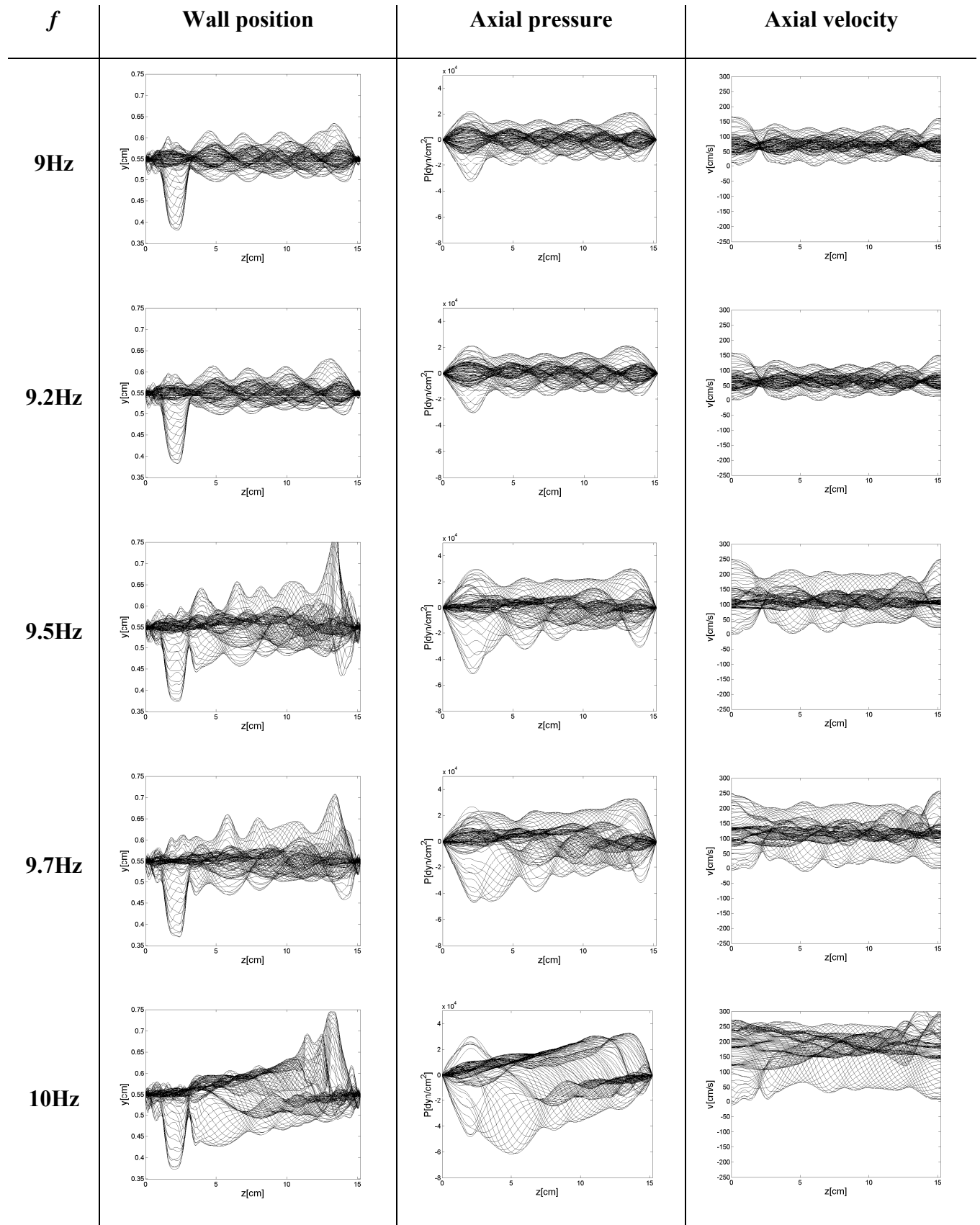


**Figure 13 (c)**

**Figure 13.** Velocity profiles. (a) Instantaneous axial velocity field and velocity profiles at 11 cross sections along the tube. (b) Enlarged view of the different velocity profiles. (c) Velocity profile at the exit of the pump (#11) for selected times over a period of time.

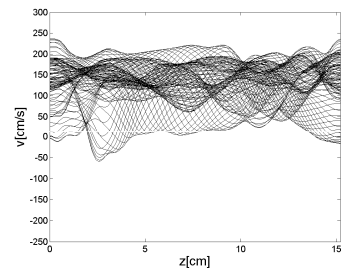
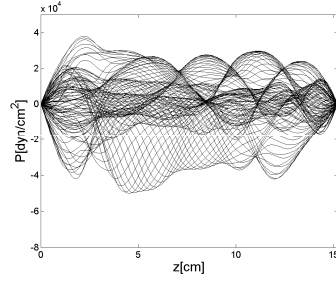
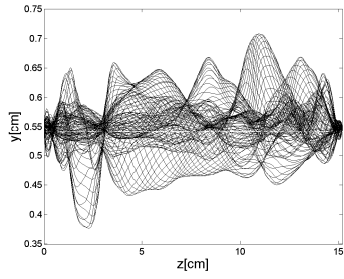
### **3.11 Wall position, axial velocity and axial pressure longitudinal distribution**

For each frequency in the positive flow domain, the wall displacement, axial pressure longitudinal distribution and axial velocity longitudinal distribution is plotted over a period of time once periodicity in the flow is achieved.

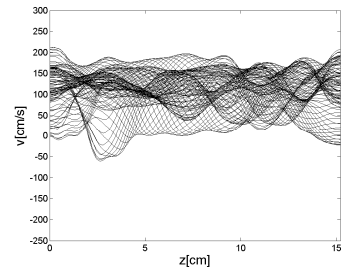
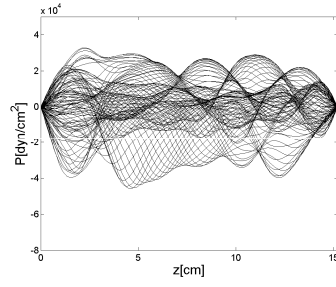
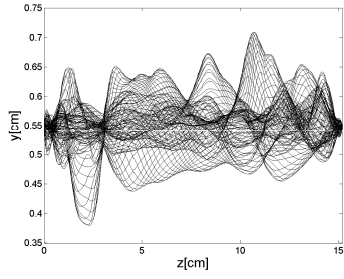




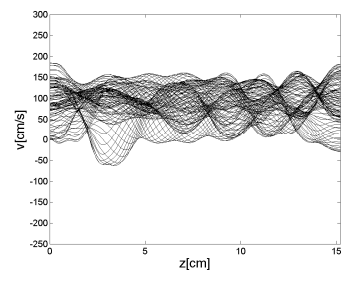
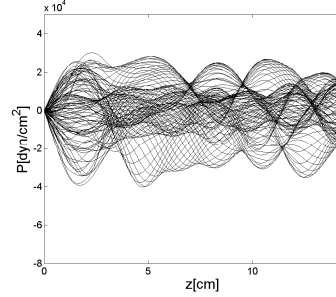
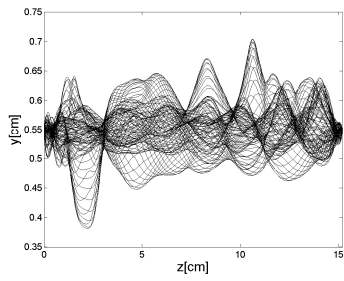
11Hz



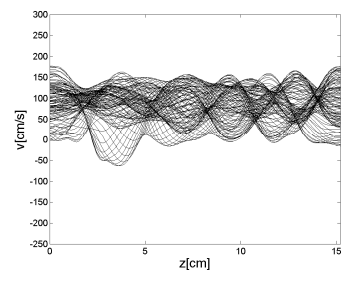
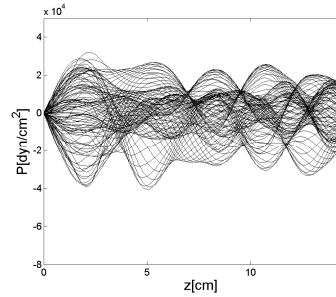
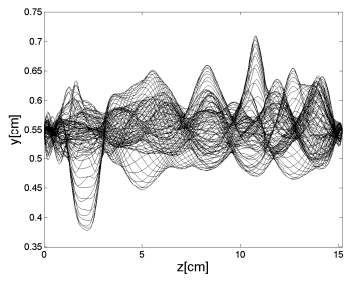
11.2Hz



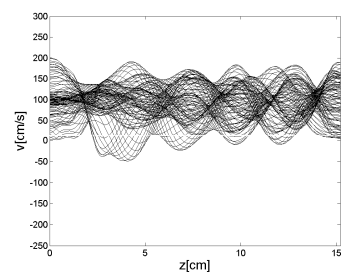
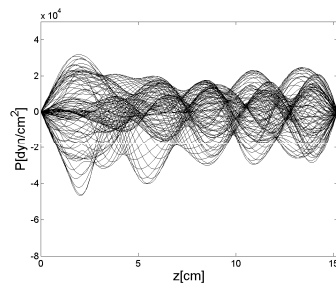
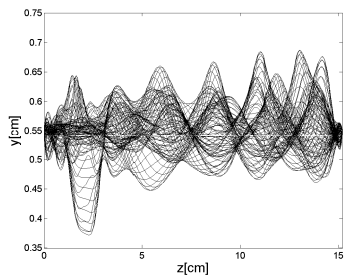
11.5Hz



11.7Hz



12Hz



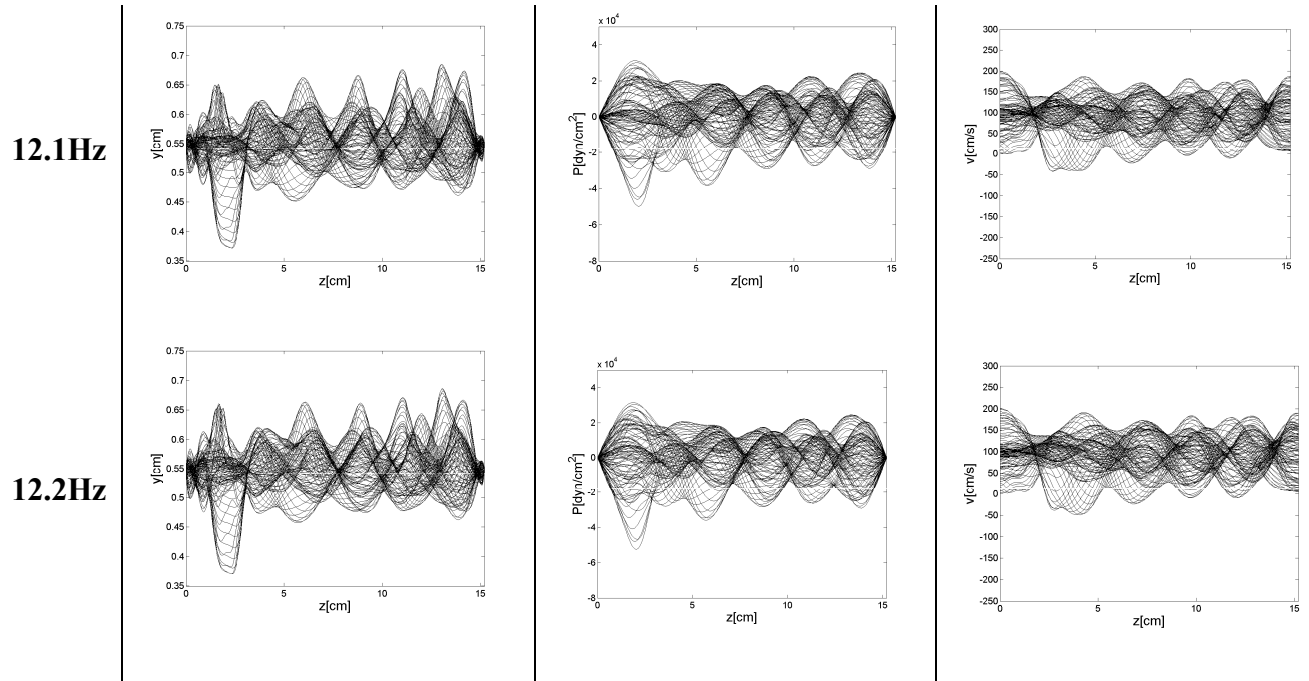


**Figure 14.** Wall displacement, axial pressure longitudinal distribution and axial velocity longitudinal distribution over a period of time once periodicity in the flow is achieved.

### 3.12 Mechanical work done by the elastic tube

An energy balance on the fluid domain inside the long portion of the elastic tube past the pincher allows us to compute the mechanical work of the elastic tube done on the fluid. Because the energy balance is made for the portion of the tube devoid of active compression (i.e. pincher), this calculation aims to focus on the energetic role of the elastic tube itself in pumping.

We use a fixed control volume (CV) delimited by the “input” and “output” cross sections, the axis of symmetry and the fluid-structure interface. The “input” cross section is located downstream next to the pinching zone at  $z=4.56$  cm, and the “output” upstream, just before the exit of the pump at  $z=13.68$  cm, away from the exit enough to avoid the

results to be biased by the “too-close” compression zone and the zero pressure boundary condition, respectively (figure 15).

In the absence of added heat, the conservation of energy principle applied to the system (fluid inside the control volume) states that the time rate of change of the system total energy ( $E$ ) is balanced by the time rate of change of the work done to the system ( $W$ ).<sup>60</sup>

$$\frac{DE}{Dt} = \frac{DW}{Dt} \quad (20)$$

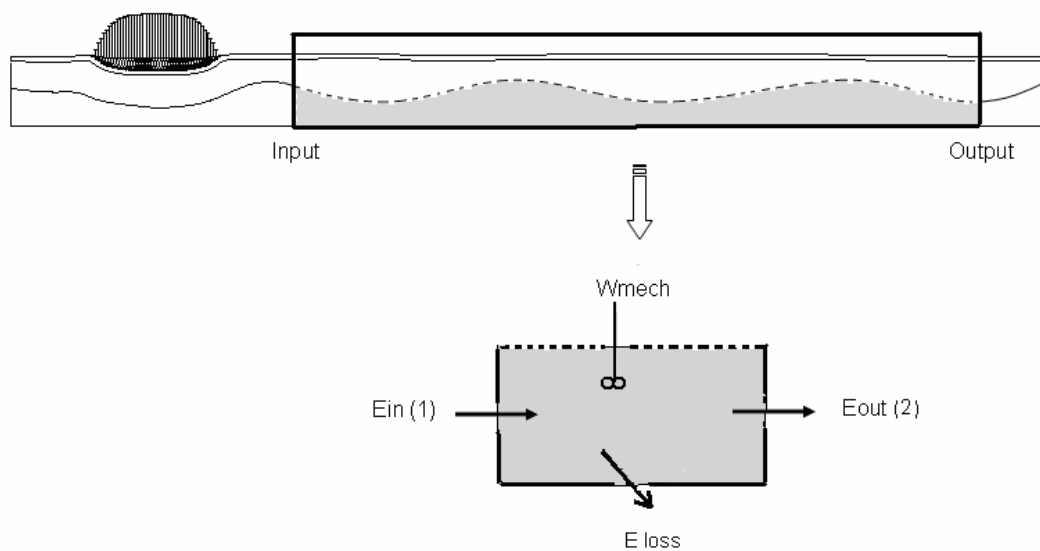


**Figure 15.** (Top) Input and Output cross sections defining the portion of the tube for which mechanical work is calculated. (Bottom) Control volume and fluid energy balance. A fixed control volume (solid line box) enclosing the wall (dashed line) is used in order to consider the wall motion as a shaft work. Pumping work defined as shaft work minus

the losses is balanced by the differential of energy between the output ( $E_{out}$ ) and input ( $E_{in}$ ) of the system.

In the absence of gravitational forces, the work done to the system, i.e. the work done to the fluid domain, is decomposed into the work done by the environment on the fluid (involving fluid pressure and viscous terms) and the mechanical power done on the fluid and due to wall motion or shaft work ( $W_{mech}$ ).

$$W = W_{mech} + W_{press} + W_{viscous} \quad (21)$$

On the other hand, the fluid's total energy per unit mass ( $e$ ) is decomposed to its internal and kinetic energies since gravitational forces are omitted.

$$e = e_{internal} + e_{kinetic} \quad (22)$$

Internal energy depends on temperature only, and is part of the fluid losses by internal friction ( $\dot{E}_{loss}$ ). Using Reynolds transport theorem, the material derivative of the fluid's total energy ( $E$ ) becomes:

$$\begin{aligned} \frac{DE}{Dt} &= \frac{d}{dt} \iiint \rho e dV + \iint \rho e \mathbf{v} \cdot \mathbf{n} dS \\ &= \frac{d}{dt} \iiint \rho \left( e_{internal} + \frac{\mathbf{v}^2}{2} \right) dV + \iint \rho \left( e_{internal} + \frac{\mathbf{v}^2}{2} \right) \mathbf{v} \cdot \mathbf{n} dS \\ &= \dot{E}_{loss} + \frac{d}{dt} \iiint \rho \frac{\mathbf{v}^2}{2} dV + \iint \rho \frac{\mathbf{v}^2}{2} \mathbf{v} \cdot \mathbf{n} dS, \end{aligned} \quad (23)$$

where  $dS$  is a surface differential element and  $dV$  a volume differential element of the CV.

The volume integral represents the kinetic power of the fluid inside the CV. Because of steady state periodic conditions, its contribution to the energy balance will be zero

after integration over a time period. The surface integral represents the flux of kinetic energy at the CV boundaries, and comprises the input and output cross sections only since no fluid crosses the top part of the CV and  $\mathbf{v} \cdot \mathbf{n} = 0$  on the bottom part of the CV (axis of symmetry).

On the other hand, the rate at which the environment does work on the fluid is decomposed into fluid pressure and viscous stress components. Integration along the surfaces of the CV is nonzero at the input and output cross sections only, and viscous stress or shear contribution on the two cross sections is small enough to be neglected. The pressure power becomes:

$$\dot{W}_{press} = \iint_{1 \cup 2} P \mathbf{v} \cdot \mathbf{n} dS . \quad (24)$$

Therefore the balance of rate of change of energy is as follow:

$$\dot{E}_{loss} + \iint_{1 \cup 2} \rho \frac{\mathbf{v}^2}{2} \mathbf{v} \cdot \mathbf{n} dS = \dot{W}_{mech} + \iint_{1 \cup 2} P \mathbf{v} \cdot \mathbf{n} dS , \quad (25)$$

$$\dot{W}_{mech} - \dot{E}_{loss} = \iint_{1 \cup 2} \left( \rho \frac{\mathbf{v}^2}{2} + P \right) \mathbf{v} \cdot \mathbf{n} dS = \dot{E}_{out} - \dot{E}_{in} . \quad (26)$$

We define the pumping power ( $\dot{W}_{pump}$ ) as the mechanical power done by the moving wall ( $\dot{W}_{mech}$ ) minus losses ( $\dot{E}_{loss}$ ):

$$\dot{W}_{pump} = \dot{W}_{mech} - \dot{E}_{loss} , \quad (27)$$

Finally the pumping work is found by integrating equation (26) over a period of time  $T$ :

$$W_{pump} = \int_t^{t+T} \left[ \iint_{1 \cup 2} \left( \rho \frac{\mathbf{v}^2}{2} + P \right) \mathbf{v} \cdot \mathbf{n} dS \right] dt . \quad (28)$$

We found a nonlinear relationship of the pumping work and the frequency of excitation (figure 16), reaching maximum around the resonant frequency. Significant positive work occurs for frequencies ranging from 10Hz to 10.5Hz, meaning that the elastic tube does work on the fluid. It is of particular interest since the considered portion of the tube actually does not contain active components (such as pincher). This implies that the elastic tube does not act as a resistor, but contribute to pumping by transmitting energy to the fluid. At resonance is the transfer of energy from the elastic tube to the flow maximized.

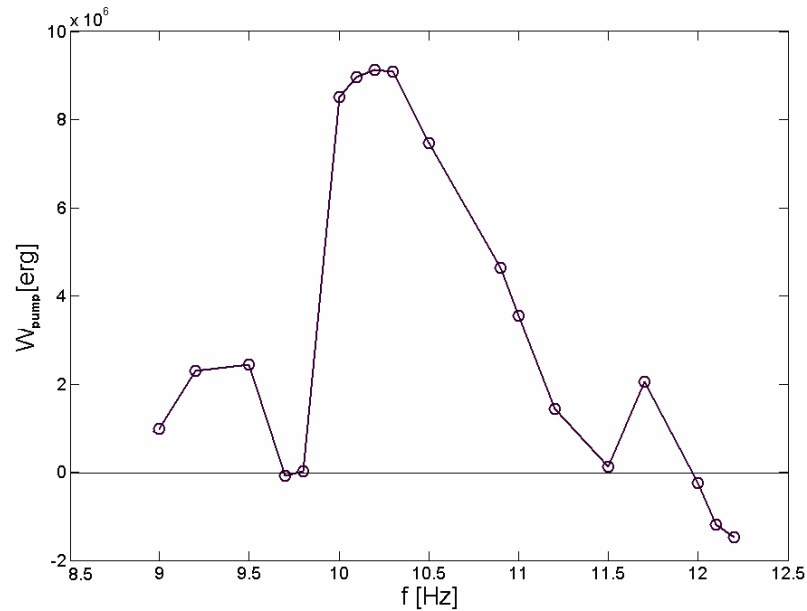


**Figure 16.** Pumping work of the elastic tube ( $W_{pump}$ , 1 Erg= $1e-7$  J) and frequency of excitation ( $f$ ).

### 3.13 Pumping efficiency

The efficiency ( $\varepsilon$ ) of a pump is the ratio of the useable work over the work dispensed to actuate the pump. In the case of the MIP, it corresponds to the work produced by the pump ( $W_{pump}$ ) over the work dispensed at the actuation zone ( $W_{actua}$ ):

$$\varepsilon = \frac{W_{pump}}{W_{actua}}. \quad (29)$$

The work done by the actuation zone is the result of the work done by each of the nodes that undergoes the prescribed compressive displacement. Nodal work is calculated using the nodal reaction force integrated over the nodal radial displacement (motions in the other directions are constrained). The model being axisymmetric, the work for the whole pinching section is recovered by multiplying by  $2\pi$ :

$$W_{actua} = 2\pi \sum_{pinching\ nodes} \int_t^{t+T} \left( \int R_y^{node} dy(t, z) \right) dt. \quad (30)$$

The work produced by the pump ( $W_{pump}$ ) represents the increase of energy of the fluid between the entrance and exit of the pump (31). It is composed of pressure and kinematic terms. Because we imposed a zero pressure boundary condition at the two extremities of the tube (entrance  $z=0$  and exit  $z=L$ ), the pressure term in equation (31) is null, which would lead to a wrong estimation of the work produced by the pump.

$$W_{pump} = \int_t^{t+T} \left[ \iint_{entrance \cup exit} \left( \rho \frac{\mathbf{v}^2}{2} + P \right) \mathbf{v} \cdot \mathbf{n} dS \right] dt \quad (31)$$

We propose to evaluate the pressure term using an equivalent model. The MIP can be seen as a tube producing a mean flow, and one can consider as an equivalent model a

similar Poiseuille tube driven by a pressure gradient (figure 17). The pressure at one extremity being zero, one can calculate, knowing the geometry and the mean flow, the pressure at the other extremity of the Poiseuille tube (32).<sup>61</sup>

$$P(z = 0) = \frac{8\mu L}{\pi R_f^4} \bar{Q} \quad (32)$$

The Poiseuille pressure represents the pressure that would be produced by the MIP for the same resulting mean flow  $\bar{Q}$ . Consequently, the work produced by the pump is evaluated by plugging the Poiseuille pressure (32) into equation (31).

The efficiency is computed for frequencies of excitation ranging from 9Hz to 12 Hz, where flow is exiting the pump in the positive direction (figure 18). We found that the efficiency ranges between 5% and 15%, except when excited at resonance, where the pump exhibits a clear peak at almost 35%. This confirms the role of resonance where the MIP reaches its maximum pumping efficiency.

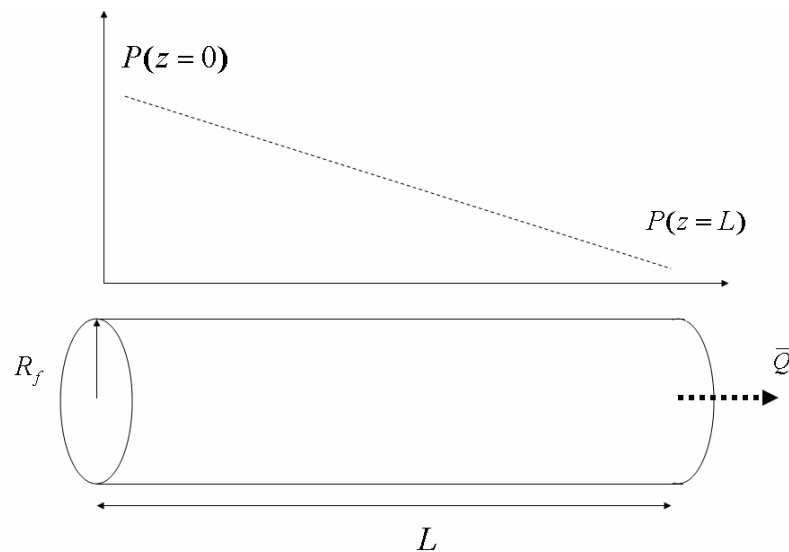


**Figure 17.** Equivalent model: Poiseuille flow driven by a pressure gradient.

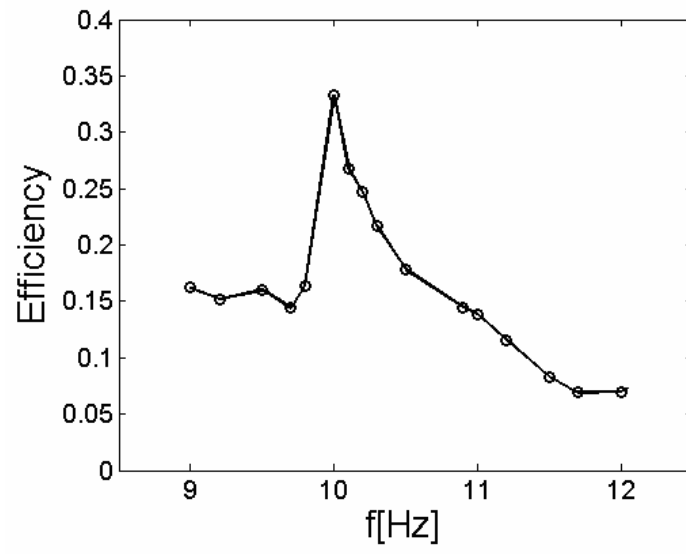


**Figure 18.** Efficiency ( $\varepsilon$ ) of the MIP and frequency of excitation ( $f$ ).

# Chapter 4

## Discussion

The multilayer impedance pump offers a new design for valveless pumping in confined environments where only small excitations are possible. The choice of materials for the pump model presented here is the optimized result of a previous series of combinations between elastic layers of different properties, with the scope to produce the desired wave amplification feature. The presented pump is an interesting resonant system, in which flow is not linear with frequency.

Several assumptions have been made. First, each layer constituting the elastic tube has been modeled as a linear elastic material. In the real case the stiffer layer may be rubber-like and the inner gelatin layer may be a viscoelastic material. This would introduce additional non-linearities and material dissipation. In appendix 3 a model of MIP using a viscoelastic gelatin is proposed. Second, the dynamics of each layer have been solved using the small displacement, small strain hypothesis. Although strains in the gelatin can reach 0.3, they are of transient nature and do not affect the linear hypothesis. The error in linearization found by performing the same simulation with the large strain assumption is less than 0.05% (see appendix 2). Third, the model has been solved assuming a laminar flow. For the fluid-filled elastic tube problem, one may want to characterize the flow as unsteady laminar or unsteady *smooth* flow. The Reynolds number calculated using the mean flow can be as high as 9,959, which for a steady flow in a pipe is past transitional. In pulsatile flow, however, the onset of turbulence occurs

only momentarily within the oscillatory cycle, when flow and velocity reach their peaks.<sup>61</sup> Therefore, the zones of turbulence may not influence the overall function of the pump. Modeling turbulence for the transient deceleration phases in the pulsatile cycles would not bring more to the understanding of the function of the MIP, which is used as a proof of concept on multilayer pumping where.

The MIP is a complex system and presents several natural frequencies. One could make an analogy between the present system (two solids coupled with a fluid), and a system of several coupled pendula, each of them having a different length. Upon excitation, each pendulum will oscillate in a manner that will exhibit a dominant frequency as well as frequencies induced by the interactions with the neighboring pendula. The system as a whole will not necessarily lock into a single resonant frequency, but will have several resonant or dominant frequencies. These dominant frequencies will be expressed at different strengths depending on the pendulum (or observable) under consideration. In a similar manner, the MIP spectrum reveals several natural frequencies. For the observable considered (flow rate at the exit) the dominant frequency is  $f=33$  Hz. We studied the pump response around the first natural frequency of the system ( $f_n=11$  Hz). We excited the pump behavior around this natural frequency, as opposed to the higher natural frequencies ( $f=41$  Hz,  $f=49$  Hz and  $f=60$  Hz) because the PSD's dominant frequency  $f_d=33$  Hz was its harmonic. The choice to study the pump at the natural frequency as opposed to the dominant frequency has been motivated by the fact that single layer impedance pumps were exhibiting the strongest response at the first harmonic of the dominant frequency of the PSD.<sup>5,27,42</sup> In addition, in the gelatin-coated pump, there is a trade-off between pinching amplitude and excitation frequency that

limits the range of frequency a specific pump model can be excited at. Due to the gelatin softness, responses to higher harmonics ( $f=22$  Hz,  $f=33$  Hz,  $f=44$  Hz,  $f=55$  Hz) or to higher natural frequencies ( $f=41$  Hz,  $f=49$  Hz and  $f=60$  Hz) are possible but would require smaller pinching amplitudes (see appendix 3). Finally, a frequency shift of about 8% is observed between the resonant frequency ( $f_{res}=10.1$  Hz) and the natural frequency ( $f_n=11$  Hz). When periodically excited, the successive pinches enhance wall motion and corrupt wave propagation. This may produce a shift between the resonant of the system deduced from the system response to periodic excitation and the natural frequency calculated from the impulse response spectral analysis.

We periodically excited the pump, and showed that the pump can produce bi-directional flow depending on the excitation frequency. The ability to reverse flow direction by adjusting the frequency of excitations has been reported by several open and closed loop experimental setups.<sup>13,28,29,51,52</sup> Positive flow, i.e. flow exiting the pump from the extremity the farthest to the compression zone, is achieved for frequencies close to the resonant frequency ( $f=[9$  Hz,  $12$  Hz]) and reaches maximum at resonance ( $f_{res}=10.1$  Hz). Negative flow is observed at frequencies below the resonant frequency ( $f=[8$  Hz,  $9$  Hz]). We then focused on the pump response around the resonant frequency, when net mean flow is positive. For that range of frequencies, the pump exhibits the largest inner wall motion. The relatively large waves at the fluid interface never occlude the fluid domain. The minimum fluid radius observed throughout the computations is  $R_f=0.37$  cm. The great gelatin stretch at resonance is to be correlated to the highest mean exit positive flow. The wave interaction mechanism leading to pumping is similar

to the one of a classic IP.<sup>5</sup> At resonance their constructive interaction creates a suction zone toward the end of the pump that eventually expels the fluid in a jet like manner.

By considering the mechanical work done on the fluid by the long portion of the elastic tube past the pincher, we are able to show that the elastic tube itself acts as a pump and not as a passive resistor. For frequencies around the resonant frequency, the mechanical work is positive (tube does work on the fluid) although no active component such as a pincher is present in that portion of the tube. Upon actuation, the energy used to compress the fluid-filled elastic tube is transmitted into the elastic tube to deform it and into the fluid to move the fluid particles. The elastic tube and the fluid are exchanging energy along the tube, and at a given point along the tube (characterized by Avrahami and Gharib<sup>5</sup> as the velocity node), the elastic energy is given back to the fluid and contributes to the pumping. In addition, the mechanical work is clearly maximal at resonance, highlighting the concept of resonant pumping, where most efficient energy transmission between the passive elastic tube and the fluid is achieved. The mechanical work for frequencies 9.7 Hz, 9.8 Hz, 11.5 Hz is found close to zero although mean flow is non zero. This apparent contradiction is explained by the way the pumping work is defined. Because the pumping work is expressed as the pressure and kinetic energy difference between the input and output of the CV, a zero pumping work means that no energy *increase* is observed between the input and the output of the CV.

We evaluated the efficiency of the pump using a Poiseuille model in order to account for the pressure at the boundaries. This method in a comparative tool and is not intended to give the exact efficiency of the pump for each excitation frequencies. The efficiency is

found to depend non linearly on the frequency of excitation, reaching maximum at resonance, highlighting the concept of resonant pumping.

The MIP can be used for different pumping applications. By tuning material properties of the elastic layers, one can pump fluids of different viscosities. The MIP has interesting features that are especially suitable for many biomedical applications. It has a simple and compact design, and has no component such as blades or valves that could obstruct the flow. The multilayer structure limits all large wave motion to the fluid-gelatin interface with almost no external wall motion. Significant pumping (up to 5.16 L/min) is achieved for small excitation (10% external radius) and the pump offers the possibility of bidirectional pumping, or switch, depending on the excitation frequency. Biomedical applications at the macroscale include circulatory assist devices, and include polymer pumping for drug delivery at the micro- and nanoscale.

## Chapter 5

# Impedance Pumping in the Embryonic Heart

The heart is the first functioning organ in the embryo. At very early stages of development the embryonic heart is a straight valveless tube for which pumping mechanism is still under debate. Fano and Badano<sup>21</sup> who, in 1890 were first to observe the embryonic heart contractile wave, characterized this primitive heart beating as peristaltic. Since their first observations, peristalsis has remained the accepted pumping mechanism. Recent investigations on impedance pumping<sup>5,27</sup> as well as *in vitro* visualizations of zebrafish embryonic beating heart<sup>25</sup> have invalidated this hypothesis and brought evidences that the embryonic heart may function as an impedance pump instead (section 1.1.2).

Using numerical simulations the two possible embryonic heart pumping mechanisms will be investigated. The exact same multilayered wall similar to the embryonic heart tube will be excited in two different manners to model peristalsis and impedance pumping in the embryonic heart. The multilayer tube is made out of an external stiffer layer similar to the myocardium layer and a soft internal layer similar to the cardiac jelly, and is the most physiological representative embryonic heart model to date. The multilayer tube is to be excited on its outer surface, the only layer in the embryonic heart

containing contractile elements. The peristalsis model consists on the multilayer tube undergoing a sinusoidal wave of contraction along its length, whereas the impedance model uses a single excitation location such as introduced in section 2.2. Both models are excited at  $f=2\text{Hz}$ , the embryonic heart frequency, for an amplitude of 20% compatible with the myocardium shortening and both models pump a viscous fluid similar to blood.

For these conditions, results show that the peristaltic embryonic heart model produces a higher flow than the impedance one, but fails in building pressure, which is essential for the developing embryo. In addition, the peristaltic model requires more energy to actuate than impedance one. This expenditure is not compensated by the flow and pressure produced by the pump, resulting in an efficiency 5 times lower than the impedance one.

As a conclusion, compared to the embryonic heart peristaltic pump model, the impedance pump model seems to be best suited to provide in blood the developing embryo, while at the same time requiring minimum energy consumption.

## **5.1 The different embryonic heart pumping models**

A peristaltic model for embryonic heart (PerisEHM) and an impedance embryonic heart (ImpEHM) were developed using the same multilayer tube introduced in section 2.2. They only differ by their mode of excitation (peristaltic wave vs. a unique excitation location). The same material properties for the stiff and the gelatin-like layer as well as the same boundary conditions (zero pressure at the exits and around the pump, no slip boundary condition at the fluid-structure interface, fixed ends at the tube's edges) to the one introduced in section 2.2 were applied. Both pumps featured the following specifics to mimic very closely the observed *in vitro* zebrafish heart dynamics<sup>25</sup>:

- the multilayer tube was filled by a viscous fluid similar to blood ( $\mu_f = 0.035 \text{ g/cm s}$ ,  $\rho_f = 1 \text{ g/cm}^3$ );
- the amplitude of excitation was 20% of the external radius, similar to the shortening resulting from the cardiac myocytes contractions;
- the frequency of excitation was fixed to 2 Hz, similar to the one observed in the tubular heart.

### 5.1.1 *The peristaltic excitation*

The peristaltic excitation consisted in a wave of constant wavelength and constant amplitude traveling along the tube length (figure 19). The wave was imposed at the outer surface of the multilayer tube, on the layer that represents the myocytes, the contractile elements of the heart tube. Because the extremities of the tube were fixed, the peristaltic wave was assumed to start and end at 1 cm away from the edges of the pump. This way, unrealistic large stresses are avoided at the tube's extremities without impairing the physics of the peristaltic pumping. The peristaltic motion was practically modeled by prescribing sinusoidal radial displacements  $\eta(t, z)$  on nodes belonging on the external surface of the external layer the tube (33). The amplitude of peristaltic excitation was set to 20% of the external radius ( $A=0.206 \text{ cm}$ ). The frequency of the peristaltic wave was  $f=2 \text{ Hz}$  and the wavelength  $\lambda$  equaled the tube length  $L$ , so that the peristaltic wave was similar to the one observed *in vitro*<sup>24</sup> (figure 20).

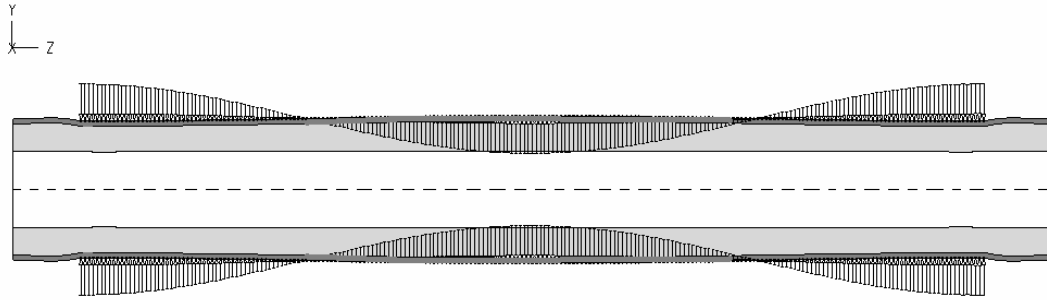


**Figure 19.** Model peristaltic embryonic heart pump. 2D longitudinal cross-sectional view of the multilayered tube with an imposed peristaltic displacement wave.

$$\eta(t, z) = A \cos \left[ \frac{2\pi}{\lambda} (z - ct) \right], \quad c = \lambda f \quad (33)$$

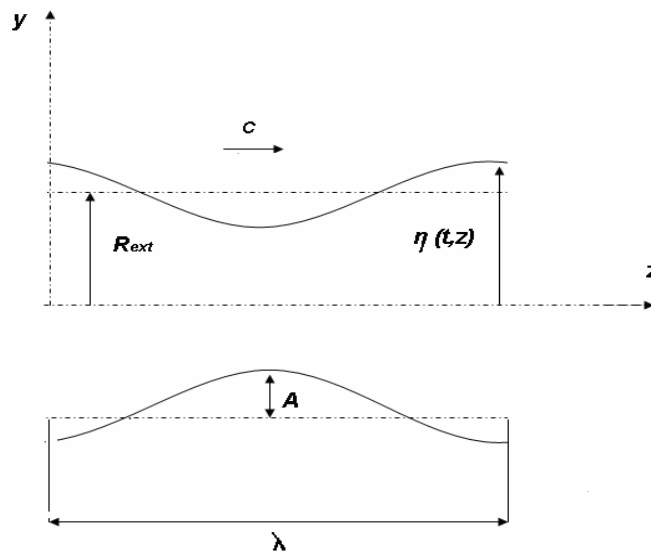


**Figure 20.** Schematic and conventions of the imposed peristaltic wave motion.  $c$  is the wave velocity.

### **5.1.2     *The impedance excitation***

The excitation of the ImpEHM was the exact same as the one described in introduced in section 2.1 (same pincher location, pincher width, pincher spatial distribution, and same duty cycle of 20%). Like in the peristaltic model, the frequency of excitation was fixed to  $f=2$  Hz, and the amplitude of the compressive displacement was fixed to 20% of the tube's external radius.

## **5.2       Flow, pressure, and energy expenditure in the two models of embryonic heart pumping**

### **5.2.1     *Flow and pressure in the peristaltic pump model***

Flow in the PerisEHM follows closely the imposed motion of the external walls. Although displacements are not directly imposed to the gelatinous layer, but to the external layer, the fluid-gelatin interface moves according to the imposed peristaltic wave, and no other wave motion is to be observed. The gelatin behaves as a passive layer transducing the peristaltic motion to the fluid domain. Its elasticity and soft constitution seems to not play a role in pumping. Exit flow is pulsatile and of the same frequency than the frequency of excitation, which is also the frequency of the traveling wave. Because the excitation amplitude is small and because the gelatin does not stretch significantly upon the passing of the contractile wave, the tube is never occluded. As expected from a partially occluded peristaltic pump<sup>31</sup> very little pressure is built up (figure 21). In addition, because the radius is never fully occluded, backflow is important. This type of peristaltic pumps which does not work by positive displacement; it relies on the viscosity

of the fluid to entrain flow. The viscous forces alone can not ensure the pressure build up. The lack of pressure inside the pump combined with the large work expended to actuate the pump results in a poor efficiency of the peristaltic pump model (see table 3).

### **5.2.2 *Flow and pressure in the impedance pump model***

The ImpEHM behaves accordingly to the MIP flow and structure described in Chapter 3. After a phase of flow build up of about 10 cycles, the flow reaches a steady state of periodic oscillations. A large number of elastic waves are traveling and reflecting during the 80% of the period when the elastic tube is not compressed. These waves are responsible for the oscillatory exit flow and pressure waveforms (figure 22). Due to a constructive wave interaction, a suction-inertial expulsion mechanism characteristic of an impedance pump and such as described in section 3.9 drives the flow in a preferential direction. Because impedance pumps are kinematic pumps, they produce flow and pressure. A single excitation location is needed to actuate the impedance pump model, providing a small energy input for consequent output flow energy (see table 3).

### **5.2.3 *Energy expenditure***

The two pumping mechanisms, peristalsis and impedance, are actuated using prescribed displacement and the actuation work is calculated by integrating the nodal reaction forces over the nodal displacement and for a period of time (30). Because a zero pressure boundary condition is used at the pump extremities, the equivalent Poiseuille flow model introduced in section 3.13 is used to calculate the pumping work by using the equivalent Poiseuille pressure (32). The efficiency of each pump is defined as the ratio of pumping work over actuation work (29).

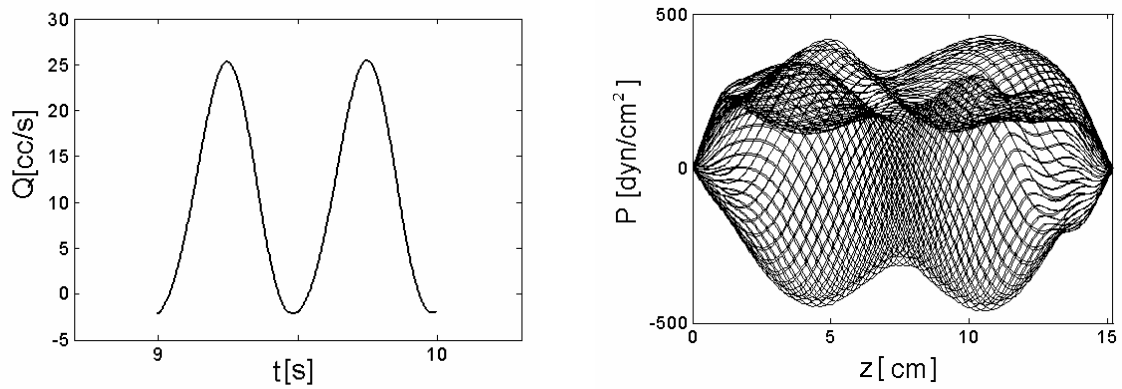


**Figure 21.** Flow and pressure in the PerisEHM. (Left) Exit flow rate and time. 2 cycles at periodic state are plotted. Mean exit flow is 11.87  $\text{cc/s}$ . (Right) Axial pressure longitudinal distribution over 1 period. Each curve is the instantaneous axial pressure distribution in the tube.

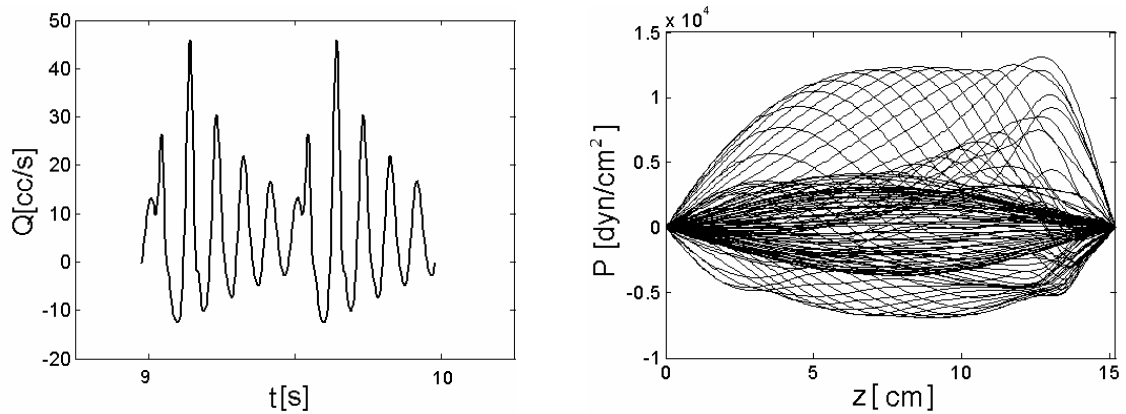


**Figure 22.** Flow and pressure in the ImpEHM. (Left) Exit flow rate and time. 2 cycles at periodic state are plotted. Mean exit flow is 6.20  $\text{cc/s}$ . (Right) Axial pressure longitudinal distribution over 1 period. Each curve is the instantaneous axial pressure distribution in the tube.

Table 3 provides a list of the flow and energy characteristics of each pump model. Flow characteristics are the mean exit flow and the range of pressure observed inside each pump (figure 21 and 22). The peak to peak pressure is a quantitative tool for estimating the pressure that would be present at each pump's exit if the zero pressure boundary condition was not present.

**Table 3.** Comparison of the flow, pressure range, pumping work, actuation work, and efficiency between the multilayer impedance and the peristaltic heart pump models

	PerisEHM	ImpEHM
Exit flow	11.87 cc/s	6.20 cc/s
Axial Pressure Peaks	+/- 4 e+2 dyn/cm <sup>2</sup>	-0.6 e+4 dyn/cm <sup>2</sup> +1.25 e+4 dyn/cm <sup>2</sup>
Pumping Work	3792 erg	1650 erg
Actuation Work	7.09 e+4 erg	6.17 e+3 erg
Efficiency	0.0535	0.2673

### 5.3 Discussion

We compared two gelatin-coated elastic tubes based on the embryonic heart structure, and excited it in two different manners as models of embryonic heart pumping. The first model, PerisEHM, featured a peristaltic wave traveling along the tube, while the second, ImpEHM, used a single periodic excitation location and pumping relied on elasticity and wave interaction.

Flow and dynamic behavior are compared. The flow in the impedance model is about 1.5 times lower than in the peristaltic model but the impedance model produces a pressure that is of an order of magnitude 25 times higher. The fact that the flow is higher in the PerisEHM is a not a direct consequence of the mode of pumping -peristalsis versus impedance-. Indeed, the ImpEHM flow performances are nonlinearly dependant on the frequency of excitation (see section 3.6), and 2 Hz may not be a natural or harmonic of the natural frequency of the impedance pump. The spectral analysis of the impulse response exit flow history of the ImpEHM was found to be very similar to the one presented in section 3.4, where 33 Hz was a dominant frequency. Therefore for the considered ImpEHM, a slightly different choice of materials properties so that 2 Hz is a natural or an harmonic of the natural frequency of the system, would lead to higher exit flows.

Pressure however, is not the result of the choice of materials, but is intrinsic to the mode of pumping. Because the walls are only partially closed, the P\_EH behaves as a viscous pump. It relies on the viscosity of the fluid to drive flow, and only small pressure is being produced. The lack of pressure produced by the peristaltic pump model has strong physiological consequences. As the embryo develops, the systemic resistance increases and the heart needs to produce enough pressure to overcome this resistance in order to irrigate all parts of the body. A pump that produces flow and only small pressure such as the peristaltic embryonic pump model becomes less efficient in delivering flow as resistance increases. The impedance pump however, whose mechanism is based on suction is capable of building pressure to accompany blood flow.

The comparison between the two pump models revealed the energetic advantage of pumping by impedance. The peristaltic pump model is 5 times less efficient than its impedant counterpart. In the PerisEHM every section along the length of the tube is undergoing at every instant an imposed displacement. In the ImpEHM however, a single location is used and active compression occurs for only 20% of the period time.

Finally, comparison of the two pump models is done for 2 periods when the ImpEHM has reached a steady state in flow. For this time frame, because of the long viscous diffusion time, the PerisEHM may not have reached its steady state. Using the impulsively actuated wavy wall model as an approximation of the wavy gelatin-fluid interface (2nd Stokes problem) one can estimate the time for the motion of the peristaltic walls to diffuse and influence the whole flow (see appendix 4). Based on the criterion that fully developed flow is reached when the axial velocity reaches 99% of the wall velocity, one finds a diffusion time of about 74 hours. This results implies that fully developed flow and peak performances in the embryonic heart excited by a peristaltic wave may not physically occur, due to the time scale difference between the viscous diffusion (74h) and morphogenesis (the heart tube shape changes every hour).

The high viscous diffusion time and the low pressure produced by a peristaltic pump are strong evolutionary incentives, and suggest that the embryonic heart may use impedance as an energetically optimized pumping model compatible with the physiological changes of the shaping heart. Through the comparison of peristaltic and impedance pumping in a multilayer tube similar to the tubular heart, we bring an additional piece of evidence that the embryonic heart may function as an impedance pump and rather than a peristaltic pump as previously accepted.

## Chapter 6

# Dynamic Role of the Cardiac Jelly

Before looping, when the embryonic heart is still a straight tube, the cardiac jelly occupies the bulk of the heart tube walls. Despite its preeminence in the tube composition, there is still no understanding on its role, if any, in pumping.

Using the latest findings in impedance pumping in the heart<sup>25</sup>, a multilayer impedance pump (MIP) which design has been inspired from the embryonic heart structure features a gelatin layer similar to the cardiac jelly has been developed. The gelatin layer in the MIP amplifies elastic waves and requires only small amplitude of excitation. However the presence of this layer reduces the fluid domain by almost 50%. Is the addition of the gelatin layer in an impedance pump (IP) a benefit to the pumping performances? By extension, would the embryonic heart with the added thick gelatinous cardiac jelly layer be an optimized valveless IP?

To explore the role of the cardiac jelly role, two models of IP with and without an added thick gelatinous layer will be compared. Finite elements based simulations are carried out for the two IP models and exit flow rates are compared. The Multilayer gelatin-coated impedance pump produces a higher flow and has a higher efficiency compared to a Single Layer IP (SLIP). The results agree with a second model of MIP with a thicker and stiffer gelatin layer. Conclusions are drawn on nature's optimal pump design of the embryonic heart.

## 6.1 Properties of the cardiac jelly

Cardiac jelly is a gelatinous acellular material lying between the endothelial lining and the myocardial layer of the heart at early stages of heart development when the heart is in tubular shape. It has been first characterized by Davis<sup>18</sup> in 1924 who gave it its name of *cardiac jelly*.

Cardiac jelly is a relatively homogenous network of collagen fibrils and fine filaments. The structural part of the jelly is ensured by the elastin and collagen scaffold, whereas its gel like appearance is controlled by glycosaminoglycan, a protein involved in the degree of hydration of the jelly. The cardiac jelly is populated by several types of proteins that participate in paracrine cell-cell communication, and proteins that promote cell migration and tissular remodelling.<sup>14,17,57</sup>

Little is known on the different roles of the cardiac jelly. As an extracellular matrix, it serves as a substratum for the diffusion of growth factors derived from the myocardium to the endocardium.<sup>17,24</sup> During the heart development, the cardiac jelly plays a central role in heart valve development and septation of the heart.<sup>57</sup>

The cardiac jelly may have a mechanical role in the formation of the heart tube and later in pumping. Davis<sup>18</sup> was first to emphasize its significance in giving mechanical cohesion to the two layers of the heart. During the fusion of the endocardial tubes that form the tubular heart, the cardiac jelly may increase the adhesiveness between the two tubules by a physical effect.<sup>18,30</sup> Barry<sup>9</sup> in 1948 used a simple geometrical reasoning to justify the presence of the cardiac jelly for pumping before valve formation. He assumed a peristaltic beat along the length of the tube similar to the one of figure 1. For such a thin-walled tube, using a tube of large radius will result in a large stroke. However, if one

considers a myocardial shortening of 20% upon contraction, this thin-walled tube will not be closed upon contraction, and the peristaltic motion will result in barely any flow. Barry showed that this dilemma can be solved by using a thick-walled tube made out of an incompressible material that would transmit the force of contraction (figure 23). In addition, he calculated that in order to achieve full closure of the heart tube, this layer should have a thickness equivalent to 45% of the external radius of the tube at rest.

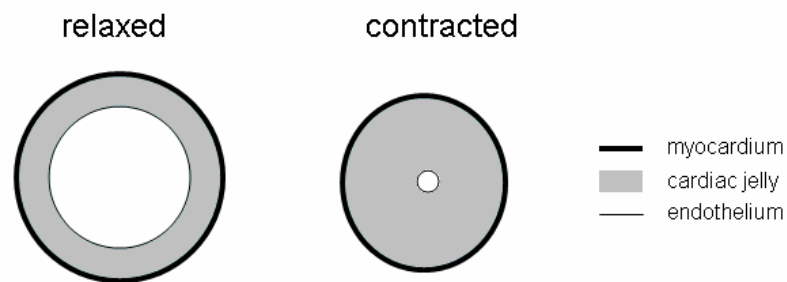


**Figure 23.** Simplified model of embryonic heart tube. Cross sections in relaxed and contracted states. A slight reduction of the external diameter leads to full closure of the tube thanks to the thick incompressible internal layer.

These results rely on the hypothesis that a peristaltic wave motion drives blood through the heart. However, the recent imaging techniques have helped to show that the embryonic heart may act as an IP instead.<sup>25</sup> In an IP, wave propagation and reflection are at the core of the pumping mechanism, and the gelatin is an especially adequate material for elastic wave propagation. The thickness of the gelatin layer ensures the amplifying of the elastic waves, while its softness ensures minimal damping and stronger wave interactions.

We propose to investigate on the gelatin as a requisite for optimal pumping in an IP. Because of its unique gel like constitution, we will focus on the elastic properties of the cardiac jelly in pumping and their contribution to achieve significant flow.

## **6.2 Numerical simulations**

### **6.2.1 Models**

We compared two IPs using finite elements numerical simulations. The first pump model was the MIP as introduced in chapter 2 (see table 2 for geometry and material properties). The second pump model was the classic SLIP model, being a simple fluid-filled elastic tube. The SLIP was the exact MIP geometry with the gelatin-like layer removed (figure 24). The two models were excited at the same frequency ( $f=10$  Hz). The same boundary conditions as defined in chapter 2 were applied to each pump. To ensure numerical validity, the classic IP has been modeled with as many elements (9,250 fluid elements and 1,250 solid elements) as the MIP for which validation tests have been conducted (section 3.1). The same 1,000 time steps per pinching cycle were used to march throughout the transient simulations, and simulations are carried on until periodicity in the exit flow is achieved.

### **6.2.2 Exit flow rate variation in time**

In the single layer and in the multilayer pump models, the exit flow (16) history plots shows a transient phase where the flow is building up before reaching a steady state of periodic oscillations and constant mean value (figure 25). When averaged over a period

of time, the gelatin-coated pump produces a net forward flow of 84.28cc/s whereas the classic pump produces only 7.77 cc/s.

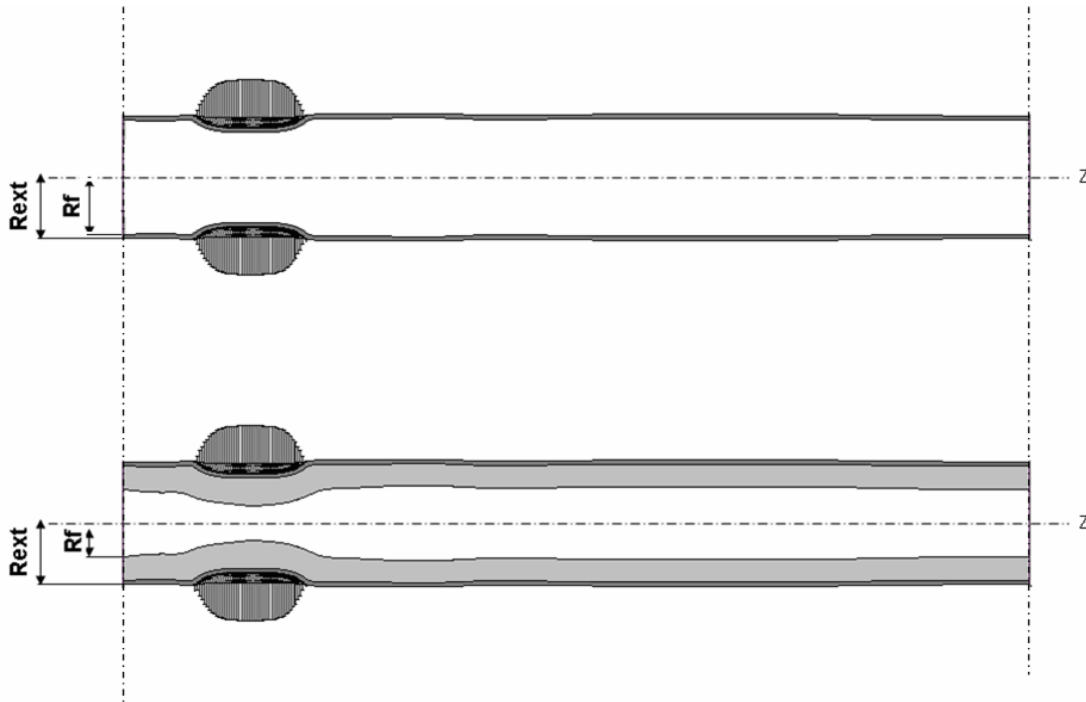


**Figure 24.** Comparative 2D axisymmetric longitudinal views. (Top) Single layer IP.  
(Bottom) Gelatin-coated multilayer IP.

### 6.2.3 *Compared performances*

Using the equivalent Poiseuille model introduced in section 3.13 we compute and compare the performances of the two pumps. Due to the thickness of its walls, the work to actuate the MIP is about 3 times greater than the work dispensed to actuate the SLIP. However, for the small excitation imposed, the SLIP is not capable of producing neither bulk flow nor pressure. As a consequence, its efficiency is practically zero. Using a gelatin layer in an IP configuration promotes the elastic wave interactions, and results in

higher pressure and flow. By the addition of the layer the efficiency jumps from 0% to 35%.

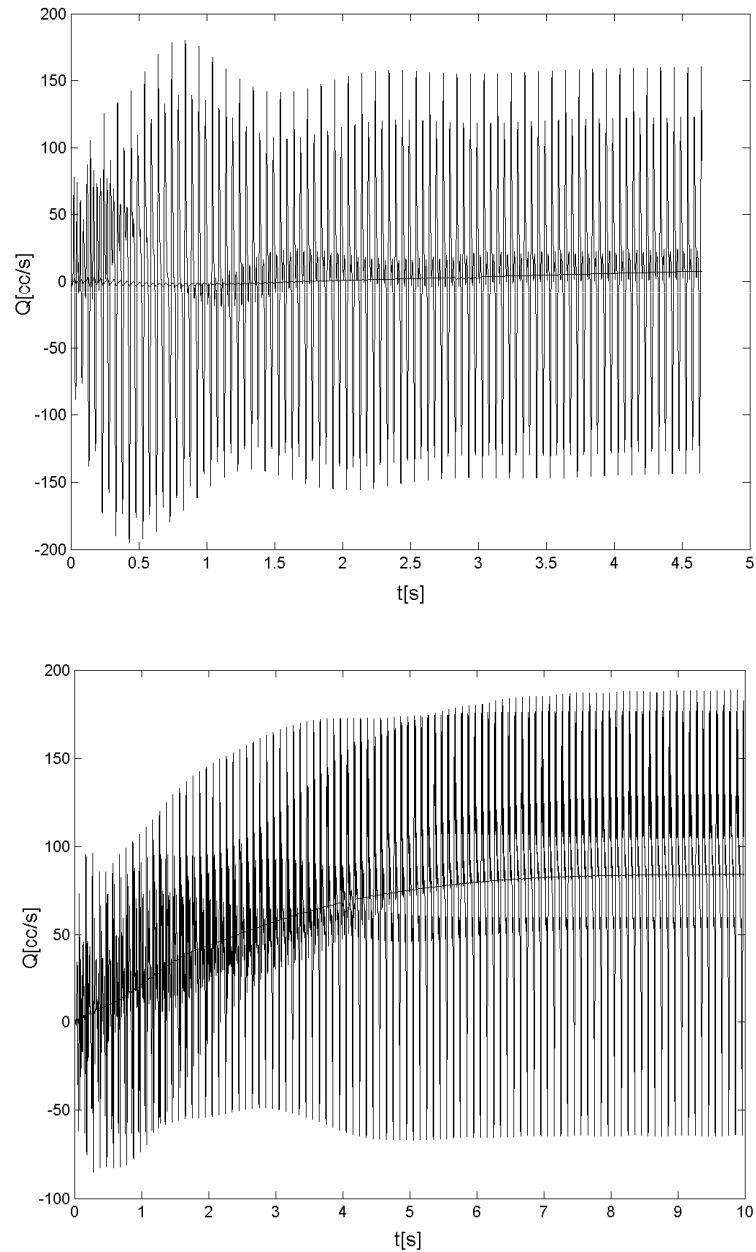


**Figure 25.** (Top) Exit flow rate history plot for the SLIP. (Bottom) Exit flow rate history plot for the gelatin-coated MIP. Excitation frequency is  $f=10$  Hz. The solid line is a filtered curve of the flow rate using a moving average window of one cycle. Mean flow in the SLIP is 7.77 cc/s. Mean flow in the gelatin-coated MIP is 84.28 cc/s.

**Table 4.** Comparison of the flow, typical pressure inside the pump, pumping work, actuation work, and efficiency between the SLIP and MIP for the same excitation conditions.

	Single Layer IP	Multilayer IP
Exit flow	7.77 cc/s	84.28 cc/s
Axial Pressure Peaks	-3 e+4 dyn/cm <sup>2</sup>	-0.6 e+4 dyn/cm <sup>2</sup>
	+2 e+4 dyn/cm <sup>2</sup>	+3 e+4 dyn/cm <sup>2</sup>
Pumping Work	25.25 erg	3.82 e+3 erg
Actuation Work	1.07e+4 erg	2.9 e+4 erg
Efficiency	0.0024	0.35

#### 6.2.4 Validation with a second MIP model

We carried on a second comparison test with a different gelatin-like layer. A slightly modified MIP that featured a stiffer ( $E_{gel} = 5 \text{ e}+5 \text{ dyn/cm}^2$ ) and thicker ( $h_{gel} = 0.7 \text{ cm}$ ) gelatin layer was compared to the SL\_IP, the latest being the same as the one introduced in section 6.2.1. The modified MIP and the SL\_IP were actuated at 10 Hz.

We find again a clear increase in the exit flow rate in this second version of gelatin-coated pump (figure 26). The mean exit flow in the gelatin pump reaches -61.31 cc/s. The negative sign means that bulk flow is directed toward the pinching zone.

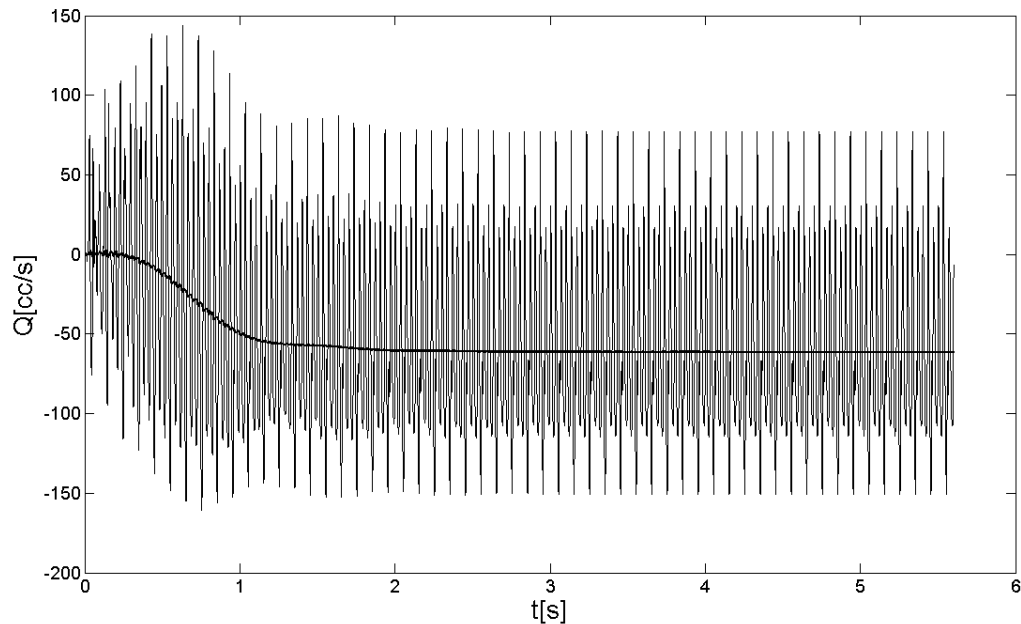


**Figure 26.** Exit flow rate history plot for the second test case of MIP with a modified gelatin layer. Excitation frequency is  $f=10$  Hz. The solid line is a filtered curve of the flow rate using a moving average window of one cycle. Mean flow reaches  $-61.31$  cc/s.

### 6.3 Nature's design: Importance of the cardiac jelly

We compared two models of IPs as models of embryonic heart pumping in the scope to understand the role of the cardiac jelly in the pumping performances. The first model is a classic SLIP. The second model is the exact same pump enliven by an internal gelatin-like layer, the MIP. This pump is a macroscopic model of the embryonic heart in which the gelatin layer represents the cardiac jelly. We excited the MIP and its single layer counterpart at a specific frequency ( $f=10$  Hz). The pump that features the gelatin layer had an exit flow rate of more than 10 times higher than the exact same pump without the gelatin. It is all the more remarkable that adding the gelatin layer reduces the fluid

volume by 42.1%. We tested a second model of MIP that featured a thicker and stiffer gelatin layer. Again, the exit flow of the gelatin-coated pump was much greater than the classic impedance pump (about 8 times). Therefore, for a classic impedance pump excited at a specific frequency, it is possible to design an associated gelatin pump that would enhance flow performance by the solely adjustment of the gelatin thickness and material properties. By extension, the cardiac jelly presence in the embryonic heart may be considered as an optimal designed layer. Its gel like mechanical properties makes it a wave amplifier and pumping enhancer. Because the gelatin allows better wave propagation, only small amplitude of muscle contraction is needed at the excitation location, which is in agreement with the small contractile capacity of the cardiac myocytes.<sup>9</sup> In conclusion, the gelatin, by its thickness and intrinsic properties, may have a role in pumping in the embryonic heart before valve formation.

# Chapter 7

## Potential Cardiovascular Applications

### 7.1 Medical applications of the MIP

The valveless MIP is a simple design that offers a promising new technique for producing or amplifying a net flow for both macro- and micro scale devices without the requirements for valves or impeller. It may prove to be beneficial as an implanted device in the cardiovascular system to support or enhance the blood flow in specific vessels. Its simple design ensures a durable and reliable performance, as well as resistance to clogging due to the pulsatile nature of the flow and the lack of valves or blades. The pump performances may be controlled using modulations in frequency, pinching amplitude or pinching duty cycle.

We propose two direct applications. First, the MIP such as presented in chapter 2 could be directly used as an intra-aortic pump. It could serve as a bridge to heart transplant for patients suffering from congenital heart disease. Second, a MIP can be created by adding an actuator to a graft already coated with gelatin. This second application would have a great pediatric use for children suffering of an underdeveloped left ventricle.

### **7.1.1 Intra-aortic pump**

Congestive Heart Failure (CHF) occurs when the heart is unable to pump blood effectively throughout the body. It accounts for 6% of the cardiovascular diseases, affects about 250,000 Americans each year, for who the mortality under medical therapy reaches 50%<sup>2</sup>. In the most severe cases, when drug treatment is not sufficient, surgical therapy may include cardiac transplantation or implantation of artificial ventricular assist devices. Over the past 10 years, advances in drug treatment have helped CHF patients in all stages of systolic dysfunction.<sup>12</sup> Nevertheless, for a certain number, heart replacement is the only possible therapy.<sup>45</sup> This procedure is restricted by the limited number of donors, and registries show ever-longer wait lists. For these patients waiting up to 2 years for the surgery, there is a strong demand in a long-term minimally invasive circulatory support.

Mechanical assist devices can work by direct systolic augmentation of the heart, by mechanical pumping to divert blood from the left ventricle directly into the aorta with sufficient force to maintain normal arterial pressure, or by diastolic augmentation. In the later case, intra-aortic balloon pumps are the most commonly used but they require permanent hospitalization and can be left in place up to a few weeks only<sup>1,10,19,46,57</sup>. In addition, complication rates range from 12% to 30 %<sup>16</sup>, and include limb ischemia, severe bleeding, balloon leak or failure. For long-term therapy, circulation need be assisted using mechanical assist devices such as left ventricular assist devices, bi-ventricular Pacers or total artificial heart. Left ventricular assist devices and total artificial hearts are electrically or pneumatically powered pumps that can produce continuous (Jarvik, DeBeckey) or pulsatile flow (Heart Mate, Novacor, Abiocr).<sup>12,33,39</sup> They can be partially or totally implantable, but always require a power pack. Other major disadvantages

include heavy drug treatments to avoid thrombosis and to prevent infection.<sup>48</sup> In addition to a poor patient's quality of life, current long-term assist devices constitute an overall costly solution.<sup>18</sup>

An ideal cardiovascular pump<sup>3</sup> should be reliable, durable, biocompatible, fully implanted, efficient, small in size, produce pulsatile flow, cause minimal thrombogenicity, and easy in placement and removal. The innovative MIP meets all these criteria, bringing intra-aortic pumps to a next generation. With the possibility of being inserted by a catheter through the femoral artery, the MIP will be positioned lying against the aortic walls. A gel-like liquid could be added *a posteriori* to recreate the thick gelatinous layer. The actuator can be made out of coils and magnets or a pneumatic chamber, and would be remotely controlled. The pump has many advantages as a cardiovascular assist device. It is fully implantable and controlled externally. It has barely any outward radial displacement when in use, and therefore would not strain the aorta. This low cost pump has no component that could obstruct the flow, damage the red blood cells and has minimal thrombogenicity. Finally due to its simple design, it is adaptable to each patient's morphology, and its use can be expanded beyond the case of heart failure.

### **7.1.2 *Gelatin-coated graft***

Hypoplastic Left Heart Syndrome (HLHS) is a fatal congenital cardiac malformation in newborns, in which the left side of the heart is underdeveloped resulting in a decrease in blood supplied to the body. Without treatment, 95% of these infants die during the first month of life, and none survive beyond four months.<sup>7,8</sup> When possible, bypassing of the left ventricle following the Total Cavo-Pulmonary Connection (TCPC) Fontan surgical

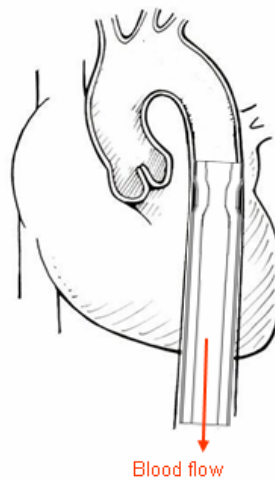


**Figure 27.** Illustration of the MIP fitting the inside of the aorta.

procedure is achieved by connecting the superior vena cava to the left pulmonary artery. As a result of this procedure, the single ventricle perfuses both the systemic and pulmonary circulations in series. Nevertheless, in many cases after the TCPC procedure the flow to the pulmonary system is not sufficient to ensure adequate pulmonary blood flow. In other cases severe conditions of systemic venous hypertension or pulmonary arterial hypotension are created. Other complications are attributed to disturbed flow dynamics in the TCPC. Typical reported failure rate and operative mortality of TCPC procedure is 9%<sup>15</sup>, and long term mortality after 15 years reaches 50%.<sup>3</sup>

Assisted cavopulmonary blood flow, by substituting a mechanical pump as a pulmonary ventricle to overcome this pressure gradient, would improve cardiac output by restoring the circulation to one more closely resembling two-ventricle physiology.<sup>47</sup> Mechanical circulatory support for adult patients who suffer from Congestive Heart Failure (CHF) is now state of the art clinically. Few studies tried to apply these clinically used cardiac assist devices for pediatric use as well in TCPC circulation.<sup>43,54,55</sup> They used

animal models to prove the improved hemodynamics of pump-supported versus passive Fontan circulation. It was shown that pump support could conceivably reverse poor hemodynamics and secondary organ failure in patients with failing TCPC circulation, could make these patients more successful transplant candidates, or could be used as destination therapy. Even though improvement was clearly proven in all these cases, the pump chosen in all these studies was not suitable enough.

An ideal pump for cavopulmonary assist would require several features including pulsatile, net unidirectional flow, minimal thrombogenicity, and minimally invasive methods for placement and removal. The anatomy of a total cavopulmonary connection is favorable for circulatory assistance in that it provides a relatively straight longitudinal axis for instrumentation. The duration of assist needed for the univentricular support would presumably depend on patient-specific physiologic variables.

The MIP can serve as a noninvasive pump to enhance blood flow in the TCPC shunt to increase pulmonary flow and pressure independently of the systemic pressure (figure 28). The pump will actually be the original connecting graft with an added internal gelatin coating and an additional excitation device placed near its proximal edge. Its pumping mechanism would rely on the graft elasticity and the impedance mismatch at the graft connections. The MIP requires only small excitations to operate. In addition, the MIP has the great advantage of directly using the graft configuration. Impedance mismatch is achieved by the graft connections. One would only need to use a graft coated with a thicker gelatin layer than the already available Dacron gelatin-coated grafts. The pump is noninvasive and can be externally controlled. Because the pump performances are based on the frequency of excitation, it is patient specific and adaptable to patient

growth, by tuning the excitation frequency. The pump has, therefore, great potential for pediatric support, where demand of small, adaptable and noninvasive devices is especially important.

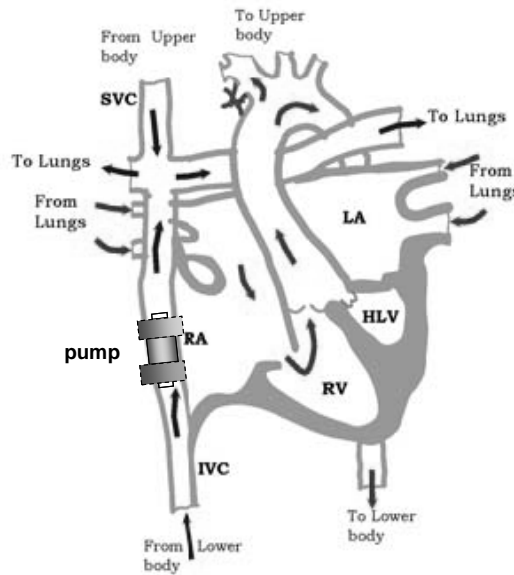


**Figure 28.** A schematic illustration of blood flow in the TCPC Fontan circulation.

(adapted from Migliavacca<sup>44</sup>), with the pump.

## 7.2 Physiologically correct model of an aorta

To test the MIP as a cardiovascular device, the time-dependent boundary conditions at the entrance and exit of the device need to be carefully applied. To do so, we propose a simple boundary condition for modeling physiological flow and pressure in the descending aorta where the pump is to be implemented.

### 7.2.1 *Nature of the flow in the descending aorta*

The vertebrate circulatory system is a closed pressurized loop in which circulation is ensured by a muscular pump, the heart. During systole (40% of the cardiac cycle) the

heart contracts and ejects blood into the aorta. During diastole (remaining 60% of the cardiac cycle) the heart relaxes and fills with blood. During that phase, the aortic valve prevents blood flowing into the aorta. The arterial tree irrigated by the aorta provides resistance to the circulatory system, while the aorta serves as a compliance chamber. Over one cardiac cycle, blood flow exiting the heart is delivered in the aorta in an unsteady pulsatile manner, and so is pressure (figure 29).<sup>36</sup>

The entire cardiovascular system may be simplified using a lumped parameter or one-dimensional (1D) model of flow. The earliest model characterizing the interaction between a pumping heart and systemic arterial tree was quantified by Otto Frank, and came to be known as the Windkessel model. It has been used to explain the rapid rise and gradual decrease of the flow and pressure waveforms.

The Windkessel model describes the cardiovascular system in terms of a compliant section in series with a resistive section. During systole, the compliant aorta acts like a capacitor to store blood. During diastole, the elastic aorta discharges the stored blood through the resistive branches of the smaller arteries to various organs. The pressure and flow waveforms given by this model are quite close to those measured in the body. Other investigators have produced more elaborate models with many elements in order to refine the waveform predictions.<sup>50</sup>

The Windkessel model is here used as an outlet boundary condition to model pulsatile flow and pressure in the descending aorta. The proposed boundary condition model ensures the generation of a pressure waveform when pulsatile velocity inlet conditions are applied. The outlet boundary condition consists in an elastic vessel modeling the compliance chamber coupled with a porous media to ensure resistance (figure 30). The

aorta model with physiological boundary condition is to serve as a test bench for aortic devices.

### 7.2.2 Aorta model with pulsatile boundary conditions

The descending adult aorta is modeled as a straight tube of circular cross section ( $R_{aorta}^f = 0.955$  cm,  $L_{aorta} = 37.2$  cm).<sup>50</sup> The aortic tube is assumed to be consisted of a unique layer ( $h_{aorta} = 0.075$  cm) of a purely elastic material within the range of biological soft tissue ( $E_{aorta} = 65 \text{ e}+7$  dyn/cm<sup>2</sup>,  $\nu_{aorta} = 0.49$ ,  $\rho_{aorta} = 1$  g/cm<sup>3</sup>). Blood is modeled as a Newtonian viscous fluid ( $\mu_f = 0.035$  g/cm s,  $\rho_f = 1$  g/cm<sup>3</sup>), and is governed by the Navier-Stokes equations (4) (5).

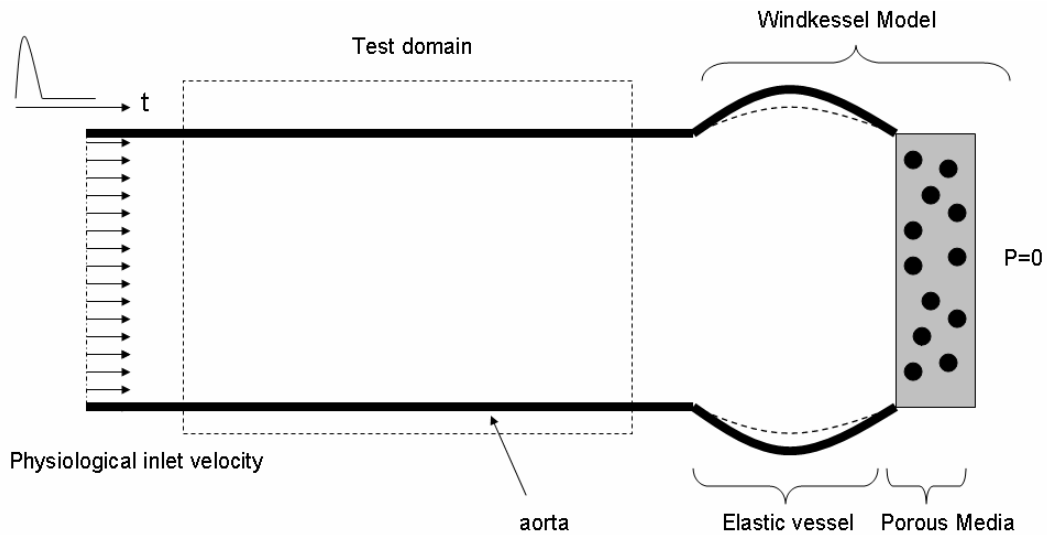


**Figure 29.** Schematic of the aorta model and the boundary conditions.

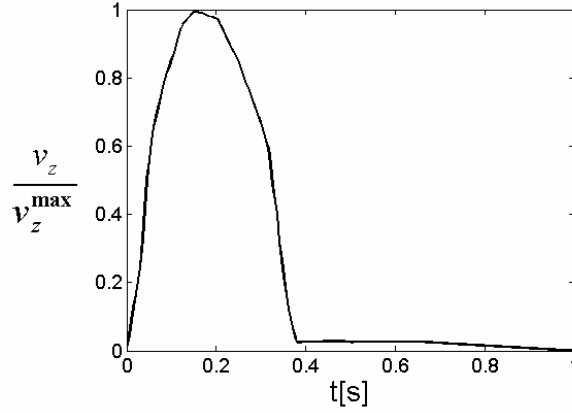


**Figure 30.** Imposed inlet velocity waveform. Plot of the axial velocity  $v_z$  is normalized by its peak value  $v_z^{\max}$  over one period ( $f=1$  Hz).

The inlet boundary condition is an imposed flat velocity profile of pulsatile waveform (from Nichols&O'Rourke<sup>50</sup>). The Windkessel model is situated at the outlet of the aortic tube. An elastic vessel ( $E_{vessel}=1.5 \text{ e}+7 \text{ dyn/cm}^2$ ,  $\nu_{vessel}=0.49$ ,  $\rho_{vessel}=1 \text{ g/cm}^3$ ) is coupled with a porous media, which is a solid domain ( $\rho_s=2 \text{ g/cm}^3$ ) saturated with the viscous fluid modeling blood (figure 31).

The flow in a porous media is governed by the Darcy's law:

$$\mu_f \boldsymbol{\kappa}^{-1} \cdot \mathbf{v} = -\nabla P + \mathbf{f}^b, \quad (34)$$

where  $\mu_f$  is the dynamic viscosity,  $\mathbf{v}$  the velocity vector and  $\boldsymbol{\kappa}$  the permeability tensor of the porous media,  $\nabla P$  the pressure gradient along the porous media, and  $\mathbf{f}^b$  the external body force vector. The porosity  $\phi$ , being the ratio of the volume occupied by the fluid to the volume of the mixed medium, was fixed to 0.8. The permeability tensor  $\boldsymbol{\kappa}$  is assumed to have components in the direction of the flow only  $\kappa_{zz}=2 \text{ e}-4$ .

The aortic walls and the elastic vessel walls are fully coupled to the fluid, and will be solved using the Fluid-Structure Interaction solver. The porous media walls are rigid.

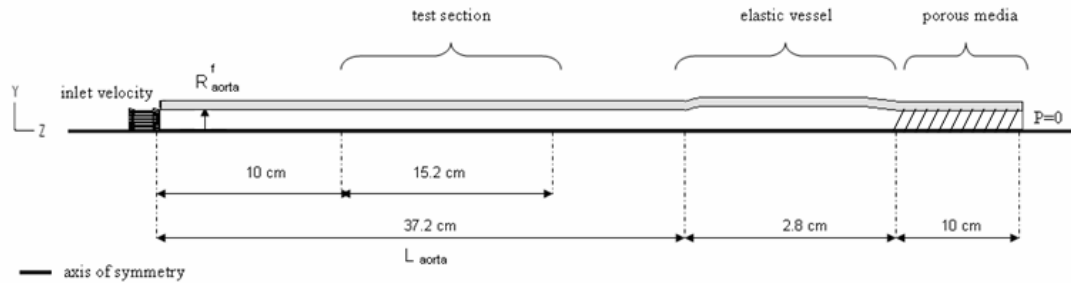


**Figure 31.** Physiologically correct model of aorta. 2D cross sectional view. Geometry and boundary conditions.

### 7.2.3 Results

#### Inlet pressure variation in time:

We fixed the inlet velocity magnitude ( $v_z^{\max}$ ) to 50.5 cm/s so that to create a flow rate corresponding to the blood flow delivered by the heart of a sick patient ( $\sim 2$  L/min). The resulting pressure is found pulsatile. Only velocity was prescribed at the inlet boundary. The inlet pulsatile pressure is the result of the Windkessel model at the outlet of the tube. The pressure peak-to-peak value is consistent with the pressure peak-to-peak value found in a human descending aorta for elderly patient, slightly on the upper limit:<sup>42</sup>  $P_{\min} = 10 \text{ e}+4 \text{ dyn/cm}^2$ ,  $P_{\max} = 21 \text{ e}+4 \text{ dyn/cm}^2$ . Although the aortic walls have been modeled as fairly rigid, the pulsatile inlet flow generates waves in the aortic walls that are visible through the small fluctuations of the pressure waveform (figure 32).

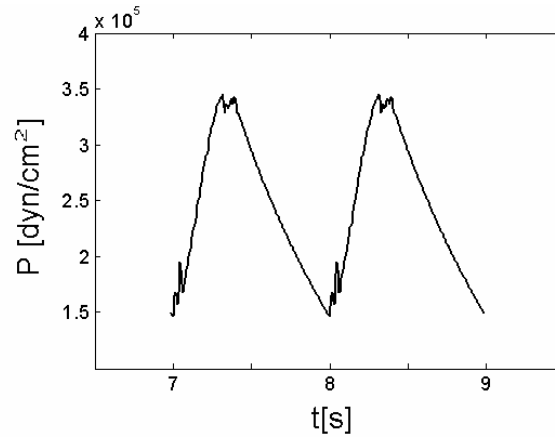


**Figure 32.** Resulting inlet axial pressure from the inlet imposed velocity profile.

Variation in time at the inlet for a node belonging to the axis of symmetry during 2 cycles.

Velocity and pressure variation at a cross section in the test domain:

In the test domain, the pressure and velocity waveform are conserved and of slightly higher values than to the incoming flow. They are still in physiological range and of waveform very similar to the one found in the descending aorta (The peak-to-peak pressure of a healthy middle-aged male patient is  $125 / 78$  mmHg =  $16.6 \text{ e}+4 / 10.4 \text{ e}+4$  dyn/cm<sup>2</sup> and peak velocity is 50 cm/s).

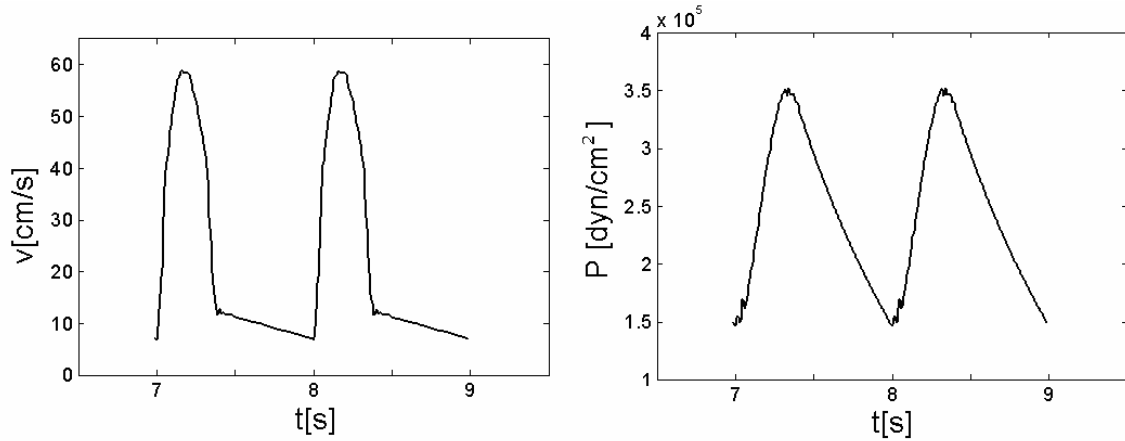


**Figure 33.** (Right) Axial velocity variation in time.(Left)axial pressure variation in time .

Plots are for the node located at mid length of the test domain on the axis of symmetry.

#### 7.2.4 Summary

We propose a boundary condition that has the advantage of modeling the correct physiological pressure waveform when a pulsatile physiological velocity inlet condition is applied. The values of the flow rate and pressure are within the range of an elderly patient with a weak heart (aorta's wall modeled fairly rigid, weak mean flow rate, high blood pressure). This model can serve as a bench test for testing aortic devices. In appendix 3 a model of MIP inserted in the aorta with physiological boundary conditions is given.

# Chapter 8

## Conclusion

This work introduced a new and innovative Impedance Pump (IP) design, the Multilayer Impedance Pump (MIP), where a thick internal gelatin layer is used to amplify elastic waves and that allow small excitation only. By exploring flow and structure response to frequencies of excitation, the resonance nature of the pump has been demonstrated. Higher flow and greater wall motion are achieved when the pump is excited around its natural frequency. Energy transmission is also more efficient at resonance, resulting in a higher efficiency for the pump excited at the resonance frequency.

Because the MIP is directly inspired from the embryonic heart structure, the use of the MIP model has allowed shedding light on nature's optimized design. First, by comparing the multilayer tube for two pumping modes (peristalsis and impedance), impedance pumping revealed to be more energetically advantageous with respect to its peristalsis equivalent. This result brings an additional piece of evidence that the embryonic heart may use elasticity and impedance mismatch to drive unidirectionally the flow, and not a sequence of peristaltic contractions as previously thought. Second, by comparing two impedance pumps (with and without gelatin-like internal layer), the added gelatin layer has been found to have a mechanical benefit in terms of exit flow. By extension, cardiac jelly may have a role in enhancing flow in the embryonic heart.

Thanks to its unique wall structure, the MIP reveals itself an adequate pumping device for biomedical applications. To test the MIP as an intra aortic pump, a Windkessel boundary condition that creates physiological pressure and flow waveforms has been proposed. Future work will focus on a model of MIP model in the descending adult aorta to show its potential for cardiovascular applications.

# Appendix 1

## Model Validation

In order to validate the numerical code, 3 computations for which the analytic solution is well known were performed. Using a rigid tube, we test first, the Poiseuille solution for a constant pressure gradient and second, for an oscillatory pressure gradient. Thirdly, we use the same oscillatory pressure in an elastic tube and compare the numerical results with the Wormesley solution.

### Constant pressure in a rigid tube

#### *Model*

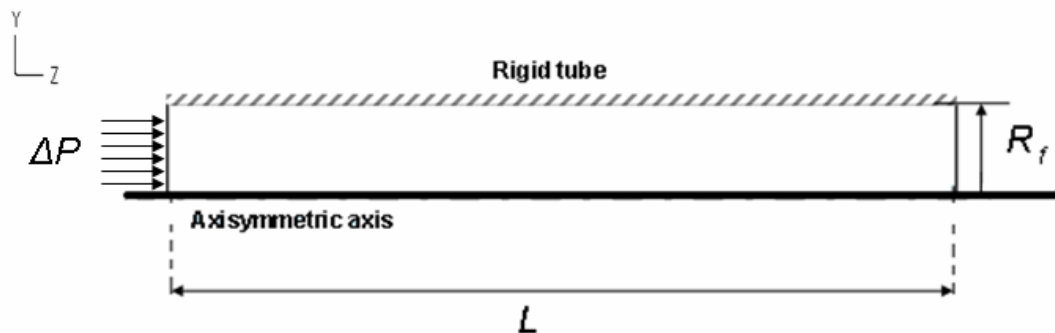


**Figure.** Schematic of the Poiseuille flow model. Flow in the rigid tube is driven by a pressure gradient.

**Table.** Characteristics of the constant pressure in a rigid tube model.

Physical parameter	Symbol	Value
Length of the pump	$L$	40 cm
Fluid domain radius	$R_f$	0.5 cm
Fluid viscosity	$\mu_f$	0.01 g/cm s
Fluid density	$\rho_f$	1 g/cm <sup>3</sup>
Pressure drop along the tube	$\Delta P$	10 dyn/cm <sup>2</sup>
Maximum axial velocity	$v_z^{\max}$	1.563 cm/s
Reynolds number <sup>b</sup>	$R_e$	156.3
Entry length <sup>c</sup>	$l_e$	6.254 cm

The first test case was the modelisation of a Poiseuille flow, being a constant pressure gradient in a rigid tube. The pressure gradient

$$\Delta P = P(z = L) - P(z = 0),$$

consisted in a constant normal traction applied at one extremity of the tube ( $P(z = 0)$ ) and a zero pressure boundary condition at the other extremity of the tube ( $P(z = L)$ ).

The tube was filled with water, and was of enough length so that flow is fully developed at the end of the tube.

---

<sup>b</sup> The Reynolds number for the Poiseuille flow is defined as:  $R_e = \frac{\rho_f v_z^{\max} D_f}{\mu_f}$  where  $D_f$  the tube's diameter ( $D_f = 2 * R_f$ )

<sup>c</sup> The entry length for the Poiseuille flow is defined as  $l_e = 0.04 R_e D_f$

The numerical model consisted in 12,000 4-noded axisymmetric elements, and the time step was set to 0.005 s.

### ***Comparison***

We compared the axial velocity profile at mid length of the tube where flow is fully developed. The Poiseuille solution for the axial velocity is dependent on the pressure gradient, the fluid viscosity and the tube geometry:

$$v_z(t, y, z_o) = -\frac{\Delta P}{4\mu_f L} (y(t, z_o)^2 - R_f^2).$$

The error between the numerical and the analytical solutions is defined to be absolute error in axial velocity relative to the analytical solution for each point  $y$  along a specific cross section located at  $z = z_o$  and at time  $t_o$  where flow is steady.

$$Error = \left| \frac{v_z^{num}(t_o, y, z_o) - v_z^{ana}(t_o, y, z_o)}{v_z^{ana}(t_o, y, z_o)} \right|. \quad (*)$$

We found a very good agreement of the numerical solution with the analytical solution, and an error of about 0.09%.

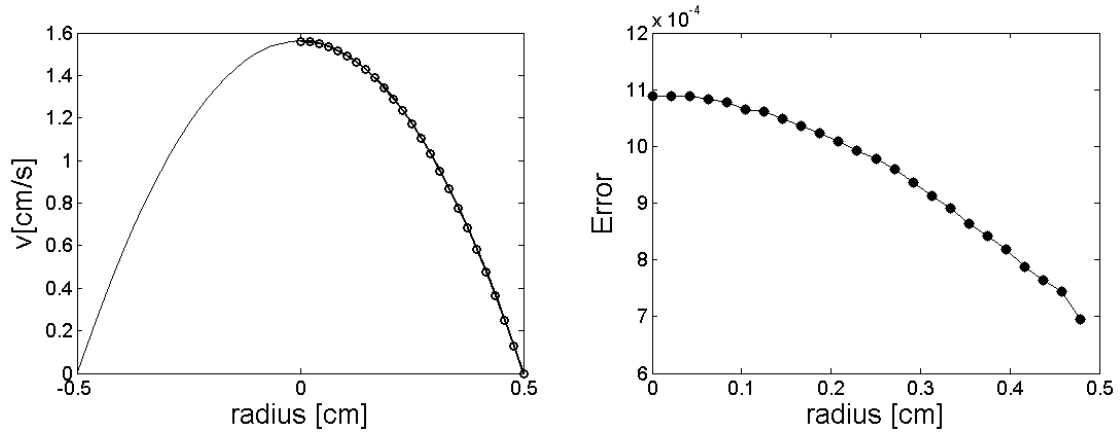


**Figure.** (Left) Velocity profile at a cross section located at mid-length of the tube. Analytical solution (thin line) and numerical solution (for positive Y only) (thick line and dots). (Right) Error in axial velocity between the numerical and the analytical solution along a cross section.

## Pulsatile pressure in a rigid tube

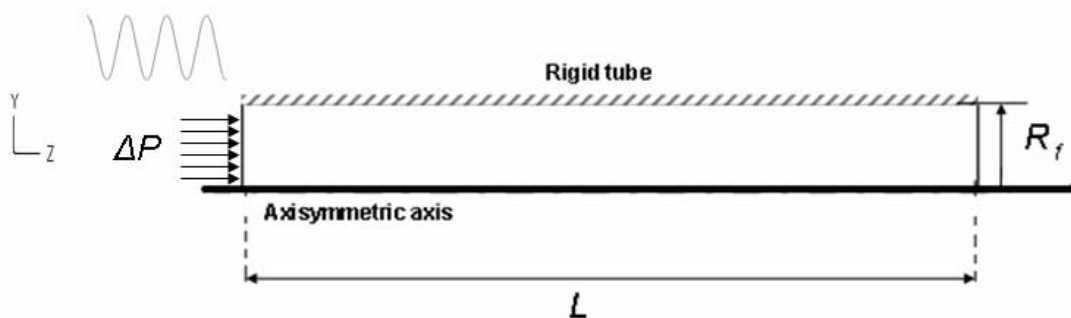


**Figure.** Schematic of the Poiseuille flow model with pulsatile inlet pressure.

The second test case consisted in the exact same rigid tube as the one from the previous section with a pulsatile pressure inlet boundary condition.

$$\Delta P(t) = P \sin(\omega t),$$

with  $|P| = P(z = 0) = 10 \text{ dyn/cm}^2$  and  $\omega = 0.36 \text{ rad.s}^{-1}$ .

The exact same numerical mesh and time step as the one from the previous section was used.

### ***Comparison***

The analytical solution is obtained by decomposing the flow into a steady and an oscillatory part. After separation of variables in the governing equation for the oscillatory part, the spatial component is found by solving a Bessel equation, and the axial velocity is expressed as: <sup>61</sup>

$$u_z(t, y, z_o) = \mathbf{Im} \left( i \frac{\Delta P R_f^2}{\mu_f L \Omega^2} \left( 1 - \frac{J_0 \left( \Lambda \frac{y(t, z_o)}{R_f} \right)}{J_0(\Lambda)} \right) \cdot e^{i\omega t} \right)$$

where  $J_0$  is the Bessel function of order zero, and  $\Omega$  a non dimensional parameter function of the material properties of the fluid, the fluid radius and the frequency of the imposed pulsatile pressure gradient:

$$\Omega = \sqrt{\frac{\rho_f \omega}{\mu_f}} R_f,$$

and

$$\Lambda = \frac{(i-1)\Omega}{\sqrt{2}}.$$

The error between the numerical and the analytical solutions is computed using equation (\*) at discrete times  $t_o$  during a period once periodic state in flow is reached.

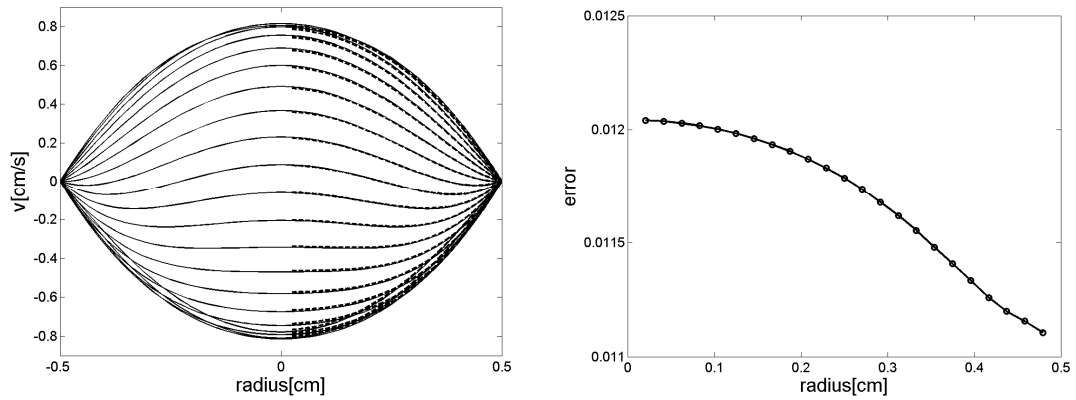


**Figure.** (Left) Velocity profile at a cross section located at mid-length of the tube. Analytical solution (solid line) and numerical solution (for positive  $Y$  only) (dashed line). (Right) Error in axial velocity between the numerical and the analytical solution along a cross section for different instants of a period of time.

## Pulsatile pressure in an elastic tube

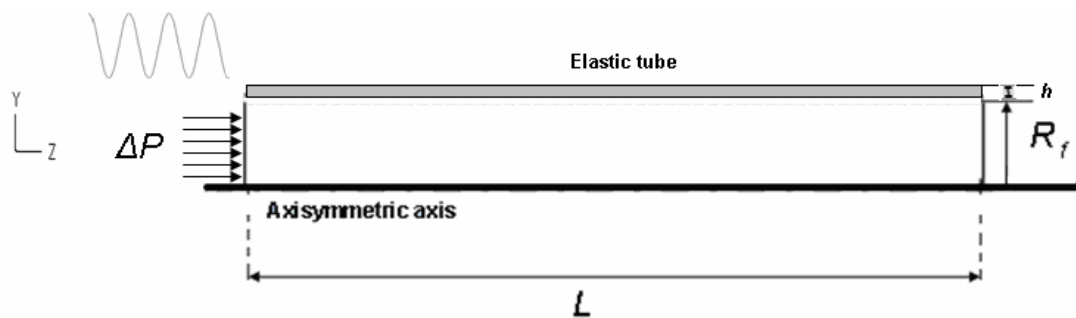


**Figure.** Schematic of the pulsatile pressure in an elastic tube model.

The third test case consisted in the modeling of a pulsatile flow in an elastic tube by imposing a pulsatile pressure at one extremity of the tube, the other extremity being constrained to a constant pressure of zero value. The elastic tube was modeled using a

purely linear elastic material ( $E_s, \nu_s$ ), and the thickness of the tube ( $h$ ) was small compared to the fluid radius.

**Table.** Characteristics of the pulsatile flow in an elastic tube model.

Physical parameter	Symbol	Value
Length of the pump	$L$	40 cm
Fluid domain radius	$R_f$	0.5 cm
Elastic tube thickness	$h$	0.05 cm
Elastic tube stiffness	$E_s$	1 e+5 dyn/cm <sup>2</sup>
Elastic tube Poisson's ratio	$\nu_s$	0.3
Elastic tube density	$\rho_s$	1 g/cm <sup>3</sup>
Fluid viscosity	$\mu_f$	0.01 g/cm s
Fluid density	$\rho_f$	1 g/cm <sup>3</sup>
Pressure drop along the tube	$\Delta P$	10 dyn/cm <sup>2</sup>

In order to avoid any wave reflection in the elastic tube, an absorbing boundary condition was used at the end of the tube ( $z=L$ ). The absorbing boundary condition consisted on a very long elastic tube (160 cm) made out of the exact same elastic tube. At the entrance of the tube, motion of the tube in the longitudinal direction was constrained, but radial motion was allowed.

### ***Comparison***

Similarly to the case of pulsatile flow in a rigid tube, the analytical solution is obtained by decomposing the flow into a steady and an oscillatory part and coupling the Navier Stokes equations with the equations of the wall motion. The velocity in the elastic tube has an axial and a longitudinal component. After separation of variables in the governing equation for the oscillatory part, the spatial component is found by solving a Bessel equation, and the axial velocity is expressed as:<sup>61</sup>

$$u_z(t, y, z) = \mathbf{Im} \left( i \frac{\Delta P R_f^2}{\mu_f L \Omega^2} \left( 1 - G \frac{J_0 \left( \Lambda \frac{y(t, z)}{R_f} \right)}{J_0(\Lambda)} \right) \cdot e^{i\omega \left( t - \frac{z}{c} \right)} \right)$$

where  $c$  is the wave speed found by solving a quadratic equation in  $z$  where

$$z = \frac{E_s h}{(1 - \nu_s^2) \rho_f R_f c^2}.$$

$G$  is an elasticity factor given by:

$$G = \frac{2 + \zeta(2\nu_s - 1)}{\zeta(2\nu_s - g)},$$

where

$$\zeta = \frac{E_s h}{(1 - \nu_s^2) \rho_s R_f c^2},$$

and

$$g = \frac{2J_1(\Lambda)}{\Lambda J_0(\Lambda)}.$$

The error between the numerical and the analytical solutions is computed using equation \* at discrete times  $t_o$  during a period once periodic state in flow is reached.

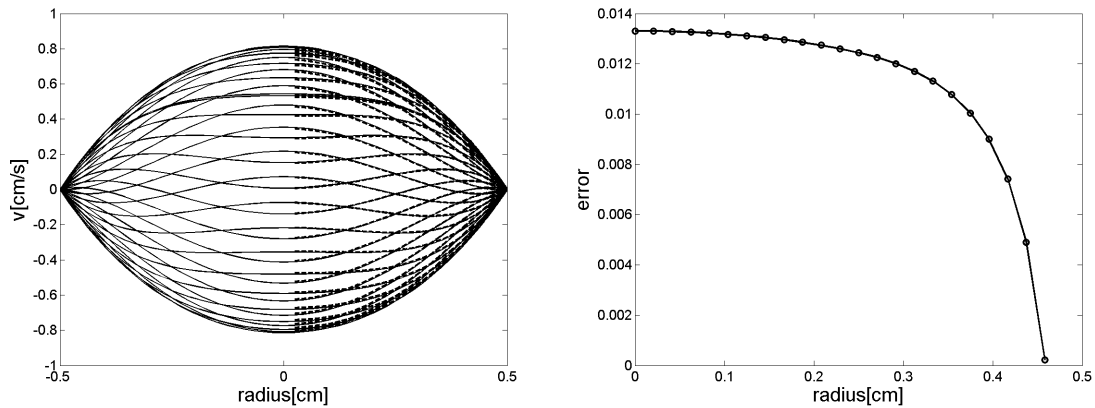


**Figure.** (Left) Velocity profile at a cross section located at mid-length of the tube. Analytical solution (solid line) and numerical solution (for positive  $Y$  only) (dashed line). (Right) Error in axial velocity between the numerical and the analytical solution along a cross section for different instants of a period of time.

## **Appendix 2**

### **Wave dynamics**

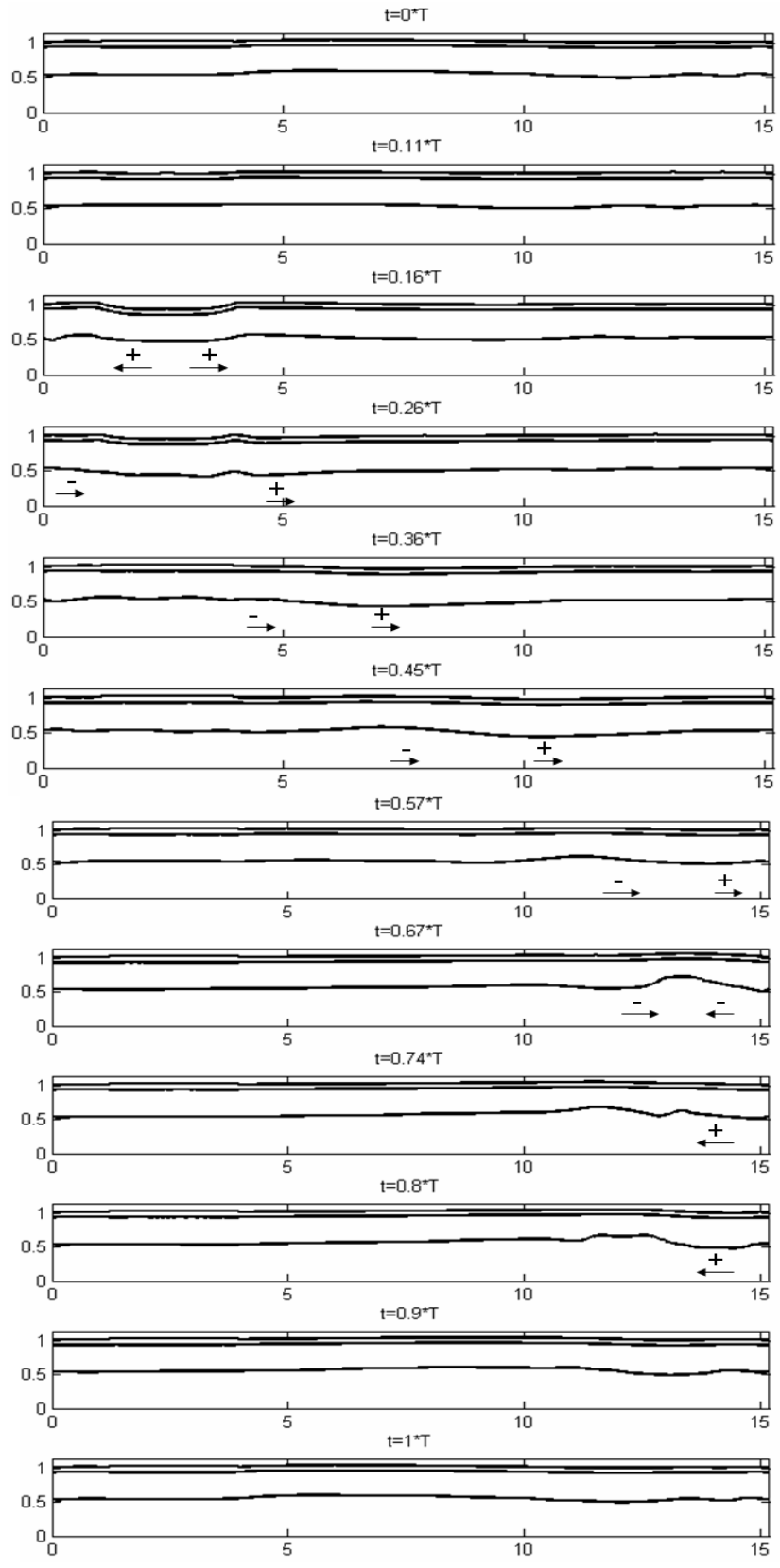


Figure (a)

95

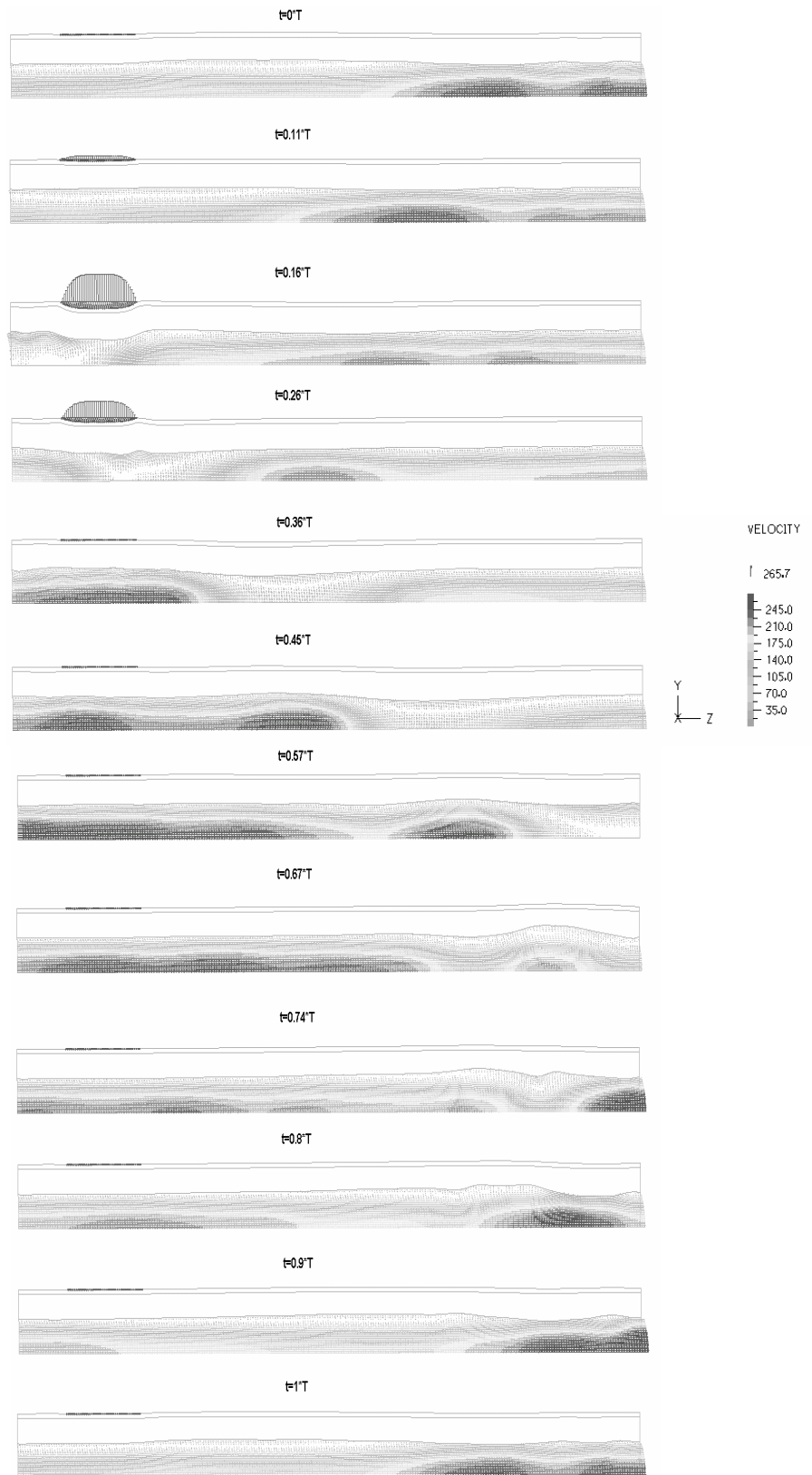


Figure (b)

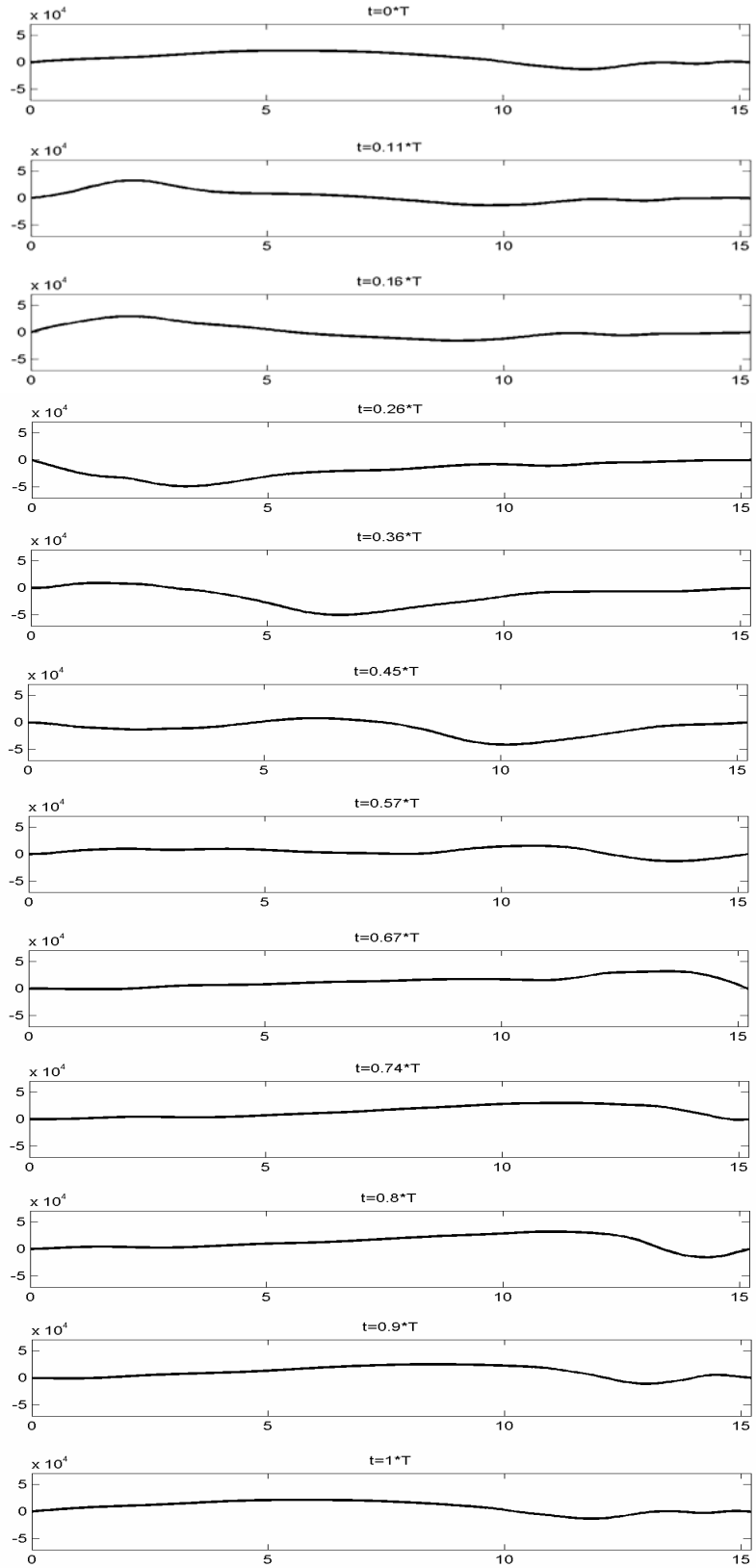


Figure (c)

**Figure.** Illustration of the propagating waves in the multilayer impedance pump.

Example for  $f=10.1$  Hz. (a) Selected frames of the model outline over one period of time at periodic conditions. The time  $t$  of each selected frame is expressed as a fraction of the period  $T$ . (b) Corresponding snapshots of the axial velocity fluid field for each of the selected times (c) Axial pressure longitudinal distribution for each of the selected times.

## Appendix 3

### MIP with a viscoelastic material

A model of MIP using a viscoelastic gelatin that is time dependant and temperature independent has been implemented. The MIP model is identical to the one described in section 2.1.

The stiffness, Poisson's ratio and density of the gelatin, are the same as in section 2.1 (see table). The gelatin being treated as a viscoelastic material, the state of stress in the gelatin follows:

$$s_{ij}(t) = 2G_{gel}(0)e_{ij}(t) + 2\int_0^t e_{ij}(t-\tau)\frac{dG_{gel}(\tau)}{d\tau}d\tau,$$

$$\sigma_{ij}(t) = 3K_{gel}(0)e_{kk}(t) + 3\int_0^t \varepsilon_{kk}(t-\tau)\frac{dK_{gel}(\tau)}{d\tau}d\tau,$$

where  $t$  is the time,

$$s_{ij} = \sigma_{ij} + \frac{1}{3}\delta_{ij}\sigma_{kk},$$

is the deviatoric stress,  $\delta_{ij}$  is the Kronecker delta,  $\sigma_{ij}$  is the stress,

$$e_{ij} = \varepsilon_{ij} - \frac{1}{3}\delta_{ij}\varepsilon_{kk},$$

is the deviatoric strain,  $\varepsilon_{ij}$  is the strain,  $G_{gel}(t)$  is the shear modulus and  $K_{gel}(t)$  is the bulk modulus defined by:

$$G_{gel}(t) = \frac{E_{gel}(t)}{2(1+\nu_{gel})},$$

$$K_{gel}(t) = \frac{E_{gel}(t)}{3(1-2\nu_{gel})}$$

In the viscoelastic formulation, the shear and bulk moduli are expressed in terms of a Prony-Dirichlet series where variation of temperature is neglected.

$$G_{gel}(t) = G_{gel}(0) + G_o e^{-d_1 t},$$

$$K_{gel}(t) = K_{gel}(0) + K_o e^{-d_2 t},$$

where  $G_{gel}(0)$  is the final shear modulus,  $K_{gel}(0)$  the final bulk modulus,  $G_o$  and  $K_o$  are constant coefficients, and  $d_1$  and  $d_2$  are the relaxations parameters for the shear and bulk modulus respectively.

**Table.** Characteristics of viscoelastic gelatin.

Physical parameter	Symbol	Value
Stiffness	$E_{gel}$	5 e+4 dyn/cm <sup>2</sup>
Poisson's ratio	$\nu_{gel}$	0.49
Density	$\rho_{gel}$	1 g/cm <sup>3</sup>
Shear modulus	$G_{gel}$	8.3 e+5 dyn/cm <sup>2</sup>
Bulk modulus	$K_{gel}$	1.67 e+4 dyn/cm <sup>2</sup>
Shear coefficient	$G_o$	8.3 e+5
Bulk coefficient	$K_o$	1.67 e+4
Shear relaxation parameter	$d_1$	1,000
Bulk relaxation parameter	$d_2$	1,000

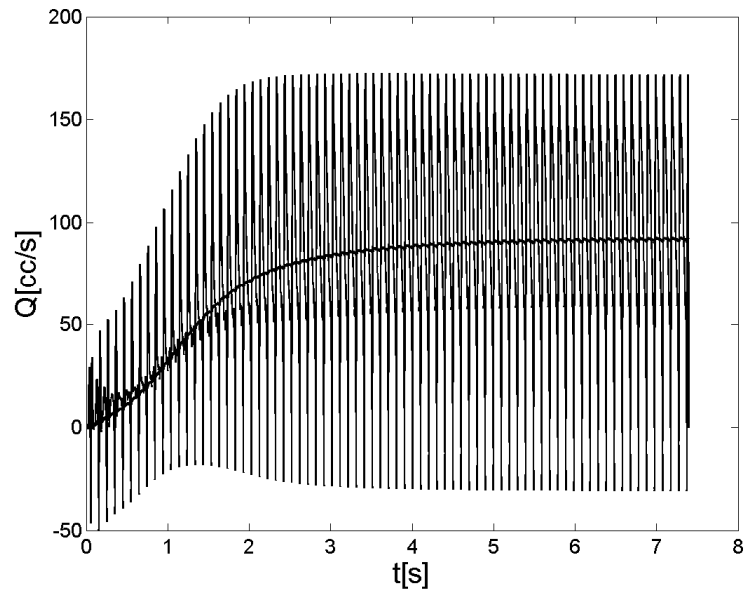


**Figure.** Exit flow rate time history for the MIP using a viscoelastic gelatin layer.

Frequency of excitation is 10.1 Hz. Mean exit flow reaches 90.6 cc/s.

This viscoelastic MIP model demonstrates that the MIP exhibits the same behavior when a viscoelastic material is used to represent the gelatin. Results show that the nonlinearities introduced by the viscoelastic material can be beneficent to the pumping if appropriate material properties are chosen.

## Appendix 4

### Error in linearization

#### Analytical

The error in solving for small strains can be estimated by calculating the error in strain linearization for the maximum strain observed (30%):

$$\varepsilon_{ij} = \frac{1}{2}(u_{i,j} + u_{j,i} - u_{k,i} \cdot u_{k,j}) = \frac{1}{2}(u_{i,j} + u_{j,i}) - \underbrace{\frac{u_{k,i} \cdot u_{k,j}}{2}}_{error}$$

$$error = \frac{1}{2} * (0.3)^2 = 0.045 < 5\%$$

#### Numerical

In addition, we performed a comparison between two numerical simulations of the MIP, one with the small strain assumption and one with the large strain assumption for the pump excited at 11.5 Hz. We found a relative error in exit flow rate of 4.6104 e-4 (less than 0.05%), which confirms the analytical results.

$$error = \mathit{mean}_{t \in [t_0, t_0 + T]} \left( \frac{Q^{small\ strain}(t, z_o) - Q^{large\ strain}(t, z_o)}{Q^{small\ strain}(t, z_o)} \right)$$

## Appendix 5

### High frequency results

The MIP defined in section 6.2.2 was excited at 5% of its external radius (instead of the 10% from the original MIP model) and frequencies ranging from 30 to 45 Hz.

#### Impulse response

The same impulse excitation as the one described in section 3.2 was applied to the MIP model excited at 5% of its external radius. The spectrum of the exit flow rate is similar to the one described in section 3.2, confirming the invariance of the model's natural frequencies with respect to pinching amplitudes.

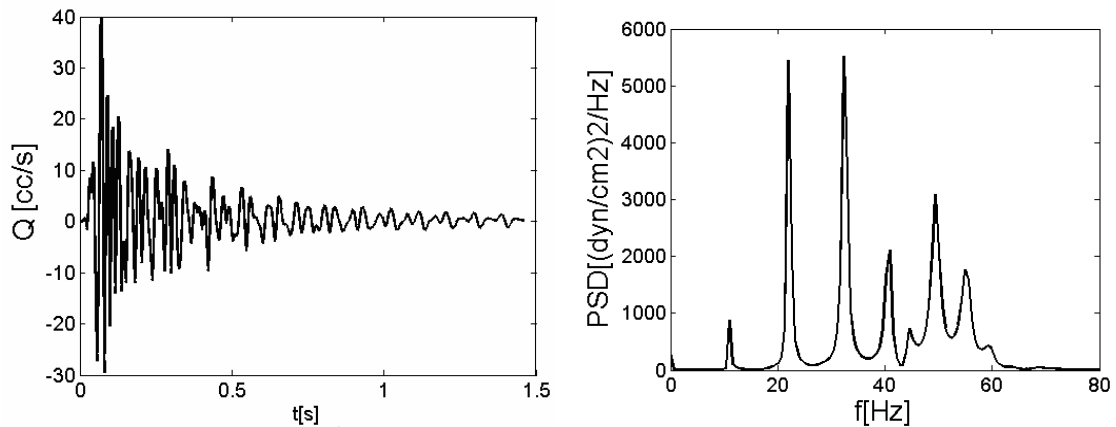


**Figure.** Impulse response of the MIP model excited at 5% of its external radius.

(Left) Exit flow rate variation in time under triangular impulse excitation. (Right) The associated Power Spectrum Density (PSD).

## Exit flow rate and frequency of excitation

The mean exit flow rate ( $\bar{Q}$ ) is calculated for frequencies of excitation ranging from 30Hz to 45Hz. It is found positive and seem not to have a specific correlation with the natural frequencies exhibited by the spectrum analysis. Although the excitation amplitude is only 5% of the external radius, flow reaches up to 50 cc/s.

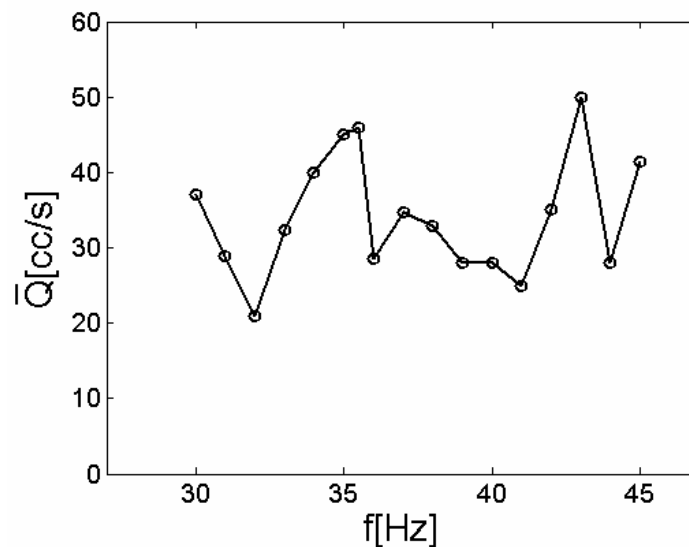
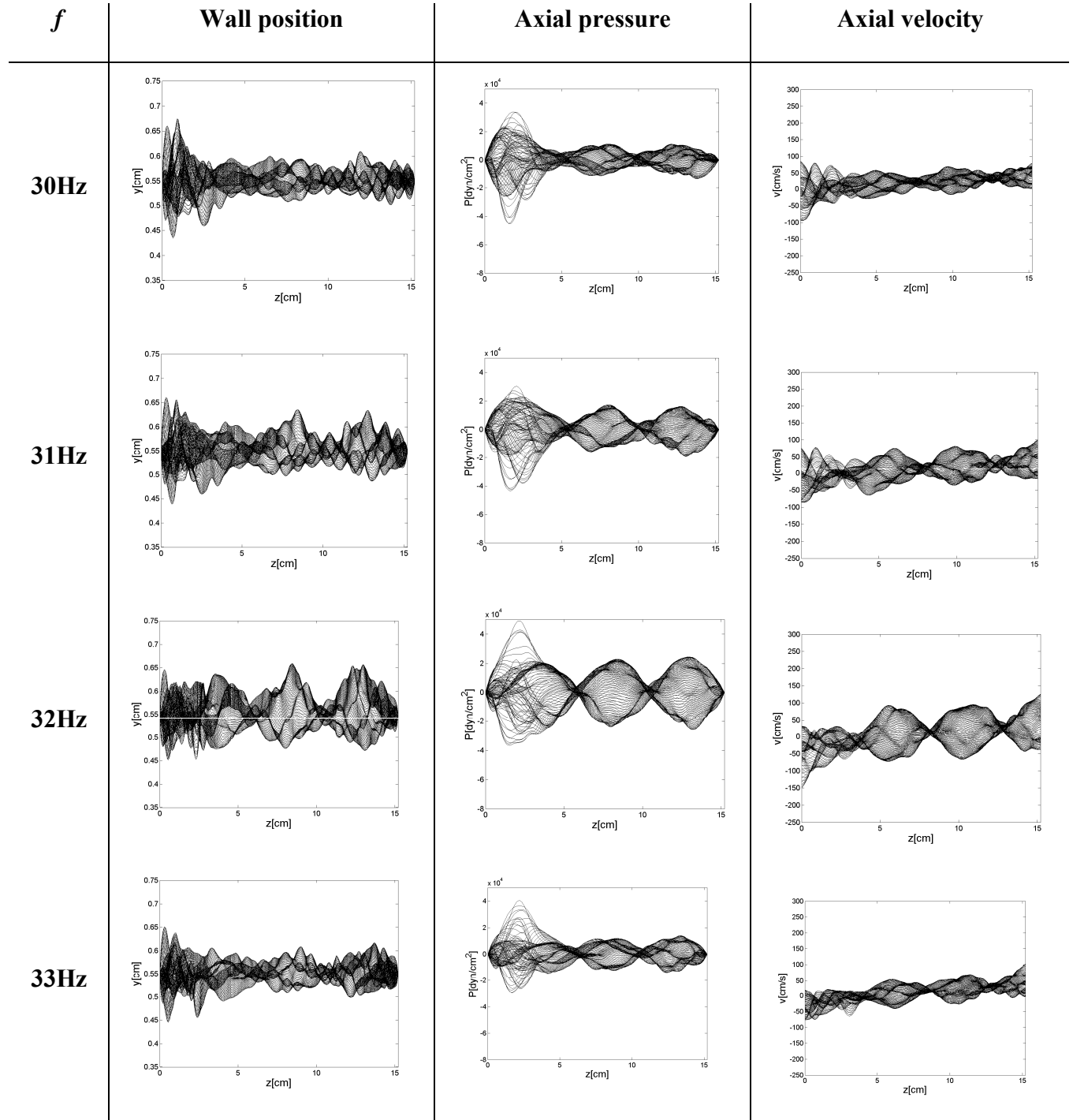


**Figure.** Mean exit flow rate ( $\bar{Q}$ ) as a function of the excitation frequency ( $f$ ).

## Wall displacement, axial pressure longitudinal distribution & axial velocity longitudinal distribution

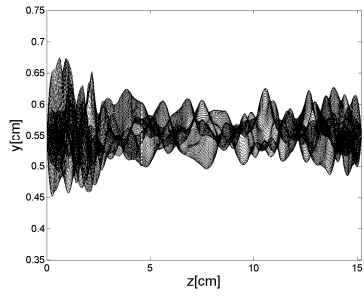
The wall displacement, axial pressure longitudinal distribution and axial velocity longitudinal distribution is plotted over a period of time once periodicity in the flow is achieved.







44Hz



107

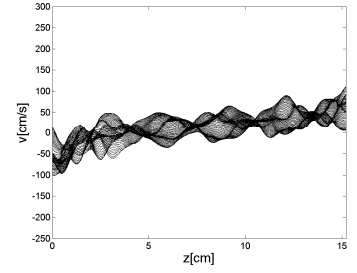
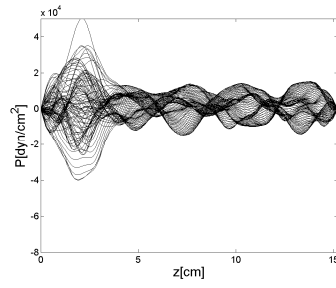


**Figure.** Wall displacement, axial pressure longitudinal distribution and axial velocity longitudinal distribution over a period of time once periodicity in the flow is achieved.

## Appendix 6

### Viscous diffusion time

We estimate the diffusion time for the entire flow to be affected by the wall motion by using the impulsively actuated oscillatory wall (2<sup>nd</sup> Stokes problem).

Considering an impulsively oscillatory wall in the  $Z$  direction of velocity  $U$  and of frequency  $f$ , the velocity  $u$  in the fluid can be expressed using the self-similar variable  $\eta$  :

$$u = U e^{-\eta} \cos(2\pi f t - \eta), \quad \eta = y \sqrt{\frac{\pi}{\nu t}}.$$

The fluid at the distance  $y=d$  away from the moving wall will have 0.99 of the wall velocity ( $U$ ) when :

$$\eta = -\ln\left(\frac{u}{U}\right) \Rightarrow d \sqrt{\frac{\pi}{\nu t^*}} = 0.0101.$$

The time  $t^*$  to reach 99% of the wall velocity at the axis of symmetry of the pump model ( $d=0.55\text{cm}$ ) is then:

$$t^* = \frac{\pi}{\nu} \left( \frac{d}{0.0101} \right)^2 \approx 2.6\text{e} + 5\text{s} \approx 74\text{h}.$$

## References

- <sup>1</sup> ACC/AHA/SCAI, *2005 Guideline update for percutaneous coronary intervention*, (2005).
- <sup>2</sup> AHA, *Heart disease and stroke statistics - 2005 Update*, (2005).
- <sup>3</sup> N. Alphonso, M. Baghai, P. Sundar, R. Tulloh, C. Austin and D. Anderson  
“Intermediate-term outcome following the Fontan operation: A survival, functional and risk-factor analysis,” *Eur. J. Cardio-Thorac. Surg.*, **28**, 529 (2005).
- <sup>4</sup> D. Auerbach, W. Moehring, and M. Moser, “An analytic approach to the Liebau problem of valveless pumping,” *Cardiovasc. Eng.*, **4** (2) 201 (2004).
- <sup>5</sup> I. Avrahami and M. Gharib, “Computational studies of resonance wave pumping in compliant tubes,” *J. Fluid Mech.*, to appear, (2006).
- <sup>6</sup> T. J. Baldwin, H. S. Borovetz, B. W. Duncan, M. J. Gartner, R. K. Jarvik, W. J. Weiss, and T. R. Hoke, “The national heart lung and blood institute pediatric circulatory support program,” *Circulation*, **113** (1) 147 (2006).
- <sup>7</sup> D. M. E. Bardo, D. G. Frankel, K. E. Applegate, D. J. Murphy and R. P. Saneto, “Hypoplastic Left Heart Syndrome,” *Radiographic*, **21** (3) 705 (2001).
- <sup>8</sup> O. Barnea and W. P. Santamore, “Estimation of oxygen delivery in newborns with a univentricular circulation,” *Circulation*, **98**, 1407 (1998).
- <sup>9</sup> A. Barry, “The functional significance of the cardiac jelly in the tubular heart of the chick embryo,” *Anat. Rec.*, **102** (1948).
- <sup>10</sup> H. Bolooki, *Clinical applications of the intra-aortic balloon pump*, ISBN # 0-87993-401-8, Futura Publishing Company (1998).

- <sup>11</sup> A. Borzi and G. Propst, "Numerical investigation of the Liebau phenomenon," *ZAMP*, **54** (6) 1050 (2003).
- <sup>12</sup> M. L. Bouvy, E. R. Heerdink, H.G.M Leufkens, and A. W. Hoes, "Patterns of pharmacotherapy in patients hospitalized for congestive heart failure," *Eur. J. Heart Fail.*, **5** (2) 195 (2003).
- <sup>13</sup> H.-J. Bredow, "Untersuchung eines ventillosen Pumpprinzips," *Fortschr.-Ber. VDI*, Reihe **6** (7) 1 (1968).
- <sup>14</sup> D. L. Brutsaert and L. J. Andries, "The endocardial endothelium," *Am. J. Physiol.*, **263** (32) 985 (1992).
- <sup>15</sup> U. K. Chowdhury, B. Airan, S. S. Kothari, S. Talwar, A. Saxena, R. Singh, G. K. Subramaniam et al., "Specific issues after extracardiac Fontan operation: Ventricular function, growth potential, arrhythmia, and thromboembolism," *Ann. Thorac. Surg.*, **80**, 665 (2005).
- <sup>16</sup> M. Cohen, M. S. Dawson, C. Kopistansky, and R. McBride, "Sex and Other Predictors of Intra-Aortic Balloon Counterpulsation-Related Complications: Prospective Study of 1119 Consecutive Patients," *Am. Heart J.*, **139** (1) 282 (2000).
- <sup>17</sup> S. Corda, J.L. Samuel, and L. Rappaport, "Extracellular matrix and growth factors during heart growth," *Heart Fail. Rev.*, **5** 119 (2000).
- <sup>18</sup> C. L. Davis, "The cardiac jelly of the chick embryo (abstract)," *And. Rec.*, **27** (1924).
- <sup>19</sup> P. L. Digiorgi, M.S. Reel, B. Thornton, E. Burton, Y. Naka and M.C. Oz, "Heart transplant and left ventricular assist device costs," *J. Heart Lung Trans.*, **24** (2) 200 (2005).

- <sup>20</sup> A. I. Dobrolyubov and G. Douchyz, "Peristaltic Transport as the Travelling Deformation Waves," *J. Theor. Biol.*, **219**, 55 (2002).
- <sup>21</sup> G. Fano and F. Badano, "Etude physiologique des premiers stades de développement du cœur embryonnaire du poulet," *Arch. Ital. de Biol.*, **13**, 387 (1890).
- <sup>22</sup> J. J. Ferguson III, M. Cohen, R. J. Freedman Jr, G. W. Stone, M. F. Miller, D. L. Joseph, and E. M. Ohman, "The current practice of intra-aortic balloon counterpulsation: Results from the benchmark registry," *J. Am. Coll. Card.*, **38** (5) 1456 (2001).
- <sup>23</sup> M. C. Fishman and K. R. Chien, "Fashioning the vertebrate heart: Earliest embryonic decisions," *Development*, **124** (11) 2099 (1997).
- <sup>24</sup> T. P. Fitzharris and R. R. Markwald, "Cellular migration through the cardiac jelly matrix - a stereoanalysis by high-voltage electron-microscopy," *Devel. Biol.*, **92** (2) 315 (14) (1982).
- <sup>25</sup> A. S. Forouhar, M. Liebling, A. Hickerson, A. Moghaddam, H.-J. Tsai, J. R. Hove, S. E. Fraser, M. E. Dickinson and M. Gharib, "The embryonic vertebrate heart tube is a dynamic suction pump," *Science*, **312** (5774) 751 (2006).
- <sup>26</sup> V. Hamburger and H. L. Hamilton, "A series of normal stages in the development of the chick embryo," *J. Morphol.*, **88**, 49 (1951).
- <sup>27</sup> A. I. Hickerson, *An Experimental Analysis of the Characteristic Behaviors of an Impedance Pump*, Dissertation, California Institute of Technology, (2005).
- <sup>28</sup> A. I. Hickerson, D. Rinderknecht, and M. Gharib, "Experimental study of the behavior of a valveless impedance pump," *Exper. Fluids*, **38** (4) 534 (2005).

- <sup>29</sup> A. I. Hickerson. and M. Gharib, “On the resonance of a pliant tube as a mechanism for valveless pumping,” *J. Fluid Mech.*, **555**, 41 (2006).
- <sup>30</sup> J. M. Hurlle and J. L. Ojeda, “Cardiac jelly arrangement during formation of tubular heart of chick-embryo,” *Acta Anat.*, **98** (1977).
- <sup>31</sup> M. Y. Jaffrin and A. H. Shapiro, “Peristaltic Pumping,” *Ann. Rev. Fluid Mech.*, **3**, 13 (1971).
- <sup>32</sup> E. Jung, and C. Peskin, “2D simulations of valveless pumping using immersed boundary methods,” *SIAM J. Scient. Comp.*, **23** (1) 19 (2001).
- <sup>33</sup> A. Kantrowitz, “A moment in history: introduction of left ventricular assistance,” *ASAIO*, **10**, 39 (1987).
- <sup>34</sup> T. Kenner, M. Mose, I. Tanev , and K. Ono, “The Liebau-effect or on the optimal use of energy for the circulation of blood,” *Scr. Med. (Brno)* **73**, 9 (2000).
- <sup>35</sup> M. G. Kinsella, T. P. Fitzharris “Control of cell-migration in atrioventricular pads during chick early heart development - Analysis of cushion tissue migration invitro,” *Devel. Biol.*, **91** (1) 1 (1982).
- <sup>36</sup> D. N. Ku, “ Blood flow in arteries,” *Ann. Rev. Fluid. Mech.*, **29**, 399 (1997).
- <sup>37</sup> G. Liebau, “Über ein ventillosoes Pumpprinzip,” *Naturwiss.*, **41**, 327 (1954).
- <sup>38</sup> J. Litmathe, U. Boeken, P. Feindt, R. Marktanner, and E. Gams, “Mechanical assist devices as bridging systems to transplantation: a current review, possible risks and perspectives,” *Transplant. Proceed.*, **36** (10) 3123 (2004).
- <sup>39</sup> A. K. Mahmood, J. M. Courtney, M. Akdis, H. Reul and S. Westaby, “Critical review of current left ventricular assist devices,” *Perfusion*, **15** (5) 399 (2000).

- <sup>40</sup> F. J. Manasek and J. M. Icardo, "Fibronectin distribution during early chick-embryo heart development," *Dev. Biol.*, **95** (1) 19 (1983).
- <sup>41</sup> J. Manner, "Cardiac looping in the chick embryo: a morphological review with special reference to terminological and biomechanical aspects of the looping process," *Ana. Rev.*, **259**, 248 (2000).
- <sup>42</sup> C. G. Manopoulos, D. S. Mathioulakis, and S. G. Tsangaris, "One-dimensional model of valveless pumping in a closed loop and a numerical solution," *Phys. Fluids*, **18**, 017106 (2006).
- <sup>43</sup> H. Matsuda, Y. Taenaka, N. Ohkubo, M. Ohtani, K. Nishigaki, S. Ohtake, T. Miura et al., "Use of a paracorporeal pneumatic ventricular assist device for postoperative cardiogenic shock in two children with complex cardiac lesions," *Artif. Organs.*, **12**, 423 (1988).
- <sup>44</sup> F. Migliavacca and G. Dubini, "Computational modeling of vascular anastomoses," *Biomech. Model. Mechanobiol.*, **3**, 235 (2005).
- <sup>45</sup> D. N. Miniati, R. C. Robbins, "Heart transplantation: A thirty-year perspective," *Ann. Rev. Med.*, **531**, 89 (2002).
- <sup>46</sup> S. D. Mouloupolous, et al., "Diastolic balloon pumping in the aorta—A mechanical assistance to the failing circulation," *Am. Heart J.*, **63**, 669 (1962).
- <sup>47</sup> W. R. Milnor, *Hemodynamics*, 2<sup>nd</sup> edition, Williams and Wilkins, Baltimore, (1989)
- <sup>48</sup> D. A. Moroney and K. J. Vaca, "Infectious complications associated with ventricular assist devices," *Am. J. Crit. Care*, **4**, 204 (1995).

- <sup>49</sup> A. Nakamura, F. J. Manasek, "An experimental study of the relation of cardiac jelly to the shape of the early chick embryonic heart," *J. Embryol. Exp. Morphol.*, **65**, 235 (1981).
- <sup>50</sup> W.W. Nichols and M.F. O'Rourke, *McDonald's Blood Flow in Arteries*, 4th ed., London, Arnold (1998).
- <sup>51</sup> J. T. Ottesen, "Valveless pumping in a fluid-filled closed elastic tube-system: one-dimensional theory with experimental validation," *J. Math. Biol.*, **46**, 309 (2003).
- <sup>52</sup> B. Patten, "Initiation and early changes in the in the character of the heart beat in vertebrate embryos," *Physiol. Rev.*, **29** (1) 30 (1949).
- <sup>53</sup> H. J. Rath and I. Teipel, "Pumping effect in valveless elastic tubes," *ZAMP*, **29** (1) 123 (1978).
- <sup>54</sup> R. K Riemer, G. Amir, S. H. Reichenbach and O. Reinhartz., "Mechanical support of total cavopulmonary connection with an axial flow pump," *J. Thorac. Cardiovasc. Surg.*, **130**, 351 (2005).
- <sup>55</sup> M. D. Rodefeld, J. H. Boyd, C. D. Myers, B. J. Lalone, A. J. Bezruczko, A. W. Potter and J. W. Brown, "Cavopulmonary assist: Circulatory support for the univentricular Fontan circulation," *Ann. Thorac. Surg.*, **76**, 1911 (2003).
- <sup>56</sup> D. Sedmera, T. Pexieder, N. Hu, and E. B. Clark, "Developmental changes in the myocardial architecture of the chick," *Ana. Rec.*, **248**, 421 (1997).
- <sup>57</sup> J. A. Schroeder, L. F. Jackson, D. C. Lee, and T. D. Camenisch, "Form and function of developing heart valves: coordination by extracellular matrix and growth factor signaling," *J. Mol. Med.*, **81**, 392 (2003).

- <sup>58</sup> M. Takeuchi, Y. Nohtomi, H. Yoshitani, C. Miyazaki, K. Sakamoto, and J. Yoshikawa, "Enhanced coronary flow velocity during intra-aortic balloon pumping assessed by transthoracic doppler echocardiography," *J. Am. Coll. Cardiol.*, **43** (3) 368 (2004).
- <sup>59</sup> H. Thomann, "A simple pumping mechanism in a valveless tube," *ZAMP* **29**, 169 (1978).
- <sup>60</sup> F. M. White, *Viscous fluid flow*, 5th edition, McGraw-Hill (2003).
- <sup>61</sup> S. Zamir, *The physics of pulsatile flow*, New York, Springer (2000).